REPUBLIC OF CAMEROON

REPUBLIQUE DU CAMEROUN

MINISTRY OF HIGHER EDUCATION

MINISTERE DE L'ENSEIGNEMENT SUPERIEUR

Ecole Nationale Supérieure des Travaux Publics

Università degli Studi di Padova

DEPARTMENT OF CIVIL ENGINEERING

DEPARTEMENT DE GENIE CIVIL

DEPARTMENT OF CIVIL, ARCHITECTURAL

AND ENVIRONMENTAL ENGINEERING

LOSS OF PRELOAD IN PRESTRESSED BRIDGE CABLES: CASE STUDY OF THE SECOND BRIDGE OVER THE DIBAMBA RIVER IN THE LITTORAL REGION OF CAMEROON

Master thesis / Mémoire de fin d'études
In order to obtain a / En vue de l'obtention du
Master in Engineering in Civil Engineering / Diplôme d'Ingénieur de Génie Civil

Presented by / Présenté par

NGUIFFO SA'A Promethe
Student number: **16TP21103**

Supervised by / Supervisé par
Prof. Eng. Carmelo MAJORANA
Full Professor of Structural Mechanics – University of Padova, DICEA, Italy

Co-supervised by / Co-supervisé par

Dr. Eng. Guillaume Hervé POH'SIE
Assistant Professor of Structural Engineering, ENSTP - Ydé

Dr. Eng. Emanuele MAJORANA
Assistant Professor of Structural Engineering, University of Padova, DICEA, Italy

Defended on July 20, 2022 Infront of the jury composed of:

President: Pr. NKENG George ELAMBO
Examiner: Dr. WOUNBA Jean François
Reporter: Dr. POH'SIE Guillaume Hervé

Academic year / Année académique
2020/2021

DEDICATION

I dedicate this endeavour work to my brother,

Eng. ***TEVOU Steve***

ACKNOWLEDGEMENT

This thesis is the result of combined direct and indirect contributions of numerous individuals whose names may not all be mentioned. Their contributions are wholeheartedly appreciated and indebtedly acknowledged. Nonetheless, it is with respect and pleasure that I address my thanks to:

- The **President** of the jury for the honour of accepting to preside this jury;
- The **Examiner** of the jury **Dr WOUNBA Jean Francois** for accepting to make criticisms aimed at ameliorating this work;
- The Director of the National Advanced School of Public Works (NASPW), **Prof. NKENG George ELAMBO** and **Prof. Eng. Carmelo MAJORANA** of the University of Padua, Italy who are the principal supervisors of this Master's in Engineering (MEng) curricula at NASPW in partnership with the University of Padua;
- The Head of the Department of Civil Engineering, **Prof. MBESSA Michel** for his tutoring, advice and availability;
- My supervisors **Prof. Eng. Carmelo MAJORANA**, **Dr. Eng. Emanuele MAJORANA** and **Dr. Eng. Guillaume Hervé POH'SIE** for the guidance, criticisms and availability throughout the making of this work;
- The **teaching staff** of the **NASPW** and the **University of Padua** for their quality teaching and motivational skills;
- The **administrative staff** of the **NASPW** for their sense of professionalism,
- All my classmates and especially **my friends** of the **7th batch** of Master's in Engineering (MEng) for the spirit of togetherness;
- My parents, **NGUIFFO ETIENNE** and **NANFACK NGUIFFO HELENE** for their love and invaluable educational facilities, guidance and support;
- The whole **NGUIFFO** family for the moments of joy, happiness and for their love and affection since my childhood;
- My friends **Kenneth Franck**, **Douanla Jonathan**, **Kuitche Gerard** and **Matsi Merveille** for all the great moral support and special time spent together.

LIST OF ABBREVIATIONS

AASHTO	American Association of State Highway and Transportation Officials
ACI	American Concrete Institute
ASCE	American Society for Civil Engineers
CHBDC	Canadian Highway Bridge Design Code
CSA	Canadian Standards Association
EN 1992-1-1	Eurocode 2: Design of concrete structures – Part 1-1.
LRFD	Load and Resistance Factor Design
LRFR	Load and Resistance Factor Rating
LM	Load Model
NCHRP	National Cooperative Highway Research Program
SLS	Serviceability Limit State
PCI	Precast/Prestressed Concrete Institute
PPR	Partial prestressing ratio
TS	Tandem System
UDL	Uniform Distributed Loads
ULS	Ultimate Limit State

LIST OF SYMBOLS

A	Cross-sectional area
A_c	Cross sectional area of concrete
A_c	Cross sectional area of prestressing steel
A_s	Cross sectional area of non-prestressed steel reinforcement
A_{sl}	Area of tensile reinforcement
b_w	Smallest width of the cross section in the tensile area
C_{dir}	Direction factor
C_{season}	Season factor
C_p	Pressure coefficient
C_e	Exposure coefficient
$C_{e(z)}$	Exposure factor
E	Young's modulus of elasticity
$E_{c,eff}(t, t_o)$	Effective modulus of concrete at the time of loading t.
EN	European Norm
E_{cm}	Secant modulus of elastic concrete
E_p	Design value of modulus of elasticity of prestressing steel
e	Eccentricity of prestressing tendons
f_{ctm}	Mean axial tensile strength
$f_{ctm,fl}$	Mean flexural tensile strength of concrete
f_{pu}	Ultimate strength of prestressing steel
f_{pk}	Characteristic tensile strength of prestressing steel
$f_{p0.1k}$	characteristic 0.1% proof-stress of prestressing steel.
$f_{ct,eff}$	Mean value of tensile strength of concrete at formation of the first crack
f'_{max}	Maximum Compressive strength of concrete at different life stages
f'_{min}	Minimum compressive strength of concrete at different life stages
f'_t	Top fibre stress
f'_b	Bottom fibre stress
f_{pj}	Stress in prestressing steel at jacking

F_w	Wind force
h	Height of the cross section
I	Moment of inertia of the girder section
K	Loss factor
k_t	Factor which depends on the load duration
k_1	Coefficient which takes into account the bond properties of the bonded reinforcement
k_2	Coefficient which takes into account the distribution of the strain
K_{id}	Transformed section coefficient that accounts for time dependent interaction
l_{set}	Length of anchorage slip
M_{Ed}	Design value of applied bending moment
M_{Rd}	Design moment resistant
N_{Ed}	Axial force in the cross section due to loading or prestressing
P_0	Prestressing force
q_k	Characteristic uniformly distributed variable action
q_b	Reference kinetic pressure
t_0	Age of concrete at the time of loading
TS	Tandem System
V	Shear force
V_{Ed}	Net design shear force
V_{Rd}	Design strength in shear
$V_{Rd,c}$	Design shear strength for a beam without shear reinforcement
x	Neutral axis depth at ultimate limit state
Z_{top}	Section modulus of the top fibers
Z_{btm}	Section modulus of the bottom fibers
α	Index or factor
$\beta_{cc}(t)$	Function describing the development of concrete strength with time
γ_c	Partial factor for concrete
γ_G	Partial factor for permanent actions
γ_P	Partial factor for actions associated with prestressing
γ_Q	Partial factor for variable actions
γ_S	Partial factor for reinforcing or prestressing steel

Δf_{ES}	Prestress Loss due to elastic shortening
ΔP_{c+s+r}	Time dependent loss of prestress due to creep, shrinkage and relaxation
$(\Delta P_{di})_{L_{di}}$	Loss of prestress due to anchorage seating calculated with Eurocode 2
$\Delta P_{\mu}(x)$	Loss due to friction calculated with the Eurocode
Δf_{pCR}	Prestress losses due to creep of concrete
Δf_{pR1}	Prestress losses due to tendon relaxation
Δf_{pSD}	Prestress losses due to shrinkage
Δt	Temperature gradient
$Q_{k,i}$	Characteristic quasi permanent combination
ε_c	Compressive strain in concrete
ε_{yk}	Yield strain of steel
ε_{ud}	Recommended strain limit
ε_{uk}	Characteristic strain of steel
ε	Ratio of bond strength of prestressing and reinforcing steel
ε_1	Adjusted ratio of bond strength taking into account the different diameters of prestressing and reinforcing steel
$\emptyset$	Nominal diameter of prestressing steel
$\emptyset_s$	Adjusted bar diameter
$\varphi(\infty, t_o)$	Final creep coefficient of concrete
θ	Sum of the absolute values of angular change of prestressing steel path from jacking ends.
ρ	Reinforcement ratio for bonded steel
σ_c	Compressive stress in concrete
σ_p	Stress in prestressing steel
σ_{pi}	Initial stress in prestressing steel immediately after tensioning
$\sigma_{p,max}$	Maximum permissible stress in prestressing during jacking
σ_s	Stress in the non-prestressed steel reinforcement
$\psi, \psi_0, \psi_1, \psi_2$	Factors defining respective values of variable actions

ABSTRACT

Accurate determination of prestress losses as well as ways to reduce them has always challenged the prestressed concrete industry. The main objective of this work was to contribute to the reduction of these losses in prestressed bridge tendons. Specifically, to evaluate prestress losses using both the AASHTO LRFD 2017 Specifications and the EN 1992-1-1:2004, to compare the results obtained from both norms and to propose solutions for the reduction of these losses. To achieve this objective, a literature review was done in order to understand the prestressing concept and to compare the loss prediction methods used in the past. The case study for this work was a prestressed concrete girder bridge of total length 445 m, made of 12 spans each of length 37 m. The Bridge was modelled, and a construction stage analysis was performed in the computer program, Midas Civil 2022 (v1.2) from where the losses were calculated. The prestress loss results provided by both norms were further analyzed and compared on the basis of the accuracy, the reliability, the performance and detailing level. The following conclusions could be drawn from this study: more than 50 % of the losses were frictional losses, followed by time-dependent losses. Regarding the results of the prestress losses obtained with the two norms, a discrepancy of 17 % for frictional losses, 4 % for losses due to elastic shortening, 14.42 % for anchorage seating losses and 4.70 % for time-dependent losses was noticed. The main reason for these discrepancies was due to the fact that the design parameters incorporated by both methods are different. The creep, shrinkage and friction coefficients proposed by both methods as well as the partial safety and strength reduction factors are all different. The AASHTO LRFD 2017 Specification provided more accurate results because it does not only take into account the time dependent material properties and the age modulus of concrete, but it provides more detailed results on the loss of prestress not only during the construction stage of the bridge but also during its service life. For prestress loss reduction, a detailed analysis of the girder revealed that increasing the elastic modulus by 10 % and decreasing the creep coefficient by 20 % reduced prestress losses by 4.35 % and 3.19 % respectively. In addition, the addition of mild strands and top prestressing strands in prestressed concrete girder was found to be some solutions to reduce these losses.

Keywords: Prestressed bridges, prestress losses, prestressing tendons, elastic modulus, creep

RESUME

La détermination précise des pertes de précontrainte ainsi que les moyens de les réduire ont toujours été un défi pour l'industrie du béton précontraint. L'objectif principal de ce travail était de contribuer à la réduction de ces pertes dans les câbles de pont précontraints. Plus précisément, il était question pour nous de : évaluer les pertes de précontrainte en utilisant à la fois les spécifications AASHTO LRFD 2017 et la norme EN 1992-1-1 :2004, comparer les résultats obtenus à partir des deux normes et proposer des solutions pour la réduction de ces pertes. Pour atteindre cet objectif, une revue de la littérature a été faite afin de comprendre le concept de précontrainte et de comparer les méthodes de prédiction des pertes utilisées dans le passé. Le cas d'étude pour ce travail était un pont à poutres en béton précontraint d'une longueur totale de 445 m, composé de 12 travées de 37 m chacune. Le pont a été modélisé et une analyse des phases de construction a été faite dans le logiciel Midas Civil 2022 (v1.2) à partir duquel les pertes ont été calculées. Les résultats des pertes de précontrainte fournis par les deux normes ont été analysés et comparés sur la base de la précision, de la fiabilité, de la performance et du niveau de détail. Les conclusions suivantes ont pu être tirées de cette étude : plus de 50 % des pertes étaient des pertes de frottement, suivies des pertes liées au temps. En ce qui concerne les résultats des pertes de précontrainte obtenus avec les deux normes, il a été constaté un écart de 17 % pour les pertes par frottement, de 4 % pour les pertes dues au raccourcissement élastique, de 14,42 % pour les pertes dues à l'assise des ancrages et de 4,70 % pour les pertes liées au temps. Ces divergences sont principalement dues au fait que les paramètres de conception incorporés par les deux méthodes sont différents. Les coefficients de fluage, de retrait et de frottement proposés par les deux méthodes ainsi que les facteurs de sécurité partielle et de réduction de la résistance sont tous différents. La spécification AASHTO LRFD 2017 a fourni des résultats plus précis car elle ne prend pas seulement en compte les propriétés des matériaux liées au temps et le module d'âge du béton, mais elle fournit des résultats plus détaillés sur la perte de précontrainte non seulement pendant la phase de construction du pont mais aussi pendant sa durée de vie. Pour la réduction de la perte de précontrainte, une analyse détaillée de la poutre a révélé que l'augmentation du module élastique de 10 % et la diminution du coefficient de fluage de 20 % réduisaient les pertes de précontrainte de 4,35 % et 3,19 % respectivement. En outre, l'ajout des câbles de précontrainte supérieurs dans la poutre en béton précontraint s'est avéré être une solution pour réduire ces pertes.

Mots clés : Béton précontraint, pertes de précontrainte, câbles de précontrainte, module d'élasticité, fluage.

LIST OF FIGURES

LIST OF TABLES

TABLE OF CONTENTS

GENERAL INTRODUCTION

Reinforced concrete is the most widely used structural material for the construction of mankind's infrastructure and one of its disadvantages is that tensile cracks due to bending occurs which encourage steel corrosion. Therefore, there is little benefit to be gained by using higher strength steel or concrete, since the resulting width of the cracks at working loads would be unacceptable in order to satisfy serviceability requirements thus, the concept of prestressing.

Prestressed concrete, an ideal combination of concrete and high strength steel, has emerged as an efficient material for modern construction. The idea of using prestressed concrete as a structural building system was defined by Eugene Freyssinet. In many countries, the development of prestressing in the building industry has had its greatest boom in the 1960s. This is due to the technical and economic benefits of prestressed concrete, as it permits longer spans and increased girder spacing (Hassoun, 2012).

Efficient design of prestress concrete bridges demands an accurate prediction of prestress losses. The prestress losses are defined as the loss of tensile stress in the prestressing tendons which acts on the concrete component of the prestressed concrete section. These losses can induce excessive deflections and cracking in large span prestressed concrete girders hence reducing the bridge durability. Despite the numerous programs that have been conducted on prestress losses, accurate determination of these losses as well as ways to reduce it has always challenged the prestressed concrete industry (Jayaseelan, 2019).

Faced with this difficulty, the research herein aims at reducing prestress losses in prestressed concrete bridges. In order to achieve this objective, prestress losses are evaluated using both the AASHTO LRFD 2017 Specifications and the EN 1992-1-1:2004. The results obtained using both norms are compared and solutions are proposed for prestress losses reduction. This study is divided into four parts. The first part consists of a literature review on the various prestressing systems, a clever understanding of the concept with an introduction to prestressed concrete bridges as well as the evaluation and comparison of the various loss prediction methods developed in the past years. The second part presents the methodology of the study, it elaborates on the collection of data, the analysis and the prestress loss calculation procedures used for both norms. In The third part, the results of prestress losses obtained for both norms are presented, compared and solutions for prestress loss reduction are finally proposed.

CHAPTER 1: LITERATURE REVIEW

Introduction

The interest of improving the load carrying capacity and durability of structural members is growing over time. There is therefore a need for new technology and new techniques to provide resistant, durable and less costly solutions. This chapter presents the background information related to prestress concrete and an attention is made on prestress losses. The generalities begin with a historical view of prestressed concrete, Its constituents and material properties, it's bond mechanism and classification. In addition, the various time dependent material properties are highlighted and an overview of prestressed concrete bridges as well as the various prestressing equipment are discussed. The principles, types and methods of applying prestress forces are also discussed in detail. Furthermore, a special review of prestress losses is presented and because they represent the core of this study, the various methods used in the past to estimate prestress losses as well as the comparison between these methods are presented. Finally, the analysis programs together with the advantages and disadvantages of the prestressing technology are presented. The literature review is written based on previously published books and articles concerning prestressed concrete and prestressed concrete bridges (Hassoun, 2012).

1.1. Prestressed concrete

Prestressed concrete is a particular form of concrete and its application is used to offset the occurrence of tensile stresses in concrete, which is weak in tension by applying an initial compressive force to the concrete to reduce or eliminate the internal tensile forces and thereby control or eliminate cracking, thus increasing its performance (Boukendakdji et al., 2017). The main concept of prestressing is illustrated in Figure 1.1.

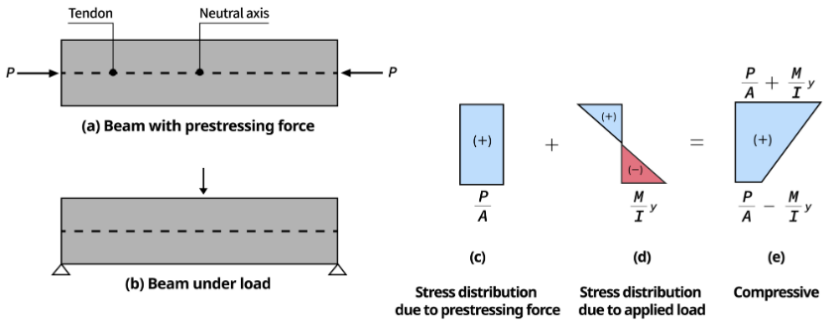

Figure 1.1. The concept of prestressed concrete (fib, 2004).

1.1.1. Historical background

Prestressing is not a new concept. Back in 2700 B.C., the Egyptians used wires and turnbuckles to hold the ship together (Members & Connor, 2001), but it was Eugène Freyssinet (1879-1962) who first applied this principle in 1928. Freyssinet is reported to have built an experimental arch in 1908, which incorporated prestressing tendons, and in 1930 he utilized prestressing during the construction of the Plougastel Bridge in France. In Germany, Dyckerhof and Widmann used post-tensioned bars during the construction of the arch bridge at Alsleben in 1927. During this time, much was still being learnt about prestressed concrete and the nature of time-dependent effects. Engineers were experimenting the ways of using prestressed concrete in building and other applications. The first prestressed concrete bridges were built in the mid-1930s with the Oued Fodda Bridge in Algeria (1936), Aux Bridge in Saxony (1936) and the Oella Bridge in Germany (1938) leading the way, but it was not until after the Second World War that prestressed concrete became firmly established in bridge building. Eugène Freyssinet is generally considered the inventor of modern-day prestressing, and it was his six bridges across the Marne River in France, built between 1945 and 1950, that established the technique. The first of these, the Luzancy Bridge is presented in Figure 1.2, is a 55 m-long structure built as a "frame" with the abutments. The remaining five are each 73 m long and again built as a frame with the deck gently curving up towards the centre, where the deck depth is only 1 m. The decks are either a concrete box or concrete "I" beam arrangement, with prestressing being used vertically in the webs as well as horizontally along the deck (Hewson, 2011).

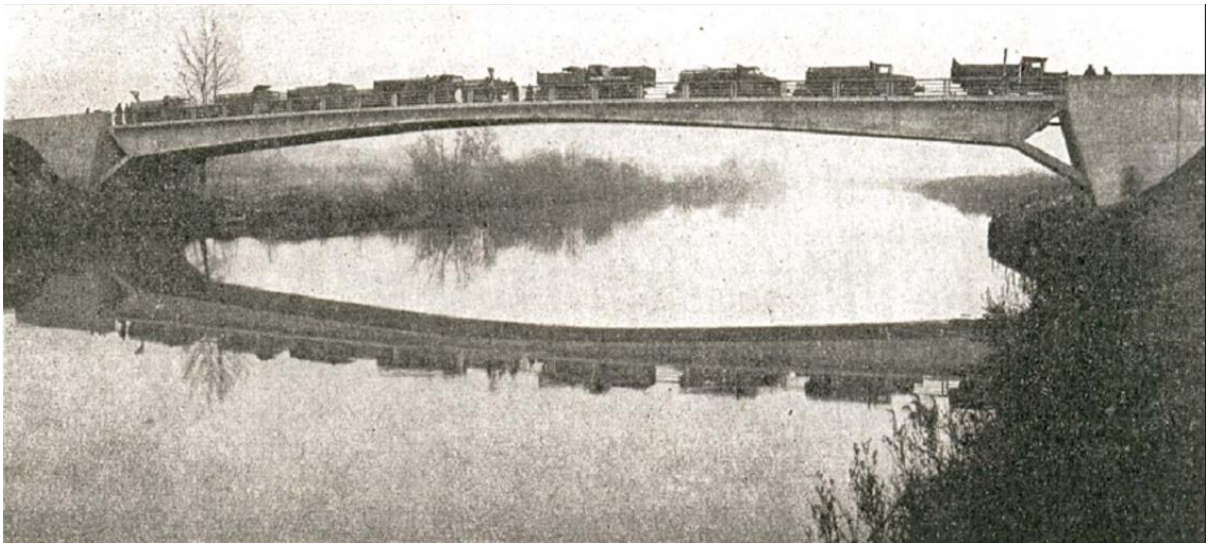

Figure 1.2. Luzancy bridge of Eugène Freyssinet 4 (Schacht & Marx, 2014).

1.1.2. Prestressing materials and their properties

The deformation of a prestressed concrete member throughout the full range of loading depends on the properties and behaviour of the constituent materials. In order to satisfy the design objective of adequate structural strength, the ultimate strengths of both concrete and steel need to be known. In addition, factors affecting material strength and the non-linear behaviour of each material in the overload range must be considered.

1.1.2.1. Steel used for prestressing

Prestressing steel used in prestressed concrete must be of high strength quality, usually of ultimate strength, f_{pu} of 1730 to 1860 MPa. Ideally a tendon material should not only have high strength but also show sufficient ductility before failure, have good bonding properties, low relaxation, good resistance to fatigue and corrosion, be economical, easy to handle, and remain elastic up to relatively high stress. There are three basic types of high-strength steel commonly used as tendons in prestressed concrete construction: Cold-drawn relieved round wire (with diameter range of 2.5-12.5mm and strength range of 1570-1860MPa), Stress-relieved strand (made of 7-wire and 19- wire strands) and high strength alloy steel bars (with diameter ranging from 20-50 mm and strength range from 1030-1230 MPa). (Raymond I. G., Neil C. M., 2017). These basic high strength steel types are illustrated in Figure 1.3.

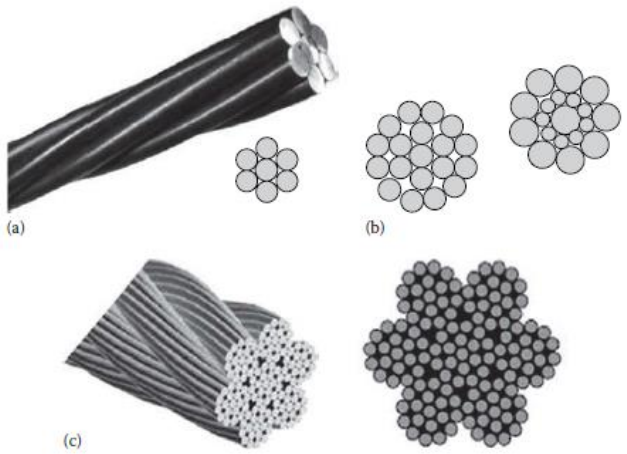

Figure 1.3. Strands and cables (Gilbert et al., 2013).

Where: a) 7-wire strand, b) 19wire strand, c) Cable made of seven 19-wire strands

1.1.2.2. Specifications of Eurocode 2 for prestressing steel

According to the Eurocode 2, the following recommendations are given for prestressing steel:

a) Strength and ductility

According to EN 1992-1-1 [1], a prestressing tendon may be assumed to have adequate ductility $f_{pk}/f_{p0.1k} \geq 1.1$. where; f_{pk} is the characteristic strength and $f_{p0.1k}$ is characteristic 0.1% proof-stress of prestressing steel

b) Elastic modulus

The elastic modulus can be obtained by measuring the elongation of sample pieces of tendon in direct tension tests. affect Its variation will the calculated extension of the tendon during the stressing operation, hence should be considered both in design and during construction.

c) Steel relaxation

Three classes of relaxation are recognized in EN 1992-1-1 [1]: Class 1(wire or strand – ordinary relaxation), Class 2 (wire or strand – low relaxation), and Class 3(hot-rolled and processed bars)(Gilbert et al., 2013).

The final creep coefficient for each class is given by Table 1.1;

Table 1.1. Long term relaxation losses (at t=500000 hrs.) and corresponding to a final creep coefficient for wire, strand and bar (T= 20°C)(EN-1992-1-1_2, 2009).

		Tendon stress σ_{pi} as a proportion of f_{pk}		
Type of tendon		$\mu = 0.6$	$\mu = 0.7$	$\mu = 0.8$
Class 1	Relaxation loss (%)	15.5	19.0	23.3
	Creep coefficient, $\varphi_p(t, \sigma_{pi})$	0.155	0.190	0.233
Class 2	Relaxation loss (%)	2.5	3.9	6.1
	Creep coefficient, $\varphi_p(t, \sigma_{pi})$	0.025	0.039	0.061
Class 3	Relaxation loss (%)	6.2	8.7	12.1
	Creep coefficient, $\varphi_p(t, \sigma_{pi})$	0.062	0.087	0.121

d) Stress-strain Curve

For cross-sectional design, EN 1992-1-1 [1] allows the stress–strain curve for prestressing steel to be approximated by either of the two bilinear curves shown in Figure 1.4 as solid lines. The inclined branch (Line 1) has a strain limit $\varepsilon_{ud} = 0.9\varepsilon_{uk}$. Alternatively, the horizontal top branch (Line 2) can be used without any limit on strain.

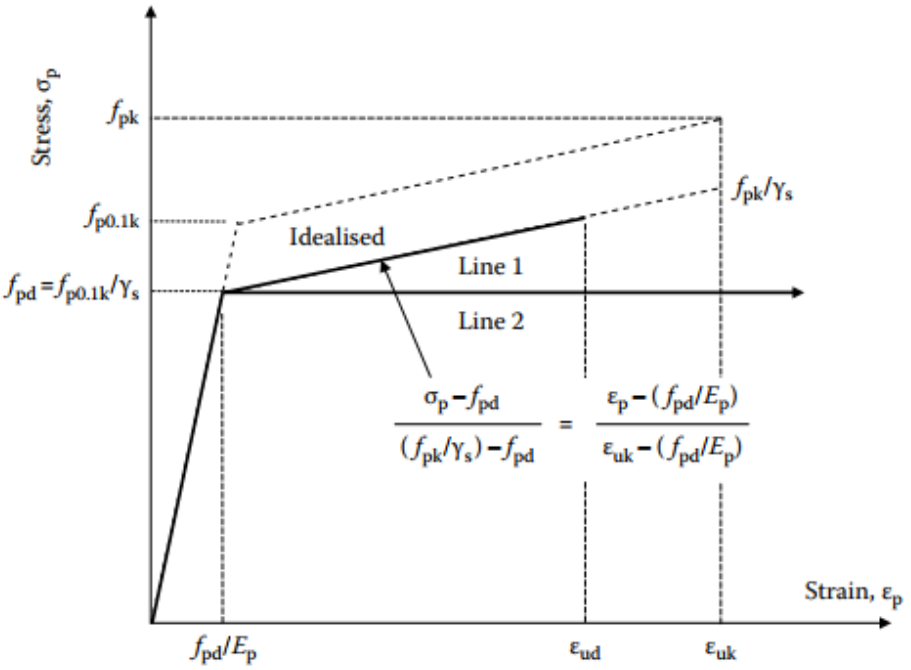

Figure 1.4. Design stress strain diagrams of prestressing steel(Gilbert et al., 2013).

1.1.2.3. Non prestressing steel reinforcement

Generally, for shear reinforcement or supplementary reinforcement in regions of high local stresses and deformations, non-prestressed reinforcing steel is commonly used in prestressed concrete structures. These reinforcement in the form of stirrups is most frequently used to carry the diagonal tension caused by shear and torsion in the webs of prestressed concrete beams, to control flexural cracks at service loads in prestressed concrete beams and slabs where some degree of cracking under full-service loads is expected and finally to reduce long-term deflection and shortening due to creep and shrinkage.(Raymond I. G., Neil C. M., 2017). Figure 1.5 shows the non prestressing steel reinforcement of a typical post tensioned girder.

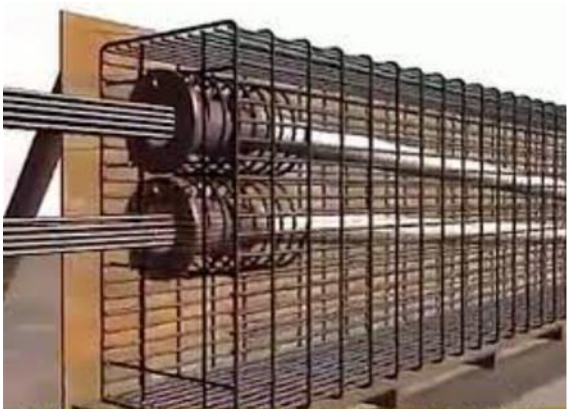

Figure 1.5. Non prestressed steel reinforcement (Bymaster et al., 2015).

1.1.2.4. Specifications of Eurocode 2 for non-prestressing steel reinforcement

According to the Eurocode 2, the following recommendations are given for non prestressing reinforcement:

a) Strength and ductility

Three ductility classes are recognized by EN 1992-1-1 [1]: Class A (low ductility); Class B (medium ductility) and Class C (high ductility). Class A reinforcement should be used if plastic methods of design are adopted.

b) Elastic modulus

In the absence of test data, the design value may be taken as equal to 200 × 103MPa, irrespective of the type and ductility class of the steel. Alternatively, E_s may be determined from standard tests.

c) Stress-strain curves

In design, EN 1992-1-1 [1] allows the idealized bilinear relationship shown in Figure 1.6 to be used with a recommended strain limit of ε_{ud}=0.9ε_{uk} and a maximum stress of kf_{yk}/γ_s. Alternatively, an elastic–plastic relationship with a horizontal top branch at f_{yd} =f_{yk}/γ_s.may be used without the need to check the strain limit;

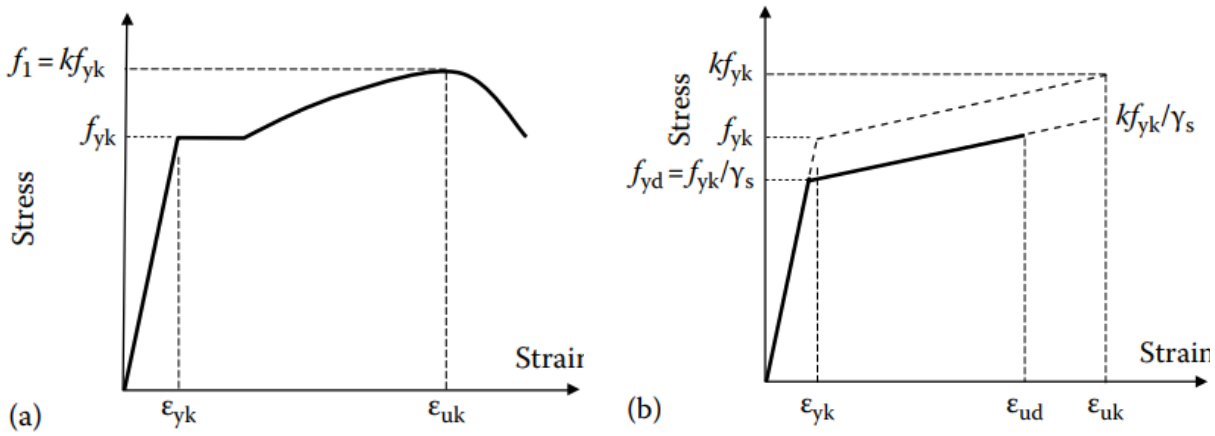

Figure 1.6. Stress–strain curves for reinforcing steel.(Gilbert et al., 2013).

Where:

(a) Actual stress–strain curve of a hot-rolled bar.

(b) Idealized stress–strain curve of a hot-rolled bar.

1.1.2.5. Prestressed concrete

For the concrete usually used in prestressed structures, the water to cement ratio is generally 0.4. A typical mix used for prestressed concrete by weight might be coarse aggregate 45%, fine aggregate 30%, cement 18% and water 7%. High strength concrete with low water to cement ratio are made more workable by adding admixtures like super plasticizers in the mix. For prestressed structures in general the quality and strength of the concrete used is higher than that used for ordinary reinforced concrete. The values of f_{ck} here ranges from 40 to 65 MPa but higher strengths are not uncommon. The forces imposed on a prestressed concrete section are relatively large hence the use of high strength concrete (having greater elastic modulus and stiffness) may delay the onset of cracking. In addition, high strength concrete usually creeps less than low strength concrete. The strength of concrete under a biaxial compression is usually greater than that undergoing a uniaxial compression(Raymond I. G., Neil C. M., 2017).

According to the ACI code, the allowable stress in concrete is based on three principles:

- Stress after the prestress transfer and before the prestress transfer
- Stresses at service loading after all losses (for Class U and class T)
- These stresses may be exceeded if it is shown by tests or analysis that performance is satisfactory

The minimum grades of concrete for prestressed applications are as follow:

- 30 MPa for post-tensioned members
- 40 MPa for pre-tensioned members

Figure 1.7 shows a prestressed concrete girder with the prestressing tendons.

Figure 1.7. Prestressed concrete girder(Boukendakdji et al., 2017).

1.1.2.6. Specifications in Eurocode 2 for prestressed concrete

According to the Eurocode 2, the following recommendations are given for prestressing steel:

a) Compressive strength

The strength of concrete is specified in EN 1992-1-1 [1] in terms of concrete strength classes which relate to the lower characteristic compressive strength at 28 days measured on cylinders f_{ck} or on cubes $f_{ck,cube}$. The standard strength classes are usually expressed as C = $f_{ck}/f_{ck,cube}$, with the minimum strength class C_{min}= $C_{12/15}$ and the maximum strength class C_{max} recommended as C_{min}= $C_{90/105}$. The concrete strength is based on the characteristic cylinder strength f_{ck} and the strength classes specified in EN1992-1-1[1] are shown in Table 1.2, together with the corresponding mechanical properties of concrete required for design. (Raymond I. G., Neil C. M., 2017)

Table 1.2. Strength and deformation characteristics for concrete(Gilbert et al., 2013).

Strength class	C12/15	C16/20	C20/25	C25/30	C30/37	C35/45	C40/50	C45/55	C50/60	C55/67	C60/75	C70/85	C80/95	C90/105
f_{ck} (MPa)	12	16	20	25	30	35	40	45	50	55	60	70	80	90
$f_{ck,cube}$ (MPa)	15	20	25	30	37	45	50	55	60	67	75	85	95	105
f_{cm} (MPa)	20	24	28	33	38	43	48	53	58	63	68	78	88	98
f_{ctm} (MPa)	1.6	1.9	2.2	2.6	2.9	3.2	3.5	3.8	4.1	4.2	4.4	4.6	4.8	5.0
$f_{ctk,0.05}$ (MPa)	1.1	1.3	1.5	1.8	2.0	2.2	2.5	2.7	2.9	3.0	3.1	3.2	3.4	3.5
$f_{ctk,0.95}$ (MPa)	2	2.5	2.9	3.3	3.8	4.2	4.6	2.9	5.3	5.5	5.7	6.0	6.3	6.6
E_{cm} (GPa)	27	29	30	31	33	34	35	36	37	38	39	41	42	44
ε_{c1} (×10⁻³)	1.8	1.9	2.0	2.1	2.2	2.25	2.3	2.4	2.45	2.5	2.6	2.7	2.8	2.8
ε_{cu1} (×10⁻³)					3.5					3.2	3.0	2.8	2.8	2.8
ε_{c2} (×10⁻³)					2.0					2.2	2.3	2.4	2.5	2.6
ε_{cu2} (×10⁻³)					3.5					3.1	2.9	2.7	2.6	2.6
n					2.0					1.75	1.6	1.45	1.4	1.4
ε_{c3} (×10⁻³)					1.75					1.8	1.9	2.0	2.2	2.3
ε_{cu3} (×10⁻³)					3.5					3.1	2.9	2.7	2.6	2.6

b) Tensile strength

An approximate value of f_{ct} is specified in EN 1992-1-1 [1] as: f_{ct}=0.9$f_{ck.sp}$. The mean strength f_{ctm} specified in the EN 1992-1-1 [1] for each class is related to the mean compressive strength by;

$$f_{ctm}=0.3\times (f_{ck})^{\frac{2}{3}} \quad \text{for } f_{ck} \leq 50MPa \qquad \textbf{(1.1)}$$

$$f_{ctm}= 2.12\text{xln}\,[1+0.1f_{cm}] \quad \text{for } f_{ck} > 50MPa \qquad \textbf{(1.2)}$$

Where:

$$f_{ctm,fl} = \max\,\{(1.6 - \frac{h}{1000})f_{ctm}; f_{ctm}\} \qquad \textbf{(1.3)}$$

1.1.3. Bond mechanism

A prestressed element ability to meet performance requirement is directly related to the quality or strength of the bond at the strand concrete interface (Naito et al., 2018). After prestress release, strand stresses are transferred to the member through the action of the bond. Without sufficient bonding, the stresses cannot be fully transferred, and the member itself cannot be brought to the desired level of precompression. Shortcomings in prestress performance caused by inadequate bond strength may include unexpected deflections or cracking at service loads. Hence the bond between the prestressed strands and the concrete is more important for the structural elements.

Bond mechanism of concrete prestress systems is mostly contributed by adhesion, mechanical interlock and friction. Adhesion plays minimal role in prestress concrete systems. Mechanical interlocking is the largest contributor to the bond. It occurs due to the spiral twisting of the outer wires that form the strand. This helical shape of the strand results in bearing stress between the strand and concrete. Friction is attributed by concrete confinement and Hoyer effect. Hoyer effect is the expansion of strand in the transfer zone after releasing the prestress force due to the poison's effect (Mohandoss et al., 2019). Figure 1.8 and Figure 1.9 illustrates the difference between bonded and unbonded tendons.

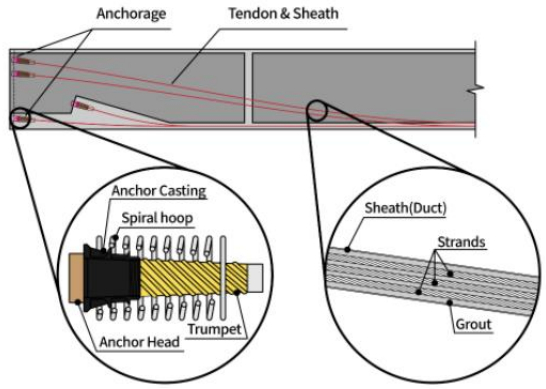

Figure 1.8. Bonded tendons(fib, 2004).

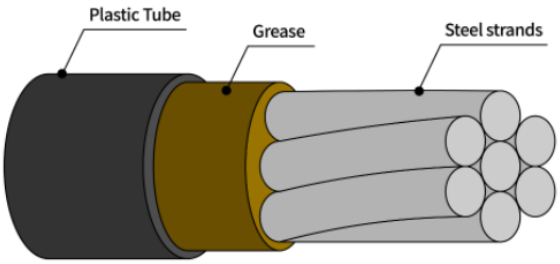

Figure 1.9. Unbonded tendons(fib, 2004).

1.1.4. Classification of prestressed concrete members

As stated by the ACI code, section 25.4.2, prestressed concrete members are spread into three classes based on the computed extreme fibre stress, f_t, in the tension zone at service loads (Mohandoss et al., 2019)

1.1.4.1. Class U (Uncracked section)

In this uncracked concrete section ($f_t \leq 7.5\sqrt{f_c'}$), the gross section properties are used to check deflection at service load. No crack will develop in this section and no skin reinforcement is

needed. Figure.1.10, shows the distribution of stresses in beams with varying amount of prestressed and non-prestressed reinforcement.

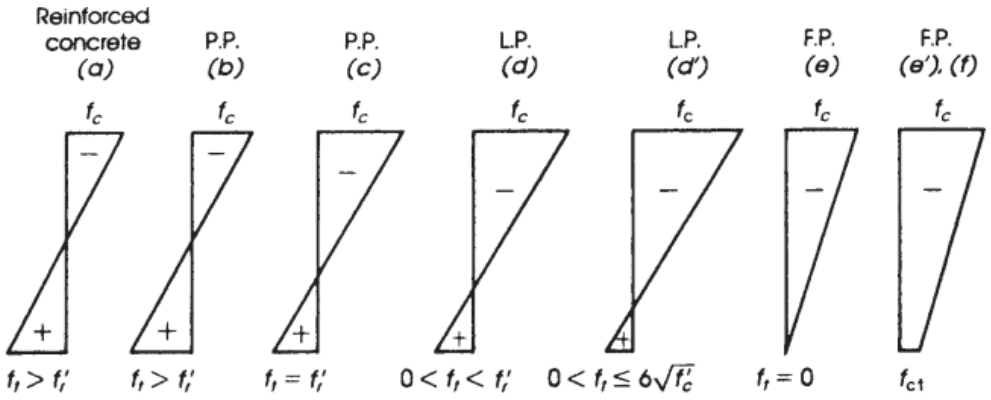

Figure 1.10. Distribution of stresses in beams with varying amounts of prestressed and non-prestressed reinforcement(Gilbert et al., 2013).

1.1.4.2. Class T (section in the transition zone)

This type of section has a tensile stress in concrete higher than the modulus of rupture of concrete, $f_t > 7.5\sqrt{f_c'}$ producing a case between cracked and uncracked sections in this case, the gross section properties are used to check stresses. No skin reinforcement is needed in the tension zone.

1.1.4.3. Class C (Cracked section)

With $f_t > 7.5\sqrt{f_c'}$, The tensile stress in the section exceeds 1.6 times the modulus of rupture. Therefore, cracks will develop as in the case of partially stressed members. In this case a cracked section property should be used to check stresses, cracking and deflections.

1.2. Time dependent material properties

The behaviour of prestressed concrete over time depends on the material properties. Creep and shrinkage of concrete, and steel relaxation are the most significant material properties affecting the long-term stresses and deformations of prestressed bridges. As time passes, volume changes due to creep and shrinkage occur in concrete. These changes create stresses, cracks, and deflections, thus affecting the serviceability of the structure.

1.2.1. Concrete creep

As shown in the figure 1.11, when a constant load is applied to concrete, initial instantaneous deformation occurs, and even though no additional load is applied, creep occurs, which increases the deformation over time. Creep deformation occurs quickly in the beginning, but the rate of

increase gradually decreases over time. When the load is removed, elastic recovery and creep recovery occur, but permanent deformation remains.

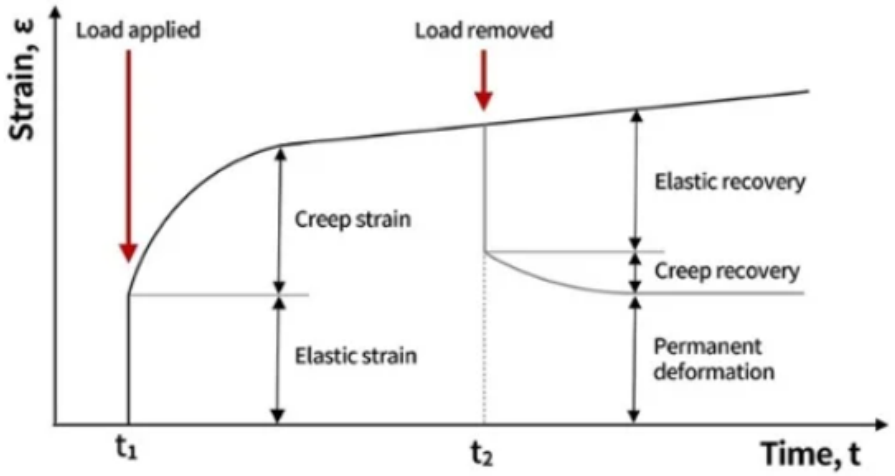

Figure 1.11. Creep strains due to loading at t_1 and unloading at t_2(S. T. Kim et al., 2017).

One of the most important factors affecting creep externally is the relative humidity of the atmosphere surrounding concrete. In environments with low relative humidity, the drying condition of the environment causes drying shrinkage, which distinguishes from the basic creep term that occurs when drying is prevented. In general, creep refers to a phenomenon that combines the two cases.

1.2.2. Concrete shrinkage

When curing and drying of concrete starts, water not used for hydration moves from the inside of the concrete to the surface and evaporates. This phenomenon causes the concrete member to shrink over time, and the deformation caused by the reduction in volume due to the shrinkage is called drying shrinkage or shrinkage strain. There are several factors that affect shrinkage, and the most influencing factors are the unit content of water in concrete and relative humidity. Furthermore, when concrete is reinforced, shrinkage strain is reduced compared to members that are not, and moisture evaporation occurs more rapidly as the surface area exposed to the atmosphere is wider.

Figure 1.12 and Figure 1.13 illustrates best illustrates this phenomenon both for normal concrete and high-strength concrete respectively.

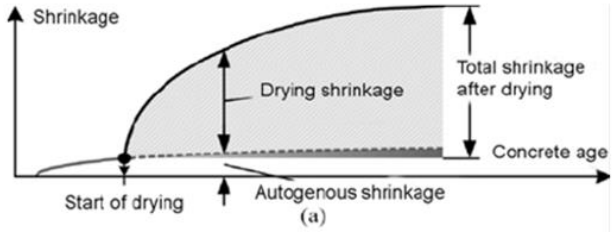

Figure 1.12. Shrinkage strain components in normal concrete (Kim et al., 2017).

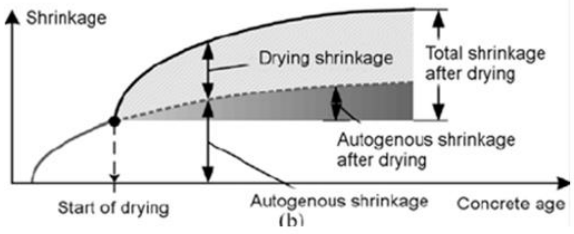

Figure 1.13. Shrinkage strain components in high-strength concrete(Kim et al., 2017)

1.2.3. Modulus of elasticity of concrete

The modulus of elasticity is an important property of hardened concrete. Concrete is a composite material, including aggregate and cement paste. The modulus of elasticity of concrete highly depends on the properties and proportions of the mixture materials. The elastic modulus of concrete has a significant effect on the behaviour of prestressed bridge girders, including deflections and stresses.

1.2.4. Compressive strength of concrete

Compressive strength is the most common performance indicator of concrete and is affected by factors, including the water-to-cementitious (w/c) ratio, mix proportion, and curing conditions. Typically, the compressive strength of concrete decreases with an increase of the w/c ratio. It also depends on the strength of the aggregate itself, and the relative ratio between the aggregate and cement paste. The higher the strength of the aggregate, the higher the compressive strength of concrete becomes. The cement type also plays an important role in the compressive strength of concrete.

1.2.5. Relaxation of prestressing steel

Steel relaxation is a loss of stress in the prestressing steel when held at a constant strain (i.e., intrinsic relaxation). The strands typically used in practice today are called low-relaxation strands. They undergo a strain tempering stage in production that heats them to about 660°F and then cools them while under tension. This process reduces relaxation losses to approximately 25% of that for stress-relieved strand (Raymond, Neil, 2017)

1.3. Methods and principles of prestressing

1.3.1. Principles of prestress

Prestressing generally involves two materials, the stressor and the stressee which, when acting together, perform better than either one taken separately(Naaman & Ph, 1983). Stresses in the

structural members must remain, everywhere and for all states of loading, within the limits of stress that the material can sustain indefinitely. The induced stresses, primarily compressive, are usually created by means of high tensile steel tendons, which are tensioned and anchored to the concrete member. Stresses are transferred to the concrete either by bond along the surface of the tendon or by the ends of the tendon (Hassoun, 2012). In the prestressed concrete design, an initial compressive stress is introduced to the beam to offset or counteract the tensile stresses produced by the external loads (Figure 1.26). If the induced compressive stress is equal to the tensile stress at the bottom fibres, then both stresses cancel themselves, whereas the compressive stress in the top fibres is doubled; in this case, the whole section is in compression. If the induced compressive stress is less than the tensile stress at the bottom fibres, these fibres will be in tension, whereas the top fibres are in compression. This principle is explained in Figure 1.26.

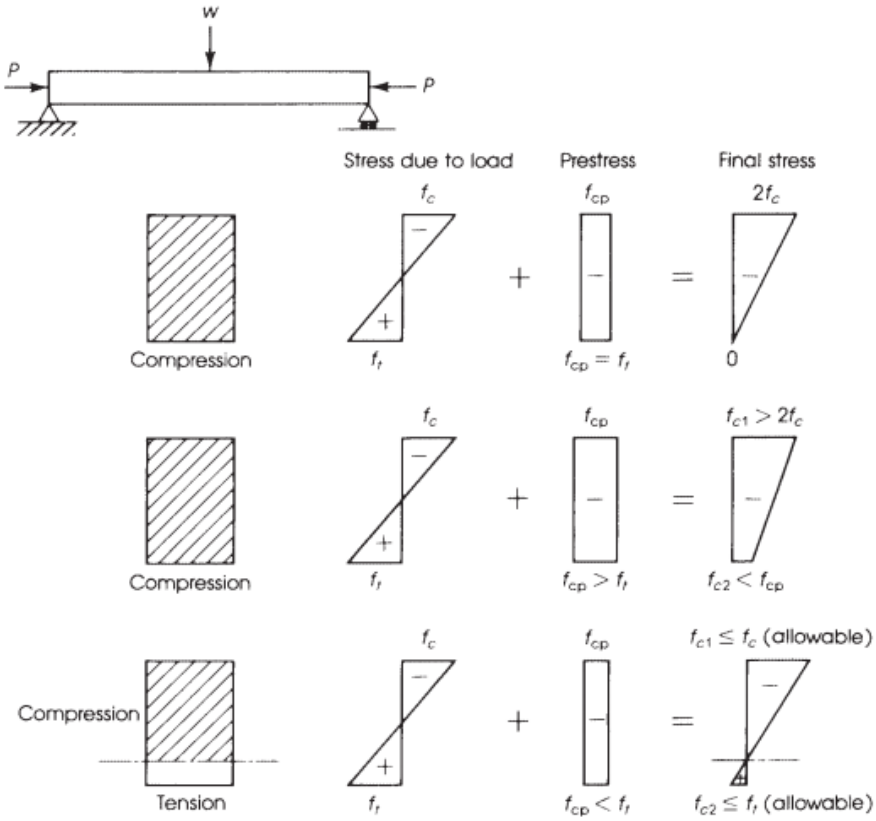

Figure 1.14. Prestressed concrete (Hassoun, 2012).

1.3.2. Types of prestressing

The various types of Prestressing of concrete can be given based on the following classifications.

1.3.2.1. Source of prestressing force

This classification is based on the methos of generation of the prestressing force. This includes;

a) Mechanical prestressing

In this type of prestressing, the devices include weights with or without lever transmissions, geared transmission in conjunction with pulley blocks, screw jacks with or without gear drives and wire winding machines. This type of prestressing is adopted for mass scale production.

b) Hydraulic prestressing

This is the simplest type of prestressing, producing very large prestressing forces. The hydraulic jack used for the tensioning of the tendons, comprises of calibrated pressure gauges which directly indicates the magnitude of the force developed during tensioning.

c) Electrical prestressing

In this type of prestressing, the steel wires are electrically heated and anchored before putting the concrete in the moulds. This type of prestressing is called Thermo-Electric prestressing.

d) Chemical prestressing

In this type of prestressing, expansive cement is used and the degree of expansion is controlled by varying the curing conditions. The expansion action of cement is restrained while setting. This generates tensile forces in the tendons and compressive stresses in the concrete.

1.3.2.2. External or internal prestressing

This classification is based on the location of the tendons with respect to the concrete section. When the prestressing is achieved by elements located outside the concrete members (for example, by cables lying outside a beam), it is called external prestressing. This technique is adopted in repair and strengthening works such as retrofitting of bridges and when the prestressing is achieved by elements located inside the concrete member (commonly, by embedded tendons), it is called internal prestressing (Menn, 1990). These two types of prestressing systems are illustrated in Figure 1.27 and Figure 1.28.

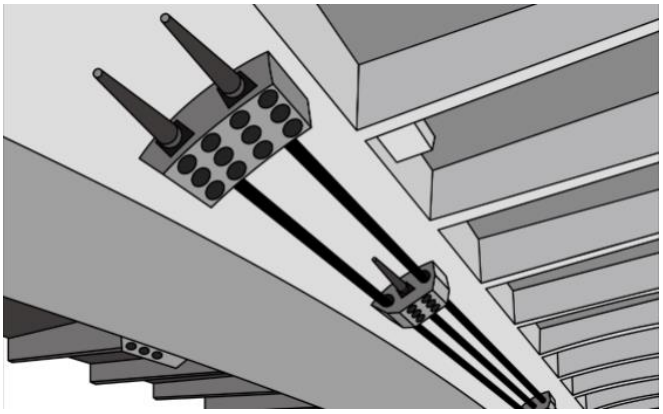

Figure 1.15. Concept of external Prestressing (fib, 2004).

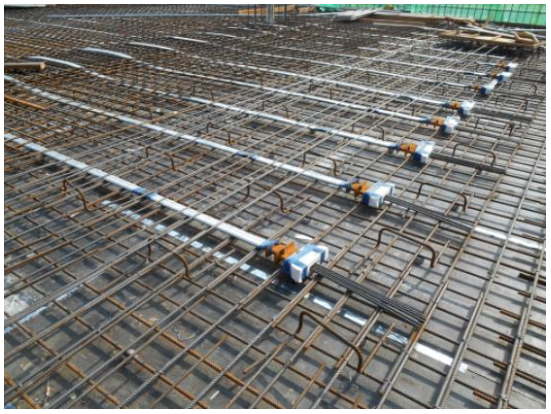

Figure 1.16. Concept of internal prestressing (fib, 2004).

1.3.2.3. Pre-tensioning or posttensioning

This is the most important classification and it is based on the sequence of casting the concrete and applying the tension to the tendons. Pre-tensioning occurs when the tension is applied to the tendons before the casting of the concrete. The precompression is transmitted from steel to concrete through bond over the transmission length near the ends and posttensioning occurs when the tension is applied in the tendons (located in a duct) after hardening of the concrete. The precompression is transmitted from steel of concrete by an anchorage device (at the end blocks) (Jayaseelan, 2019). A clearer illustration is given by Figure 1.29 and Figure 1.30.

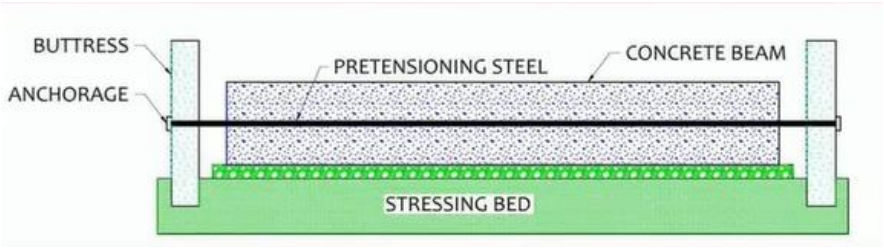

Figure 1.17. Pretensioned concrete(Bhuiyan et al., 2021).

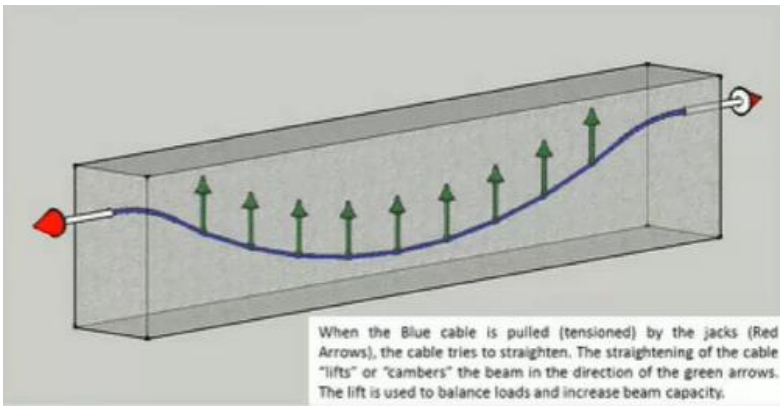

Figure 1.18. Posttensioned concrete(Bhuiyan et al., 2021).

1.3.2.4. Linear or circular prestressing

This classification is based on the shape of the prestressed member. When the prestressed members are straight or flat, in the direction of prestressing, the prestressing is called linear prestressing. For example, the prestressing of beams, piles, poles and slabs. The prestressing cable profile maybe curved and when the prestressed members are curved, in the direction of prestressing, the prestressing is called circular p restressing. For example, Circumferential prestressing of tanks, silos, pipes and similar structures (Bhuiyan et al., 2021).Figure 1.31 shows a tank illustrating clearly the concept of circumferential prestressing.

Figure 1.19. Prestressed storage tank (Bald et al., 1997).

1.3.2.5. Full, limited or partial prestressing

It's based on the amount of prestressing force. Full prestressing occurs when the level of prestress is so much so that no tensile stress is allowed in the concrete under service loading. When the level of prestress is such that the tensile stress under the service loads is within the cracking stress of the concrete, it is called Limited Prestressing and when the level of prestressing is such that under tensile stresses due to service loads, the crack width is within the allowable limit, it is called Partial prestressing (Choudhary & Akhtar, 2019). These three forms of prestressing are represented in 3 curves as illustrated in Figure 1.32.

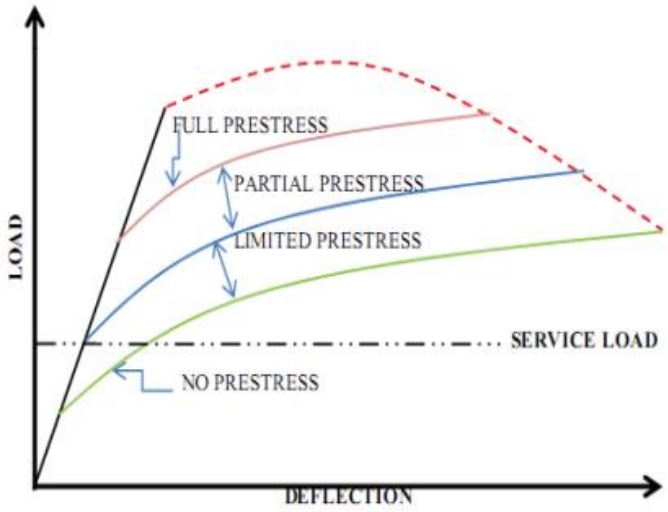

Figure 1.20. Prestressing zones (Choudhary & Akhtar, 2019)**.**

1.3.2.6. Uniaxial, biaxial or multiaxial prestressing

As the name suggest, this prestressing form is on the direction to which the member is prestressed. When the prestressing cables are parallel to one axis, it is called uniaxial prestressing. For example; Longitudinal prestressing of beams. When there are stressing cables parallel to two

axes, it is called biaxial prestressing. For example; Biaxial prestressing of slabs. When the prestressing force is parallel to more than two axes, it is called multiaxial prestressing. For example, prestressing domes (Menn, 1990).

1.3.3. Prestressing stages.

1.3.3.1. Stages of pre-tensioning

Here, the tension is first applied to the members and the concrete is cast. The various stages of the pre-tensioning operation are summarized as follows; anchoring the tendons at ends of the abutments, placing of jacks, applying tension to the tendons, casting of the concrete, curing of the concrete, cutting of the tendons. After cutting of tendons, transfer of prestress occurs with elastic shortening and camber. These stages are shown schematically in the following figures. Pre-tensioning is advantageous in that it is suitable for precast members produced in bulk and does not require large anchorage devices. But some of its limitations are that it requires a pre-tensioning bed, and requires a good bond between concrete and steel over the transmission length. These stages are best illustrated in Figure 1.33.

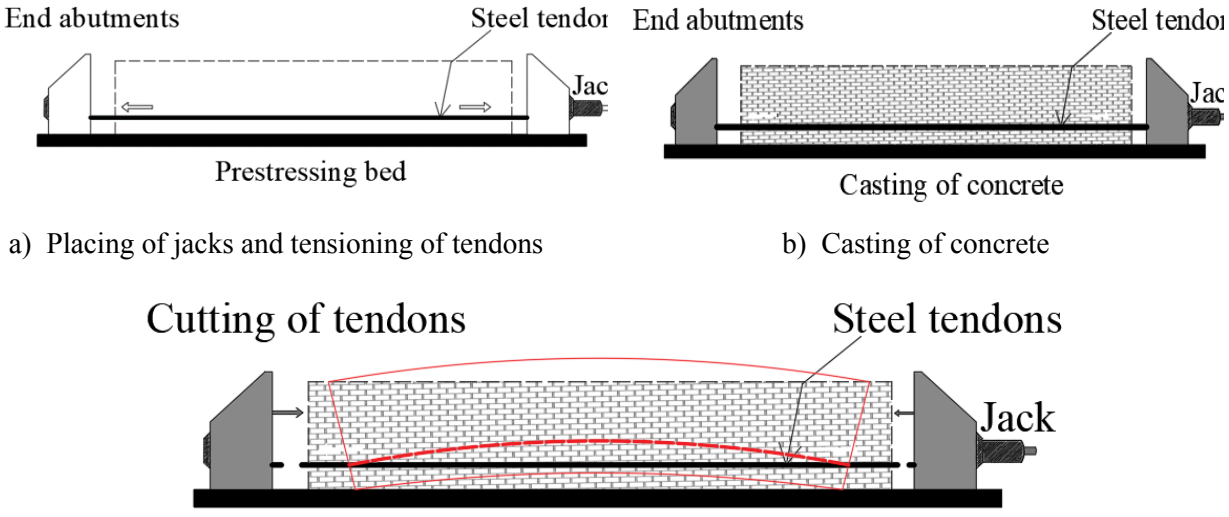

a) Placing of jacks and tensioning of tendons

b) Casting of concrete

c) Transferring of prestress

Figure 1.21. Stages of pre-tensioning.

1.3.3.2. Stages of post-tensioning

Here the tension is applied after the hardening of the concrete. The tendons are placed in ducts after the casting of the concrete. If the ducts are grouted, then it is known as bonded post-tensioning. Post-tensioning is advantageous in that it is suitable for heavy cast in place members, the waiting period is less and the transfer of the prestress depends on the transmission length. The relative disadvantage of posttensioning as compared to pre-tensioning is the requirement of

anchorage devices and grouting equipment. Stages of the posttensioning operation include; casting of concrete, placement of tendons, placement of the anchorage block and jack, applying tension to the tendons, seating of the wedges, cutting of the tendons. The stages are shown schematically in Figure 1.34.

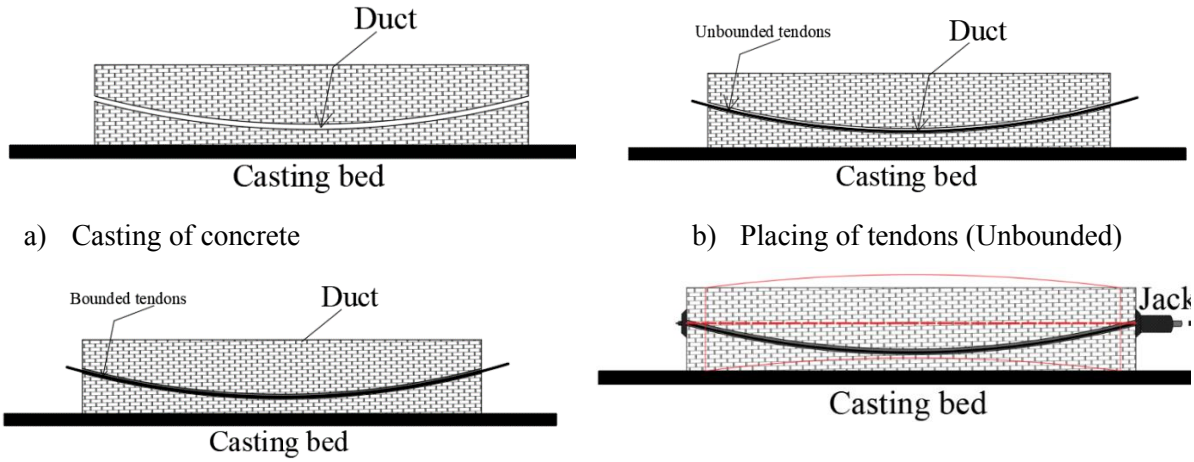

a) Casting of concrete

b) Placing of tendons (Unbounded)

c) Placing tendons (bounded)

d) Transferring of ¨Prestress

Figure 1.22. Stages of posttensioning.

1.4. Prestress losses

Prestress losses are defined as the reduction in the tensile stress in prestressing tendons. They are categorized as either instantaneous losses or long-term losses. Instantaneous losses include frictional losses, elastic shortening (ES) and seating loss or anchorage slip. Long term losses occur over a period of time. They include losses in prestress due to concrete creep (CR), shrinkage (SH) and relaxation of prestressing strands (RE). The generalized variation of stress over time is due to the various losses illustrated in Figure 1.35.

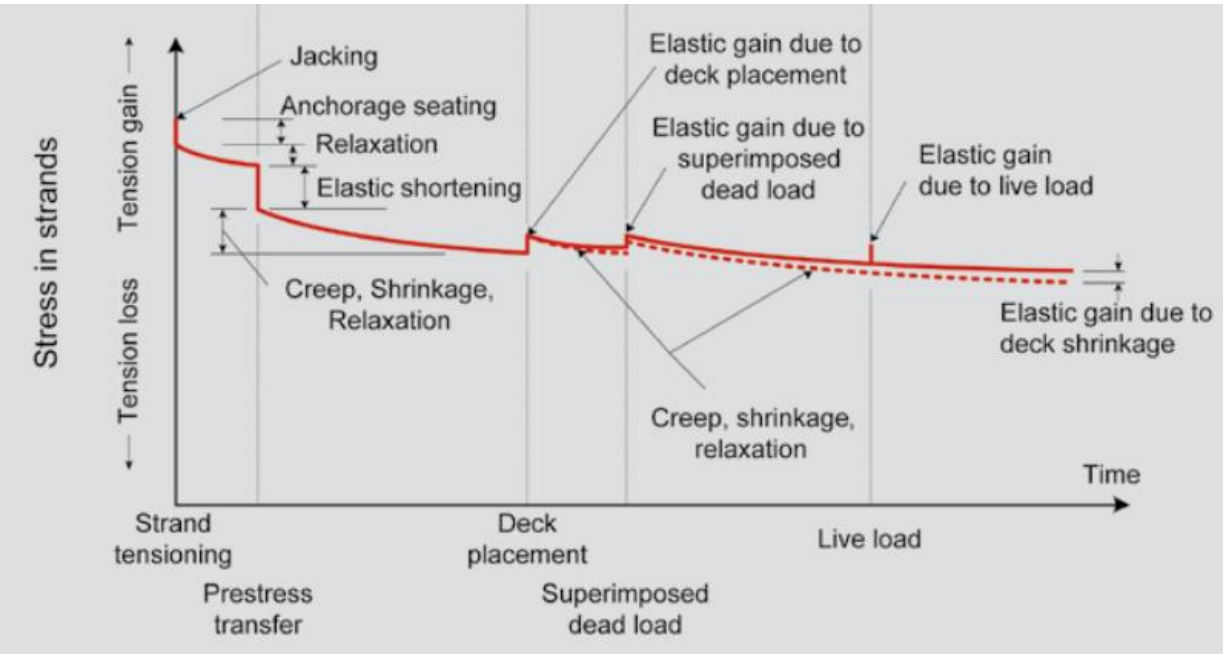

Figure 1.23. Schematic summary of prestress losses with time(HÖKELEKLİ, 2016).

1.4.1. Background

Numerous studies have shown that the current models tend to over-predict the long termtime dependent losses and hence the camber and deflection in prestress beams(reference). The ACI-ASCE Joint Committee 423 (1958) proposed the lump sum prestress loss estimates. These losses included the effects of creep, shrinkage and relaxation, but excluded the frictional and anchorage losses. The further refinement of losses led to the development of the PCI Committee recommendations (1975), the AASHTO-LRFD method (1977) and the ACI-ASCE Committee recommendations (1979). These methods for the calculation of losses failed to acknowledge the variability of material properties of concrete which then led to either overestimation or underestimation of losses [Shenoy and Frantz (1991), (Gruel, et.al, (2000), NCHRP Report 496 (2003), Hale and Russell (2006)]. The National Cooperative Highway Research Program [NCHRP Report 496 (October2003)] investigated the measurement of material properties (elastic modulus, concrete strength, volume to surface ratio and creep coefficient) and their effect on measured prestress losses and deflections. The experimental research programs performed on prestressed concrete bridge girders by Tadros et al (2001), Miller et al (2000), Pessikiet al (1996), Hale and Russell (1996) verified that the PCI Design Handbook method, ACI 318 and AASHTO-LRFD equations overestimated the prestress losses. it was concluded that accurate determination of losses was mandatory for the exact prediction of camber and deflection (Jayaseelan, 2019).

Figure 1.36 shows the collapse of a prestressed viaduct due to excess deflection. This is as a result of under estimation of prestress losses.

Figure 1.24. Damage and collapse of the Petrulla Viaduct(Anania et al., 2018).

1.4.2. Types and causes of prestress losses

The jacking force acting on the prestressed concrete fails to transmit all the forces to the concrete due to the instantaneous loss and the time dependent loss that occurs during the construction stage. Additionally, the neutral axis changes as the cross-section changes due to concrete placement according to the construction stage, and as the distance between the tendon and the neutral axis of the cross-section changes, the stress value applied to the member varies. For this reason, it is necessary to reflect the tendon force at each stage in the design through the construction stage analysis. Figure 1.37 illustrates these causes.

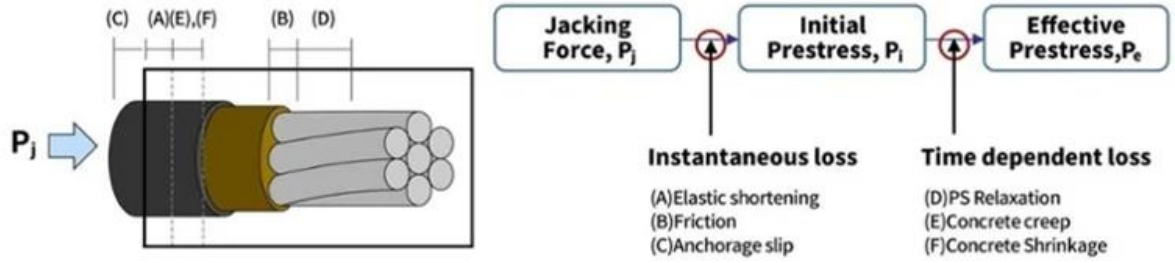

Figure 1.25. Concept diagram of jacking force due to loss(S. T. Kim et al., 2017).

Transfer of prestress refers to tensioning of a prestressing tendon, which causes compressive forces to act on the concrete as a reaction to the jacking force. As shown in the figure above, this force, which is reduced due to the instantaneous loss, acts on the concrete as initial prestress.

After the prestress is transferred into the concrete, the initial prestress decreases due to the time dependent loss. This reduced forced is called the effective prestress. Loss in prestressing force comprises two major time components: short-term losses, which occur immediately after the transfer of prestressing force and long-term losses, which occur due to time-dependent material properties (Kim et al., 2022)

1.4.2.1. Instantaneous losses

These are losses which occur after the transfer of the prestress forces

- Loss due to elastic shortening: When prestress is transferred into concrete, the concrete is compressed and shortens due to elastic shortening. At this time the tendon also shortened, resulting in losses and which is called elastic shortening loss.
- Loss due to friction: The loss due to friction is a loss caused by frictional action that occurs when the stretched tendon contacts the sheaths during the post-tensioning method. The friction loss can be divided into the loss of curvature friction due to the curvature effect of the tendon and the loss of wobble friction due to the effect of the tendon's length. Figure 1.38 illustrates these two effects.

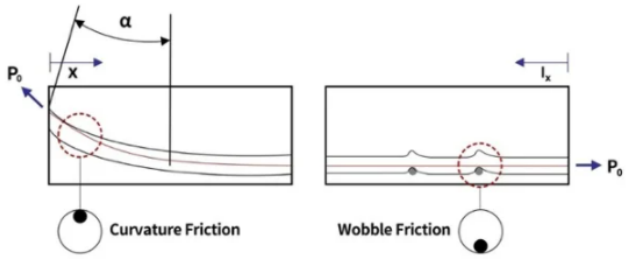

Figure 1.26. Friction in post-tensioning system(Kim et al., 2017).

- Loss due to anchorage slip: As the tendon stretched by jacking is anchored to the anchorage, the anchorage system may be slightly pushed or moved. After this process, the tendon that had been stretched shortens and prestress is lost. The length of the anchorage slip varies depending on the type of anchorage, but loss is generally calculated by assuming anchorage slip at 6mm. Figure 1.39 illustrates this more clearly.

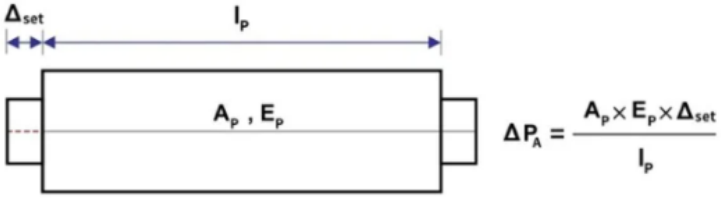

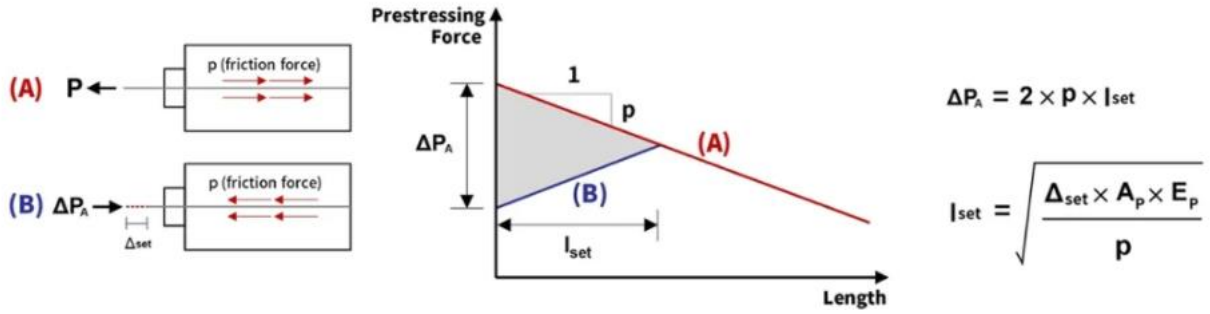

Figure 1.27. Prestress Loss due to anchorage in the presence of friction force(Kim et al., 2017).

When tendon is tensioned, a frictional force is generated from the inside to the right, so the prestress force decreases as shown in (A). Removing the prestressing jack causes the tendon to settle in the anchorage, causing slip, and a frictional force to the left. This causes prestress loss. As distance from the anchorage zone increases, the frictional force decreases. Thus, the loss is reduced like the in Figure 1.39.

1.4.2.2. Time dependent losses

The relaxation of prestressing steel interacts with the creep of concrete and is influenced by the shrinkage of concrete. It is difficult to accurately predict long-term losses because variability in material properties must be considered. Due to these problems, many design standards propose approximate solutions to estimate long-term losses by empirical research.

- Loss due to tendon relaxation

A phenomenon in which tensile stress decreases over time when the prestressing steel is maintained at a constant length under tension. This phenomenon increases as the temperature increases and the stress increases. Therefore, for prestressing steel subjected to very high levels of tensile stress, the prestress decreases more due to relaxation. Relaxation is divided into pure relaxation and apparent relaxation. Pure relaxation is the amount of decrease in tensile stress that occurs when the strain is constant, and is expressed as a percentage of the initially applied tensile stress while apparent relaxation occurs when the relaxation behaviour is changed due to the influence of concrete (creep, shrinkage), and the strain of tendon is not kept constant and decreases.

- Loss due to concrete creep:

The compressive stress caused by the concrete creep induces a shortening strain in the concrete which leads to loss of prestressing force in tendons. Two types of creep can be distinguished: Basic creep (Constant deformation of structural element subjected to a sustained load with no

loss of moisture to the surrounding) and drying creep (Long-term shortening occurring in a specimen constantly exposed to the environment).

- Loss due to concrete shrinkage:

The free water is gradually lost from the concrete as a result of concrete shrinkage, which creates a shortening in the concrete producing losses in the prestressing force

1.4.3. Loss occurrence order according to the transfer of prestress method

1.4.3.1. Pre-tensioning method

In the pre-tensioning method, the loss of prestress occurs at the jacking stage, the transfer of prestress stage, and the sustained loading stage. In the process of tensioning the tendons and anchored at the buttress, loss due to anchorage slip occurs and loss due to the initial relaxation begins. When prestress is transferred after the concrete hardens, loss due to elastic shortening occurs. When load is applied after completion of the construction, loss due to creep and shrinkage, and loss due to relaxation occur over time. Lastly, after time dependent loss occurs, the initial prestress state of the tendon becomes the effective prestress state.

- Elastic shortening occurs when there is a reduction in strain in the prestressing strands at the transfer of prestress due to the concrete member shortening.
- Anchorage seating is the movement of prestressing steel when it is allowed to rest in the anchorage, which leads to a loss of stress in the tendon.
- Relaxation of prestressing steel occurs due to the loss in tension in a prestressing strand with respect to time when it is held at a constant length.

The loss of prestress in pretensioned members is explained with Figure 1.40.

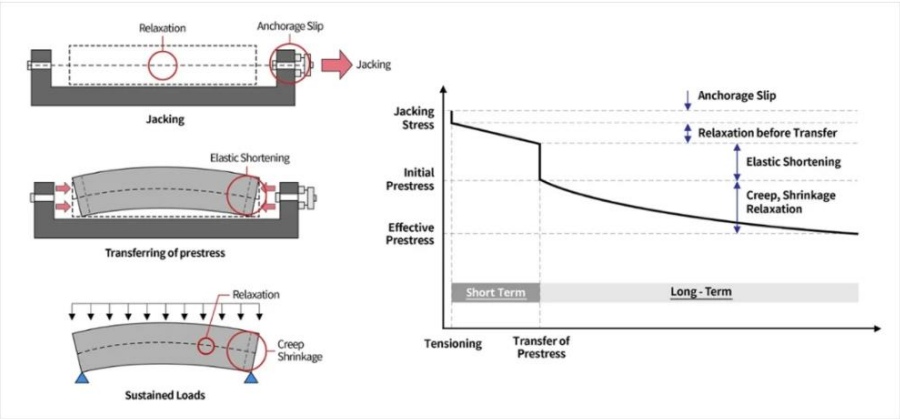

Figure 1.28. Prestress losses due to pre-tensioning (Kim et al., 2017).

1.4.3.2. Posttensioning method

In the posttensioning method, the loss of prestress occurs at the transfer of prestress stage and the sustained loading stage. When the tendons are tensioned on the hardened concrete where the sheaths are arranged, loss due to elastic shortening and loss due to friction occur at the same time. Furthermore, when the prestressing jack is removed, the prestressing tendon settles, resulting in loss due to anchorage slip. These three losses occur almost simultaneously in the process of transfer of prestress. Additionally, just as in the pre-tensioning method, time dependent losses occur under the sustained load state, ultimately becoming an effective prestress state. The loss due to friction occurs only in the post-tensioning method using sheaths. The loss of prestress in post tensioned members is explained with Figure 1.40.

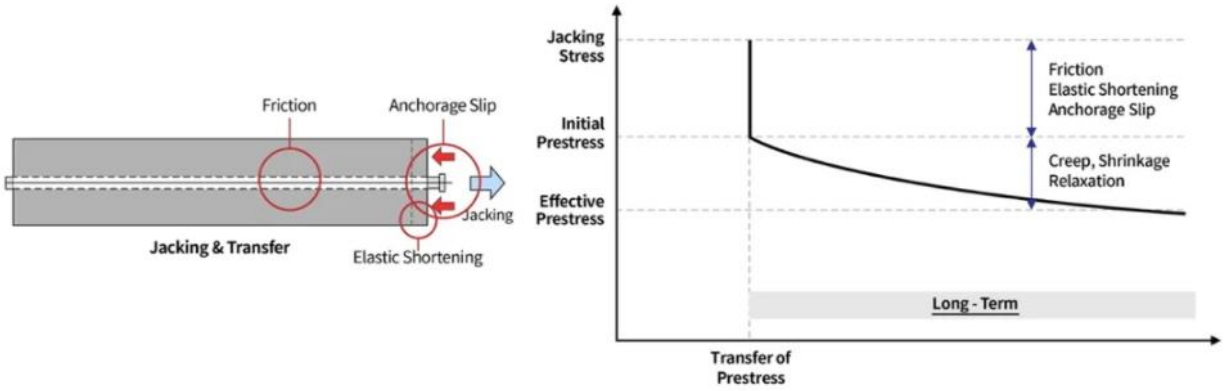

Figure 1.29. Prestress losses in post-tensioning (Kim et al., 2017).

1.4.4. Prestress losses estimation methods

1.4.4.1. PCI Design Handbook (2010)

This Handbook provides a method for approximating the prestress losses. It is refined method in that the stress changes due to each loss source are calculated separately. The total losses are estimated by adding the effects from elastic shortening, creep, shrinkage, and relaxation. The anchorage seating losses and the friction losses, when applicable, also need to be considered. This method was developed on an approximate value of basic ultimate shrinkage strain (ε_{sh}) for concrete of -550 x 10^{-6} and an ambient relative humidity correction factor of 1.5-0.0015RH

$$TL = ES + CR + SH + RE \quad \textbf{(1.10)}$$

- Loss due to elastic shortening (ES):

$$ES = K_{cr}\frac{E_s}{E_c}f_{cir} \quad \textbf{(1.11)}$$

- Loss due to creepage (CR):

$$\text{CR} = K_{cr}\frac{E_{ps}}{E_s}(f_{cir} - f_{cds}) \quad \textbf{(1.12)}$$

- Loss due to shrinkage (SH): **(1.13)**

$$\text{SH} = (8x10^{-6})\,K_{sh}E_{ps}\left(1 - \frac{0.06V}{S}\right)(100 - RH)$$

The equation was developed on an approximate value of basic ultimate shrinkage strain (ε_{sh}) for concrete for concrete of -550 x 10^{-6} and an ambient relative humidity correction factor of 1.5-0.0015RH

- Loss due to relaxation of tendons (RE):

$$\text{RE} = [K_{re} - J(SH + CR + ES)]C \quad \textbf{(1.14)}$$

The values of K_{re} and J depends on the stress level and the material characteristics of the tendon as shown in Table 1.3.

Table 1.3. Values of K_{re} and J (Raymond I. G., Neil C. M., 2017).

Type of Tendon	Kre	J
Grade 270 stress-relieved strand or wire	20,000	0.15
Grade 270 low-relaxation strand or wire	5,000	0.04
Grade 145 or 160 stress-relieved bar	6,000	0.05

The effective stress at the level of the prestressing strands is calculated as below;

$$f_{se} = f_{pi} - \text{TL} \quad \textbf{(1.15)}$$

Where; f_{pi} is the initial prestress at the time of loading. This method is limited for maximum values of prestress losses.

1.4.4.2. AASHTO-LRFD Time step method (2017)

This time step method was developed by modulating the AASHTO LRFD refined equations to accommodate the time dependent creep effects. It presents a refined method that splits the loss calculation into two stages: before and after casting the deck. The losses are calculated individually and then added together. where the elastic shortening, friction and anchorage losses have to be previously determined when applicable. This method is based on the following assumptions:

- Spans not greater than 76.2m

- Normal density concrete,
- Strength in excess of 24.13 MPa at the time of the prestress.
- Loss due to friction

AASHTO (2012) divides the time-dependent loss calculation equations into two intervals: between transfer and deck placement, and between deck placement and final time.

This method of estimating losses is fully developed in the methodology of this study.

1.4.4.3. AASHTO-LRFD Approximate lump sum estimates of time dependent losses

Table 1.4 specifies the approximate lump sum estimates of time-dependent losses resulting from creep, shrinkage of concrete, relaxation of steel in prestressed, partially prestressed members. It is applicable if the concrete creep ranges from 1.6 to 2.4, the Ultimate shrinkage coefficient ranges from 0.004 to 0.006, the ambient relative humidity ranges from 40 to 100 percent and the partial prestressing ratio should range from 0.2 to 1. This method reflects the values and trends obtained from a computerized time-step analysis of a large number of bridges (Jayaseelan, 2019).

- Pretensioned members are stressed after attaining a compressive strength of 3.5 f_{ci},
- Members are made from normal weight concrete,
- The concrete is either steam or moist-cured,
- Prestressing is by bars or strands with normal and low relaxation properties, and
- The exposure and temperature conditions are average.
- The PPR ration should range between 0.2 and 1.

Table 1.4 gives an illustration of how the time dependent losses are calculated with the AASHTO LRFD-Lump sump method.

Table 1.4. AASHTO LRFD-Lump sump estimates of time dependent losses(Jayaseelan, 2019).

Type of Beam Section	Level	For wire and strands with fpu=235,250 or 270 ksi	For Bars with fpu=145 or 160ksi
Rectangular Beams, Solid Slab	Upper	29+4 PPR	19+6 PPR
	Bound		
	Average	26+4 PPR	
Box Girder	Upper	21+4 PPR	15
	Bound		
	Average	19+4 PPR	
I-Grirder	Average	33[1-0.15(fc-6)/6]+6PPR	19+6 PPR
Single T,Double T, Hollow Core and Voided Slab	Upper	39[1-0.15(fc-6)/6]+6PPR	31[1-0.15(fc-6)/6]+6PPR
	Bound		
	Average	33[1-0.15(fc-6)/6]+6PPR	

Where PPR, the partial prestressing ratio is given by

$$PPR = {A_{ps}f_{py}}\Big/{\left(A_{ps}f_{py} + A_s f_y\right)} \tag{1.16}$$

1.4.4.4. NCHRP 496 Detailed prestress losses [Tadros et al (2003)]

This method makes use of aging coefficient approach for the computation of losses between transfer and casting of decks. The prestress losses are computed in four stages:

- Instantaneous prestress loss due to elastic shortening at transfer.
- Long-term prestress losses due to shrinkage of concrete, and creep of concrete, and relaxation of prestressing strands, between the time of transfer and just before deck placement.
- Instantaneous prestress gains due to the placement of deck weight.
- Long-term prestress losses between the time of deck placement and the final service life of the structure, due to shrinkage of the girder, creep of the girder, relaxation of prestressing strands, and shrinkage of deck concrete.

The long-term prestress losses due to shrinkage, creep, and relaxation (for the time between transfer and placement of the deck slab) are determined in three different stages. The net section properties of the non-composite section are used for the calculation of the prestress losses. The long-term prestress losses between the time of the deck placement and the final stage are determined in five stages: the shrinkage, creep of concrete, relaxation of prestressing strands, concrete deck shrinkage between the time of deck placement and the final service life of the structure (Jayaseelan, 2019).

- Loss due to elastic shortening

$$\Delta f_{pES} = n_i f_{cgp} \tag{1.17}$$

- Loss due to shrinkage

$$\Delta f_{pCR} = \varepsilon_{bid} E_p K_{id} \tag{1.18}$$

  Loss due to creep is given by

$$\Delta f_{pSR} = n_i f_{cgp} \psi_{bid} K_{id} \tag{1.19}$$

- Loss due to relaxation of prestressing strands $\Delta f_{pR2} = \emptyset_i L_i K_{id}$

$$\Delta f_{pSR} = n_i f_{cgp} \psi_{bid} K_{id} \tag{1.20}$$

- The total prestress loss is given by

$$TL = \Delta f_{pES} + \Delta f_{pCR} + \Delta f_{pSR} + \Delta f_{pR2} \quad \textbf{(1.21)}$$

1.4.4.5. Swartz (2010)

Swartz (2010) presented two methods for calculating prestress losses. One is a time-step method, and the other one is called the "Direct Method," which was developed as a simplification of the AASHTO (2012) refined method. Swartz (2010) explained that the main idea behind this time-step method is to discretize the element into several horizontal layers, and that a prestress loss approximation can be found by knowing the strain distribution at each step. At every interval, the strains are calculated by accounting for creep, shrinkage and relaxation, and the elastic response due to the loads applied. The first step in this method is to calculate the stress at each level of the discretized member. The second step is to calculate the creep strains at each element. Third, the shrinkage strain is calculated and added to the creep strain, giving the total inelastic strain. The fourth step is to get the constants that will be used to solve a system of equations to be defined later, along with the axial forces and effective moments experienced due to internal stresses. Finally, the total and elastic strains along with the elastic stress increase at each level are calculated. From the strain and curvature found from the system of equations, the strain at the level of the prestressing steel is found, then transformed to stress in the steel.

The first step in this method is to calculate the stress at each level of the discretized member. This stress will be zero in the first-time step, while in the following steps it will be the stress found at the end of the preceding interval. The second step is to calculate the creep strains at each element, by subtracting the elastic strain, from the total strain. Third, the shrinkage strain is calculated and added to the creep strain, giving the total inelastic strain. The creep coefficient and the shrinkage strain are obtained using the equations from AAHSTO (2012) previously explained. (Jayaseelan, 2019).

The total strain is given by

$$\varepsilon_{Tk}(t_i) = \sum_{j=1}^{i-1} \Delta\sigma(t_j)\left[\frac{1}{E_c(t_j)} + \frac{\psi(t_i, t_j)}{E_c(t_j)}\right] \quad \textbf{(1.22)}$$

The elastic strain

$$\varepsilon_{kelastic} = \frac{\sigma_{kelastic}}{E_c} \quad \textbf{(1.23)}$$

The creep strain at each element is given by

$$\varepsilon_{cr} = \varepsilon_{cr} - \varepsilon_e - \varepsilon_{sh} \quad \textbf{(1.24)}$$

Total inelastic strain

$$\varepsilon_l = \varepsilon_{sh} + \varepsilon_e \quad \textbf{(1.25)}$$

The fourth step is to get the constants that will be used to solve a system of equations to be defined later, along with the axial forces and effective moments experienced due to internal stresses. After all these constants and parameters have been found, the system of equations is solved simultaneously by simplifying with matrix solutions. Finally, the total and elastic strains along with the elastic stress and stress increase at each level are calculated. From the strain and curvature found from the system of equations, the strain at the level of the prestressing steel is found, then transformed to stress in the steel.

The total strain

$$\varepsilon_{Ktotal} = \varepsilon_o - y_k \Phi \quad \textbf{(1.26)}$$

The elastic strain

$$\varepsilon_{Kelastic} = \varepsilon_{Ktotal} - \varepsilon_{sh} - \varepsilon_{cr} - \varepsilon_{od} \quad \textbf{(1.27)}$$

The stress changes

$$\Delta\sigma = \sigma_{kelastic}(t_i) - \sigma_{kelastic}(t_{i-1}) \quad \textbf{(1.28)}$$

Strain in the prestressing steel

$$\varepsilon_s = \varepsilon_o - y_k \Phi - \varepsilon_j' \quad \textbf{(1.29)}$$

The elastic stress

$$\sigma_s = \varepsilon_s E_p \quad \textbf{(1.30)}$$

All the explained steps are to be repeated for the number of intervals the designer decides to use. The total losses can be found by getting the difference between the initial stress at jacking and the stress in the prestressing steel at the final time step.

1.4.4.6. European Norm 1992-1-1:2004

The EN 1992-1-1:2004 provides a simplified method for calculating prestress losses. For long term losses, one formula is used which takes into account all the losses which are time dependent. As a result, this method is very easy to use. In this method, the modulus of elasticity is estimated from the concrete compressive strength and therefore a change in the concrete compressive strength will also change the modulus of elasticity. It's generally applicable for normal weight concrete and is applicable if the concrete creep ranges from 1.6 to 4.2, the Ultimate shrinkage coefficient ranges from 0.004 to 0.008, the ambient relative humidity ranges from 20 to 100 percent and the partial prestressing ratio should range from 0.2 to 1. It does not separate the different losses and makes use of the time dependent correction factors and the equations for the prediction of losses (Raymond I. G., Neil C. M., 2017).

1.4.5. Evaluation of methods to estimate losses

The following evaluations were done for each prestress loss calculation method:

1.4.5.1. PCI Design Handbook (2010)

The method for calculating losses explained in the PCI Design Handbook (2010) is a simple process that, unlike the lump-sum methods, still separates the contributions from each source of loss. This Handbook fails to mention any important limitation to the procedure that other design methods usually specify, such as the maximum compressive strength to which it can be applied. This is the only method that does not use an age-adjusted modulus of elasticity approach. This is because this method only provides an estimate of the losses for the end of the service life, and it does not separate the process into stag.es, such as before and after deck placement as the AASHTO (2012) refined method does. Principally it's owed to the application often to building type pretensioned members (Jayaseelan, 2019).

1.4.5.2. AASHTO-LRFD Time step method (2012)

This method allows understanding the behaviour before and after casting the deck, and can be used in calculating losses for any pretensioned member, not just bridge girders. This method is only used for normal weight concrete. Another issue regarding the AASHTO (2012) refined method is its complexity. Compared to its previous version from the 2004 AASHTO Specifications, the current refined method requires a large number of steps and calculations (Garber, 2014). This method is divided into two stages considering three main events: release, deck casting, and ultimate life. Although it is true that using this method in the estimation of losses involves a lot of steps, the process becomes easier to understand and apply once an example is seen. In addition, it might be desired in some cases to know the losses before and after

the deck is cast, including the shrinkage gain due to the deck placement. Finally, if a more detailed analysis is needed, a time-step method should be used. This method tends to overestimate creep effects because it does not consider the reduction in the creep coefficient associated with the increase in concrete strength (Menn, 1990).

- The AASHTO Time Step method takes into account the incremental increase in creep and calculates the losses and camber on a day-to-day basis.
- The AASHTO Time Step method takes into account the variability in material properties and is formulated for high performance concrete when compared to the AASHTO LFRD refined method.
- This method accommodates the use of effective modulus which combines the effects due to elastic strain and creep of concrete as an elastic deformation on the concrete section.

1.4.5.3. AASHTO-LRFD Approximate lump sum estimates of time dependent losses.

This method was developed based on the prevailing AASHTO LRFD time dependent coefficients for the determination of prestress losses and deflection in prestressed concrete bridges. It does not separate the different losses and makes use of the AASHTO LRFD time dependent correction factors and the equations for the prediction of losses. Prestress losses, the camber and deflection of the girder have been determined on a day-to-day basis from a time period of t = 1 day to t = 10,000 days. Bridges are designed for the range of variables a specified below; This method shows a better agreement with test results than the Refined method, because it accounts for the variability of the loss with concrete strength (Jayaseelan, 2019).

1.4.5.4. NCHRP 496 Detailed prestress losses

This method takes into account the variability of material properties which influences the creep and shrinkage coefficient of the curing concrete. The reported literature [Hale and Russell (2006)] showed that the NCHRP 496 method predicted losses within 18% of the measured losses. This method produces better estimates of long-term prestress losses than those obtained by the AASHTO-LRFD Lump-Sum method because it does takes into account the level of prestressing or ambient relative humidity. It is applicable for non-composite members, composite precast girders, and high-strength concrete (Jayaseelan, 2019).

1.4.5.5. Swartz (2010)

The derivation of this method was based in the assumption that a perfect bond between the concrete and the strands exist. It uses an age-adjusted modulus of elasticity when calculating the total strain at each interval. However, it does not use the transformed or composite section properties accounting for this varying modulus of elasticity. Also, the method separates the

section into several horizontal layers. This process may be tedious because one must decide how many layers to use, and calculate each of their areas and distances from the top of the deck. Furthermore, this method can be harder to follow along and understand since it uses constants and solves simultaneous equations using matrices. As mentioned in the PCI-BDM (2003) discussion in Section 3.1.3, it is also recommended that this method is not used by hand calculations and it should be automated. The assumptions used for this method include constant stresses per time step, uniform shrinkage through the section, and plane sections remain plane. This method is only applicable for bonded prestressing steel since one assumption calls for a perfect bond between the steel and the concrete so that strain compatibility could be applied. Another assumption was creep superposition (Jayaseelan, 2019).

1.4.6. Comparison between the different methods of estimating prestress losses

The following comparisons were done between the various loss prediction methods:

1.4.6.1. Comparison of prestress losses between AASHTO time step and NCHRP 496 detailed method.

Figure 1.42 shown below compares the prestress losses at mid span predicted using the AASHTO Time Step method and the NCHRP 496 method. Prestress losses have been compared for two loading stages: prior to slab casting at 90 days and after 10 years. The results show that both the methods almost predict the same losses at loading stage of 90days. The long-term losses predicted using proposed method and the NCHRP 496 method were 246.08 and 229.73 MPa. Both the AASHTO Time Step and the NCHRP 496 detailed method take into account the variability of material properties which influences the creep and shrinkage coefficient of the curing concrete (Jayaseelan, 2019). The comparison between these two methods using a bar chart is illustrated in Figure 1.42.

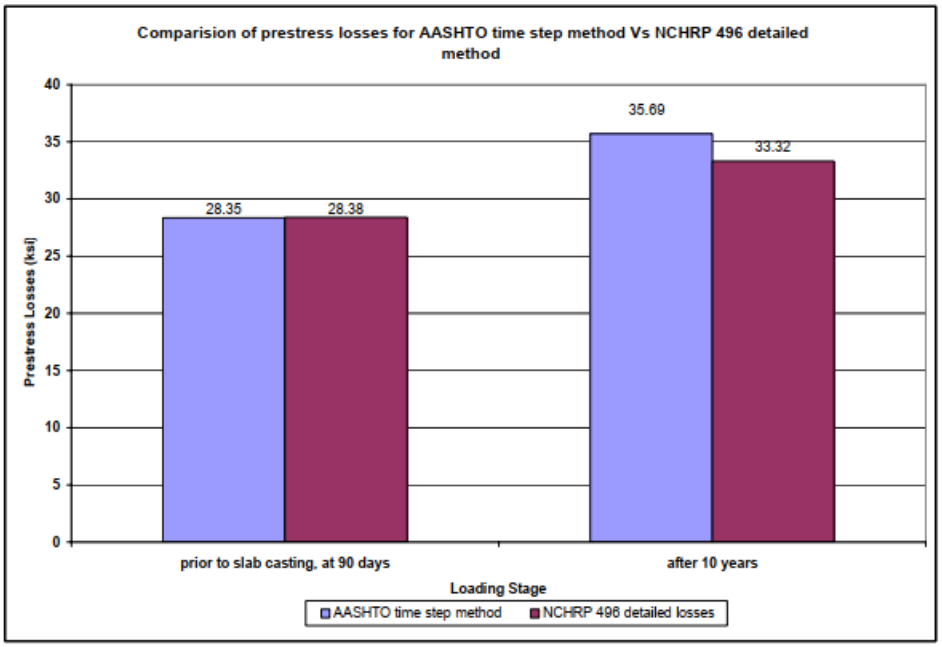

Figure 1.30. Plot showing the comparison of prestress losses at mid span using the AASHTO time step and NCHRP 496 detailed method for two stages of loading.(Jayaseelan, 2019).

1.4.6.2. Comparison of prestress losses between AASHTO Time step and AASHTO refined method.

Figure 1.43 shows that the AASHTO Time Step method predicts long term losses of about 1% lower than that predicted using the AASHTO LRFD method. The AASHTOLRFD refined method estimates long term losses and is formulated using the normal concrete strength. However, the AASHTO Time Step method takes into account the additional factors such as the age of concrete and the change in material properties and loading and calculates the creep coefficient on a day-to-day basis. In comparison to the AASHTO LRFD refined method, the Time Step method takes into consideration the reduction in creep coefficient associated with the increase in concrete strength (Jayaseelan, 2019). The comparison between these two methods using a bar chart is illustrated in Figure 1.43.

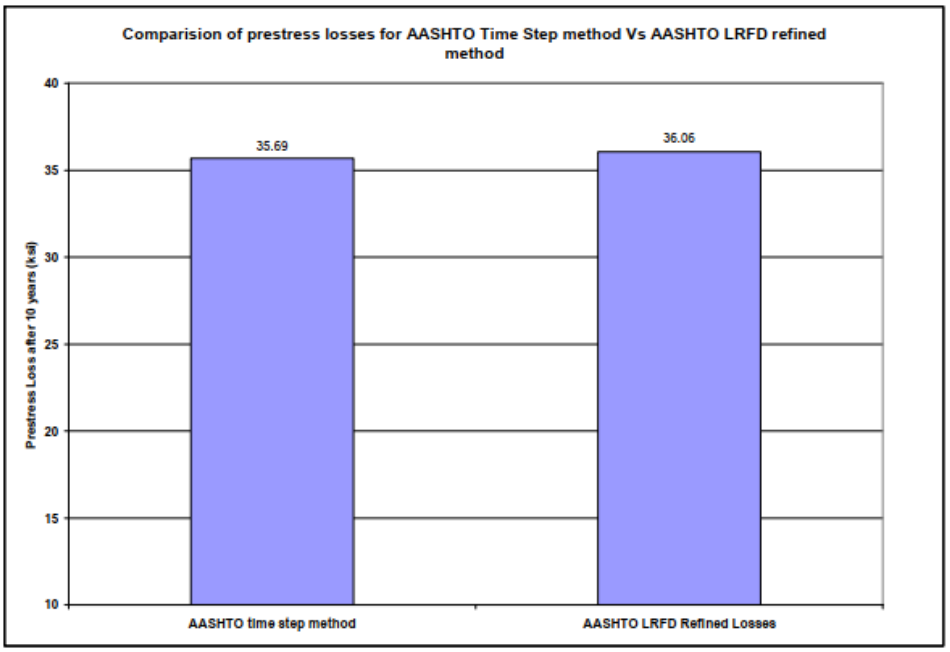

Figure 1.31. Plot showing the comparison of long-term prestress losses at mid span using the AASHTO Time step and AASHTO LRFD refined method.(Jayaseelan, 2019).

1.4.6.3. Comparison of losses between AASHTO Time step and PCI Design Handbook method.

Figures 1.44 compares the losses predicted using the AASHTO Time Step and the PCI (Zia. et al., 2017) method. The total losses at the final stage are about 55.16 MPa more than the PCI losses. The PCI Design Handbook method (Zia. et al., 2017) method assumes an ultimate creep coefficient of 2.0 for the both the stress due to prestress loads and all the super imposed dead loads. Due to this fact, the PCI Design Handbook method over estimates the losses for the loading stage prior to slab casting. The results prove that the proposed AASHTO Time Step method predicts more improved losses than the PCI Design Handbook method for intermediate loading stages. The comparison between these two methods using a bar chart is illustrated in Figure 1.44.

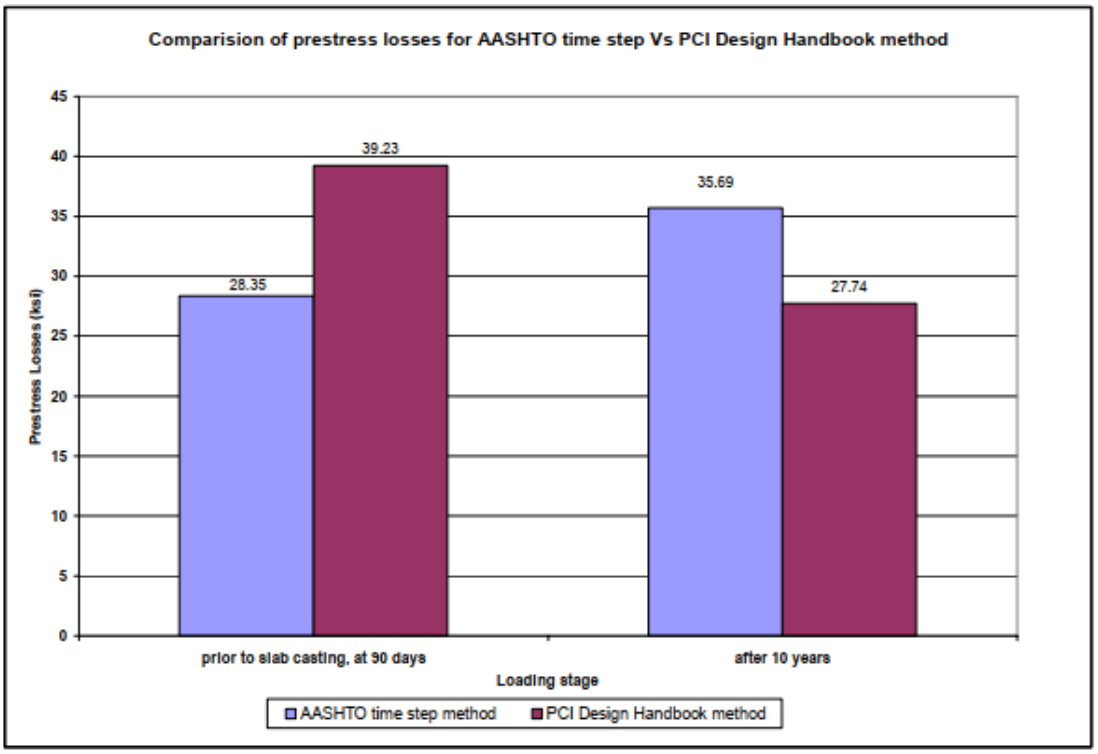

Figure 1.32. Plot showing the comparison of final prestress losses at mid span using the AASHTO Time step and PCI method.(Jayaseelan, 2019).

1.5. Analysis and design programs

Many software are used worldwide for prestress loss calculations and member verification. Among these software, Midas Civil revealed itself among the best because of the various analysis types it is capable of carrying out and Microsoft Excel is best for structural verifications.

1.5.1. Midas Civil 2022 v1.2

MIDAS Civil is a Bridge Design & Analysis software bases on the FEM analysis that combines powerful pre-and post-processing features with an extremely fast solver, which makes bridge modelling and analysis simple, quick, and effective. Also, there are several easy parameter modification tools available that can be used for parametric analysis leading to optimized and economical design.

1.5.1.1. Intuitive modelling

This software enables us to readily create nodes and elements as if drawings were drawn using the major functions of CAD programs. Powerful automatic modelling functions such as Auto Mesh Generation and various Bridge Wizards are introduced. The Bridge Wizards can create a complete bridge model for you in a blink of an eye and you are able to make any modification to

the model to match with the real structure as much as possible. Other modelling approaches such as CAD import, table format modelling, and code format modelling are also available.

1.5.2. Construction stage analysis approach

This analysis is crucial for this type of bridge where each temporal structure arrangement can lead to critical internal forces in specific members and the structure behaviour such as deflection and stress redistribution will continue to change during and after the construction due to time to time dependent material properties such as creep, shrinkage and tendon relaxation. This check is done in order to verify if the bridge is safe during the construction process.

1.5.2.1. Procedure for construction stage analysis

- After the creation of the structural model, the elements, loads and boundary conditions are created
- These elements, boundary and loads are grouped for activation and deactivation during the construction stage
- The time dependent material properties such as creep and shrinkage are then defined according to the standard AASHTO
- The defined time dependent material properties are linked to the general material properties through which the change of the concrete member material properties with time are automatically calculated and reflected
- Construction stages and time steps are then created considering the true sequence of construction
- The desired analysis condition is then defined and the analysis is carried out
- The results of the construction stage analysis and that of the complete structure analysis are then combined as necessary

1.5.2.2. Group activation and deactivation concept

In Midas Civil, four types of groups exist which can be activated or deactivated at any time of the construction process

- Structural groups
- Load groups
- Boundary groups
- Tendon groups

Elements can be activated at any age, with properties accounting for the passage of time. The partial or total force redistribution can be considered at deactivation stage. Loads can be activated

or deactivated at any time during the construction stage. Supports can be either deformed or at the original position of the nodes. Figure 1.45 explains this concept.

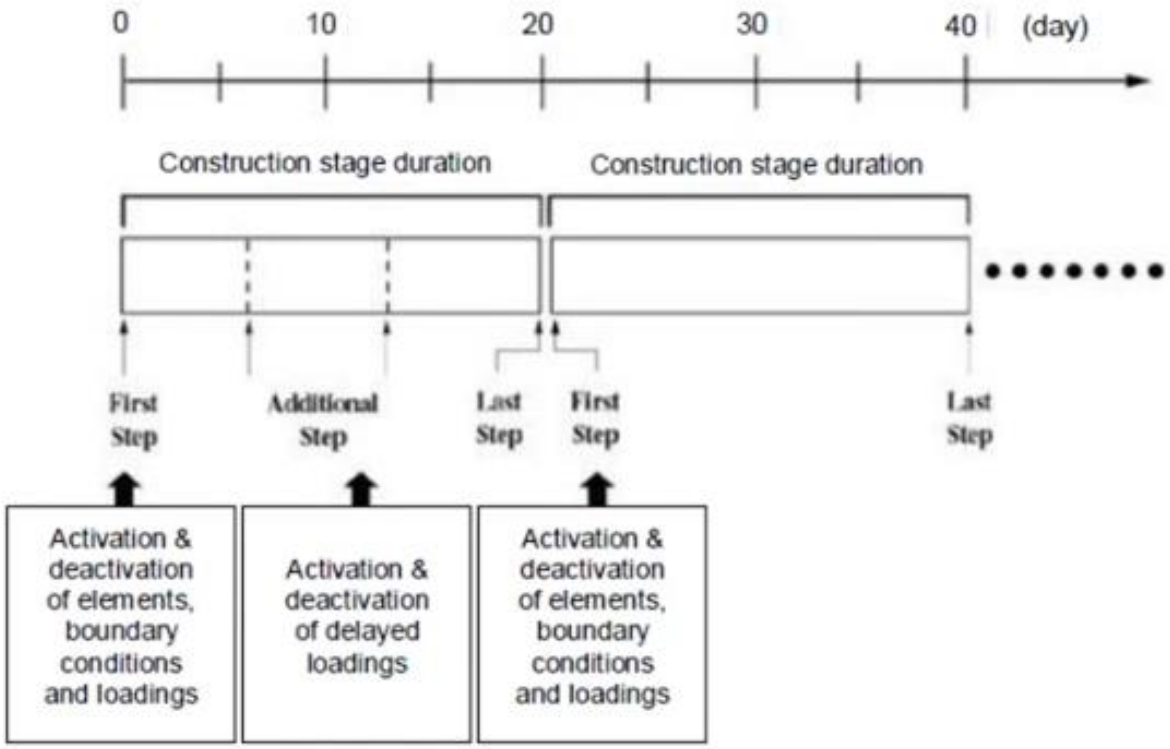

Figure 1.33. Definition of construction stages(Charbel et al., 2012).

1.5.2.3. Composite section for construction stage

With Midas Civil, one finite element with two different properties can be defined considering the pre-composite properties of the section and the composite properties of the section. These are easy to follow and the stage at which any of these properties should be considered can be chosen. Figure 1.46 shows a composite section for construction stage as presented by the software Midas Civil 2022 V1.2.

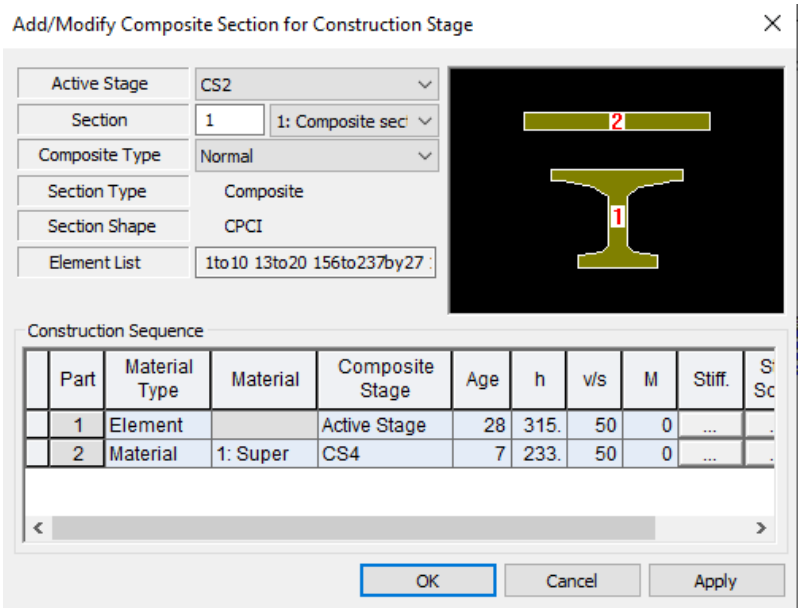

Figure 1.34. Pre-composite and composite sections(Charbel et al., 2012).

1.5.2.4. Powerful post processor

The post-processor can automatically create load combinations in accordance with specified design standards. Changing the type of display can produce various forms of graphic output. Practically all the results can be animated, namely, mode shapes, time history results of displacements and member forces, dynamic analysis results, and static analysis results. It also provides results that are compatible with MS Excel, which enables the user to review all analysis and design results systematically.

1.5.2.5. Auto design and load rating

Midas Civil has powerful design code checking and load rating features. AASHTO LRFD & LRFR, CHBDC CSA, EUROCODE, and other codes are available. The codes are constantly updated to make sure the users can best take advantage of the code checking and rating features in the program. The automatic report generation features give the users an organized and detailed report that includes formulas and code references and it gives the users the confidence in their result.

From a simple small 2D static analysis to a large complex 3D nonlinear dynamic analysis, Midas Civil is the easiest and most productive solution for the structural analysis and consequently for the evaluation of the losses in prestress over time.

1.5.3. Excel 2019

Microsoft Excel is the industry leading spreadsheet program, a powerful data visualization and analysis tool. It helps engineers to have a self-made calculator board for analysis and design of civil engineering programs.

1.6. Advantages and limitations of prestressing technology

The advantages and disadvantages of using prestressing technology are presented in this section.

1.6.1. Advantages of prestressing

The following are the advantages of using prestressing system

a) Section remains uncracked under service loading

There is a reduction of steel corrosion which implies an increase in durability, The full section is utilized which implies a higher moment of inertia (high stiffness) and less deformations (improved serviceability) and finally, there is an increase in shear capacity.

b) High span to depth ratio

Larger spans are possible with prestressing (no prestressed slab: 28:1 and Prestressed slab: 45:1), For the same span, less depth compared to reinforced concrete members (Reduction in self-weight, more aesthetic appeal due to slender sections and more economical sections).

c) Suitable for precast construction

The advantages of precast concrete are as follows; Rapid construction, better quality control, Reduced maintenance, Suitable for repetitive constructions, availability of standard shapes and reduced use of frameworks.

d) Strong structural system strong

When prestressing mechanisms are designed and engineered for a new structure, the goal is to achieve stronger structural systems with smaller deflections using least material possible.

e) Increased load carrying capacity

Prestressing the structure provides a greater load carrying capacity (Magnel, 1950) and creates savings of material up to 37 percent (Gosaye & Kaba, 2015). Prestressing help to obtain aesthetic benefits in constructing slender structure and also helps to attain greater span lengths as that of the Panama Atlantic Bridge illustrated by Figure 1.47.

Figure 1.35. The Panama Atlantic bridge(Craig, 2018).

1.6.2. Limitations of prestressing

Despite the various advantages of prestressing, this system presents some limitations:

- Prestressing requires enough expertise to jack and install the members.
- This technology is a very skilled technology hence it's not common as reinforced concrete
- It requires high strength materials and hence is very costly
- There is additional cost in auxiliary equipment and need of quality control and inspection for short span lengths.
- Prestressing can reveal to be costly, comparative analysis are therefore required depending on the span length.

Conclusion

The foremost objective of this chapter was to investigate the relevant literature pertaining to the prediction of prestress losses. A general overview of prestressing concepts, prestressing systems and principles were discussed in the chapter. A brief review of prestress bridges, their components and the different time dependent material properties were also discussed. In addition, a detail study was carried out on prestress losses. Furthermore, the loss prediction methods including the comparison between them was discussed. Finally, the software program which would be used for analysis was presented as well as the advantages and disadvantages of the prestressing technology. The proposed AASHTO Time Step method (2017) was developed by modulating the AASHTO LRFD refined equations to accommodate time dependent creep effects. The EN 1992-1-1:2004 on the other hand does not separate the different losses and makes use of the time dependent correction factors and the equations for the prediction of losses. Knowing the particularities of the prestressing technology, the structure on which such is applied, the methodology is discussed in order to attain the objective in the next chapter.

CHAPTER 2: METHODOLOGY

Introduction

The previous chapter enabled us to understand the concept of prestressing and generalities on its advantages and disadvantages. This chapter will focus on the description of the methodology work. This is the part of the study that establishes the research procedure after the definition of the problem, so as to achieve the set of objectives. It is partitioned in different sections, the first being a general recognition of the site done by documentary research. This is followed by a site view and data collection that will enable the modelling and analysis of the prestressed bridge. Thereafter, this chapter will focus on the description of the verification procedures and the governing equations used by analytical and numerical procedures which are intended to be used for the calculation of prestress losses in the critical girder of the bridge. The modern software makes it possible to analyse ever increasing number of structural problems; however, the results of this analysis are strongly dependent on the assumptions made and the understanding of the working principles of the software used, so care is always recommended when adopting numerical solutions.

2.1. Site recognition and data collection

2.1.1. Site recognition

The site recognition is based on documentary research which aims at knowing the physical parameters of the site, that is, the geographical location, the climate, the relief, geology, hydrology and on the other hand, socio-economic parameters such as demographics and economic activities in the region.

2.1.2. Data collection

The Dibamba bridge project data was obtained at the Ministry of Public Works of Cameroun. Three categories of data were collected:

2.1.2.1. Geometric data

The geometric data needed for the Prestress loss assessment of the prestressed bridge under real traffic loads include:

- Longitudinal section;
- Transversal section;
- Structural system plan view;

- Girder distribution;
- Cross beam section;
- Prestressing strand section.

2.1.2.2. Material characteristics

Defining the material properties will help to obtain the resisting forces and moments. The analysis will be a construction stage analysis so the time dependent properties of the material are required. The material properties will be divided in two parts, one for the concrete used in the deck and girders and another for the prestressing steel cable. The material characteristics needed for the prestress loss assessment of the prestressed bridge under real traffic loads include:

- Prestressing strand resistance;
- Concrete girder resistance;
- Bearing Resistance;
- Concrete slab resistance;
- Reinforcement bars traction resistance;
- Concrete cover;
- Concrete and superstructure;
- Humidity and Temperature Variation.

2.1.2.3. Traffic data

The traffic data needed for the prestress loss assessment of the prestressed bridge under real traffic loads include:

- Vehicle type;
- Vehicle information;
- Number of loading cycles produced by each vehicle type.

2.2. Actions on the structure

The actions to consider for design and prestress loss evaluations are Permanent actions, variable traffic actions, and other variable actions such as thermal variations and wind.

2.2.1. Permanent loads

Permanent loads can be sub-divided into two categories which are; permanent structural and permanent non-structural loads (superimposed dead loads). The permanent structural loads are the self-weight of the beams and the slab and are applied to the structure at the initial phase, especially the self-weight of the prestressed beams which act alone until the time when the slab

is cast. This self-weight can be computed using the density and the geometry of the structural element. On the other hand, superimposed dead loads are permanent loads that are applied after the slab has started contributing to the bridge structure. The different permanent non-structural loads are; weight of in-situ slab, weight of Concrete side-walks, weight of asphalt pavement, weight of prefabricated cornice, weight of Security railing, weight of drainage pipes.

2.2.2. Wind loads

The wind load is calculated taking into account two phases which are; phase 0 and phase 1, and they represent different stages in the construction or service stages of the bridge.

2.2.2.1. Phase 0 (Unloaded)

In this phase, concrete is not yet contributing to the structural resistance and the influence height of the wind load is the height of the beam plus slab.

2.2.2.2. Phase 1 (Loaded)

At this stage, the concrete is now contributing to the resistance and it is considered that the bridge is loaded by a car. The height considered is the height of the girder plus slab plus height of car. In the case, the height of the car is assumed to be 3 m. According to the Italian annex of the code, the force of wind can be calculated using the equation (2.7).

$$F_w = q_b C_e(z) C_{fx} A_{ref.x} \quad \textbf{(2.1)}$$

$$q_b = \frac{1}{2}\rho v_b^2 \quad \textbf{(2.2)}$$

Where:

- v_b is the basic wind velocity;
- $C_e(z$ is the exposure factor at height z;
- C_{fx} is the force coefficient in X-direction (parallel to the width and perpendicular to the span);
- $A_{ref.x}$is the reference area of the structure.

Figure 2.2 shows the transverse section of the bridge superstructure together with the effect of wind forces.

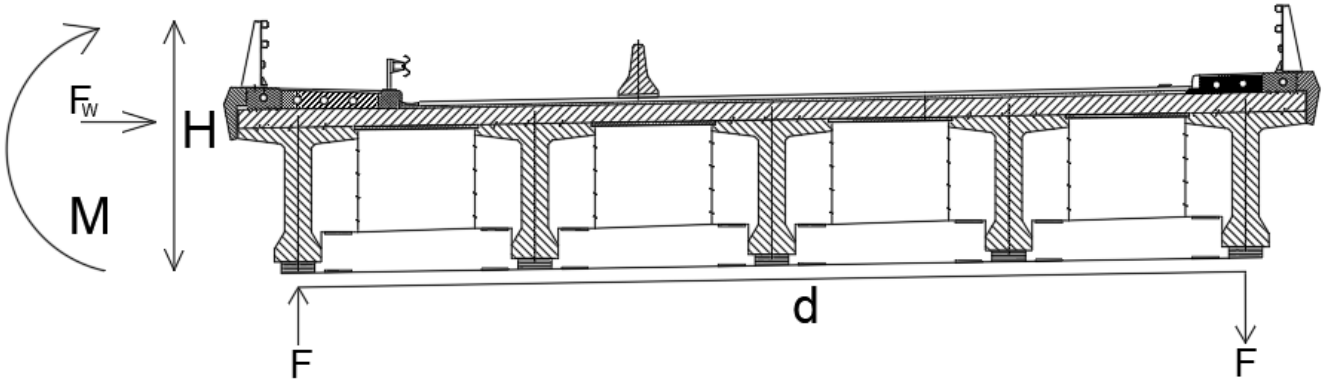

Figure 2.1. Determining the beam force due to wind on the edge beams.

After getting the value of F_w, the moment generated by it can be calculated as

$$M = F_w \cdot (H/2 - Y_G) \quad \textbf{(2.3)}$$

The resulting vertical couple of forces acting on the edge beams were calculated using

$$F = M/d \quad \textbf{(2.4)}$$

as illustrated on Figure 2.2

The value of $C_{fx}$was derived through interpolation according to Figure 2.3.

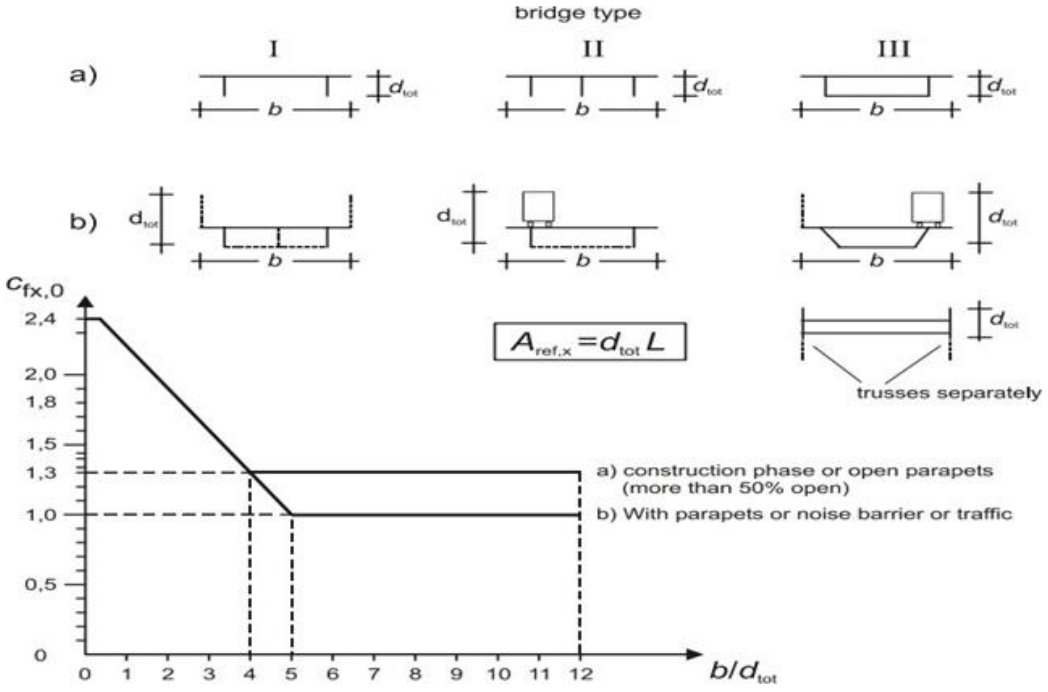

Figure 2.2. Calculation of the force coefficient (EN-1992-1-1_2, 2009).

The value of Ce(z) was obtained from Figure 2.5 according to the category of the terrain.

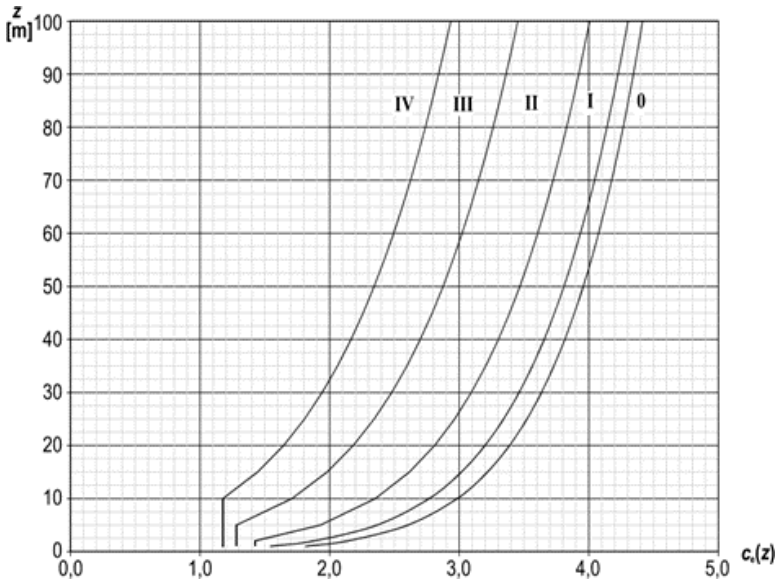

Figure 2.3. Calculation of the exposure factor (EN-1992-1-1_2, 2009).

2.2.3. Traffic Loads

In order to determine the traffic load, the number and width of notional lanes of the roadway was calculated according to the norms, and then, the load models are chosen and applied on the bridge deck. The number and width of the notional lanes was calculated according to Table 2.1.

Table 2.1. Number and width of notional lanes (EN-1992-1-1_2, 2009).

Carriageway width w	Number of notional lanes	Width of a notional lane w_l	Width of the remaining area
$w < 5{,}4$ m	$n_l = 1$	3 m	w - 3 m
5,4 m $\leq w < 6$ m	$n_l = 2$	$\frac{w}{2}$	0
6 m $\leq w$	$n_l = Int\left(\frac{w}{3}\right)$	3 m	$w - 3 \times n_l$
NOTE For example, for a carriageway width equal to 11m, $n_l = Int\left(\frac{w}{3}\right) = 3$, and the width of the remaining area is 11 - 3×3 = 2m.			

The load model chosen for this analysis is the load model 1 (LM1) where uniformly distributed loads (UDL) were applied on all the lanes with lane 1 having the highest value, and the UDL is also applied to remaining area and footpaths. Concentrated tandem loads were also applied to each lane. The characteristics of the loads applied are shown in Table 2.2.

Table 2.2. Characteristic values of LM1(EN-1992-1-1_2, 2009).

Location	Tandem system *TS*	*UDL* system
	Axle loads Q_{ik} (kN)	q_{ik} (or q_{ik}) (kN/m^2)
Lane Number 1	300	9
Lane Number 2	200	2,5
Lane Number 3	100	2,5
Other lanes	0	2,5
Remaining area (q_{rk})	0	2,5

The application of Load model 1 is shown on Figure 2.5. For the crowd loading, reference is made to Load Model 4 of UNI EN 1991-2-2005 which stipulates that for the design of footbridges, a uniformly distributed load should be defined and applied only in the unfavourable parts of the influence surface, longitudinally and transversally.

$$2.5\,kN/m^2 \leq q_{fk} \leq 5\,kN/m^2$$

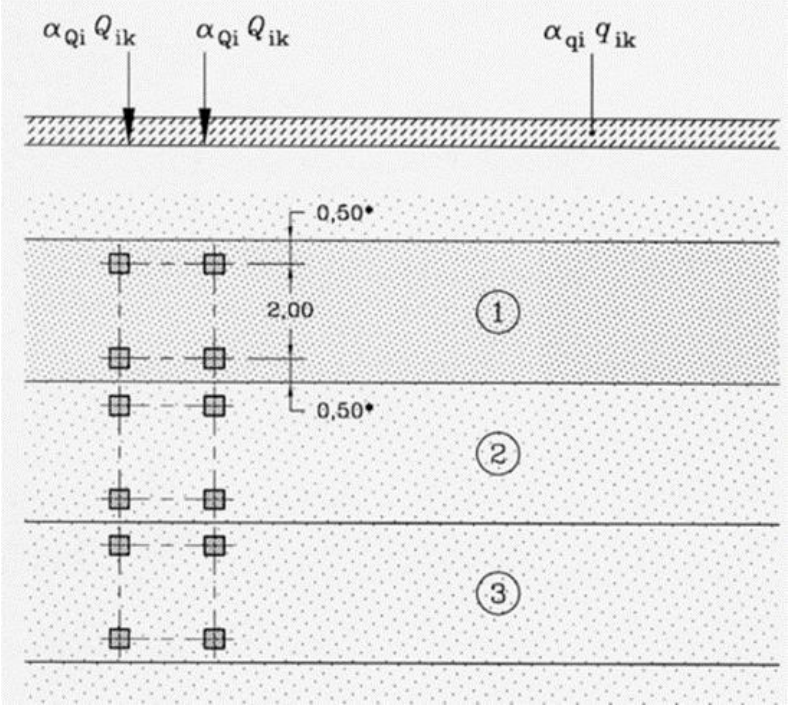

Figure 2.4. Application of LM1(EN-1992-1-1_2, 2009).

Using these load models, the distribution of the loads on the bridge deck are shown on Figure 2.6

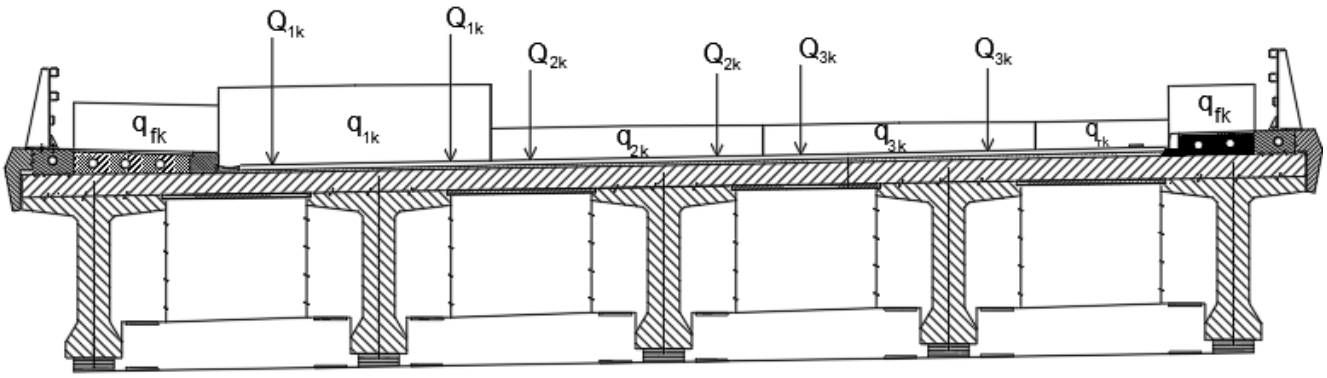

Figure 2.5. Application of traffic loads on bridge deck.

2.2.4. Thermal Action

According to the vertical linear component approach, there id a temperature variation of ΔT between the top and bottom of the slab, the effect of this temperature variation results in stresses at the top and bottom of the beam.

Table 2.3. Values of K_h depending on h_o(EN-1992-1-1_2, 2009).

h_0	k_h
100	1.0
200	0.85
300	0.75
≥ 500	0.70

To calculate these stresses, the resulting force and moment due to temperature change have to be evaluated.

$$N = A_c \varepsilon E_{cm} \quad \textbf{(2.5)}$$

$$\varepsilon = \alpha \Delta T \quad \textbf{(2.6)}$$

where:

- α is the coefficient of thermal expansion for concrete;
- Ac is the area of slab section;
- ΔT is the temperature variation;
- ε is the strain due to temperature difference.

The recommended value of ΔT is obtained from Table 2.4.

Table 2.4. Recommended values of linear temperature difference component for different types of bridge decks for road, foot and railway bridges (EN-1992-1-1_2, 2009).

Type of Deck	Top warmer than bottom	Bottom warmer than top
	$\Delta T_{M,heat}$ (°C)	$\Delta T_{M,cool}$ (°C)
Type 1: Steel deck	18	13
Type 2: Composite deck	15	18
Type 3: Concrete deck: - concrete box girder - concrete beam - concrete slab	 10 15 15	 5 8 8

The values given in the table are based on a depth of surfacing of 50 mm for road and railway bridges.

2.3. Load Combinations

There are various load combinations that can be considered both at the ultimate and serviceability limit states in order to obtain maximum actions on the structure

2.3.1. Basic Actions

The basic actions are usually considered using the Eurocode 0 manual. These basic actions are shown on Table 2.5.

Table 2.5. Basic actions.

Load	Description
G_1	Structural permanent action due to the concrete frame
P	Prestressed load
G_2	Non-Structural permanent action
ε_2	Shrinkage and creep
T_K	Thermal action
M_V	Moving load
F_w	Wind action

2.3.2. Partial factors for load combinations

Table 2.6 gives the values of the partial safety factors with respect to each load type.

Table 2.6. Partial factors for load combinations.

Partial factors	G_1	G_2	P	ε_2	T_K	TS	UDL	F_w
γ	1.35	1.5	1	1.2	1.5	1.35	1.35	1.5
ψ_o	/	/	/	/	0.6	0.75	0.4	0.6
ψ_1	/	/	/	/	0.6	0.75	0.4	0.2
ψ_2	/	/	/	/	0.5	0	0	0

2.3.3. Ultimate limit state combination

At ultimate limit state, the combination considered is the persistent combination.

$$F_d = \gamma_g G_k + \gamma_g P_k + \gamma_g \left[Q_{1k} + \sum_{i=2}^{i=n} \psi_{0i} Q_{ik} \right] \quad \textbf{(2.7)}$$

a) When the traffic load is considered as the leading variable action;

$$Q_{k,1}=1.35*G_1+1.5*G_2+P_k+1.35*(TS+UDL)+1{,}5*0{,}6*T_k+1{,}5*0{,}6*F_W \quad \textbf{(2.8)}$$

b) When the wind load is considered as the leading variable action and the traffic load is considered as the accompanying variable action

$$Q_{k,1}=1.35*G_1+1.5*G_2+P_k+(0.75*TS+0.4*UDL)+1{,}5*0{,}6*T_k+1{,}5F_W \quad \textbf{(2.9)}$$

2.3.4. Serviceability limit state combination

The different load combinations considered at the serviceability limit sate are; the characteristic combination, the frequent combination, the quasi-permanent combination.

2.3.4.1. Characteristic combination

$$F_d = G_k + P_k + Q_{1k} + \sum_{i=2}^{i=n} \psi_{0i} Q_{ik} \quad \textbf{(2.10)}$$

$$Qk,1 = G1 + G2 + Pk + (TS + UDL) + 0,6 * (T_k + F_w) \quad \textbf{(2.11)}$$

2.3.4.2. Quasi permanent combination

$$F_d = G_k + P_k + \sum_{i=1}^{i=n} \psi_{2i} Q_{ik} \quad \textbf{(2.12)}$$

$$Q_{k,i} = G_1 + G_1 + P_k + (0.5 * T_k) \quad \textbf{(2.13)}$$

2.3.4.3. Frequent combination

$$F_d = G_k + P_k + \psi_{11} Q_{1k} + \sum_{i=2}^{i=n} \psi_{2i} Q_{ik} \quad \textbf{(2.14)}$$

a) When traffic load is the leading variable load;

$$Q_{k,1} = G_1 + G_2 + P_k + (0.75 * TS + 0.4 * UDL) + 0{,}5 * T_k \quad \textbf{(2.15)}$$

b) When wind is the leading variable action and traffic load is the accompanying variable action

$$Q_{k,1} = G_1 + G_2 + P_k + 0{,}2 * F_w + 0{,}5 * T_k \quad \textbf{(2.16)}$$

2.4. Girder verification at limit states

2.4.1. Ultimate Limit State verification of the girder

Verifications at the ultimate limit state involves calculating the ultimate moment capacity of the beam and calculating the maximum shear resistance.

2.4.1.1. Calculating the ultimate resisting moment

For the design at ultimate limit state, the rectangular stress block is used. The first step is to look for the position of the neutral axis, and the total strain in the steel which is the sum of prestressing strain and bending strain.

$$M_{RD} = F_{c(g)} * a_{c(g)} + F_{c(s)} * a_{c(s)} + F_s * a_s + \sum (F_{pi} * a_{pi}) \quad \textbf{(2.17)}$$

Where; $a_{c(g)}, a_{c(s)}, a_s \; and \; a_{pi}$ is the distance from the neutral axis to the centroid of the various stress blocks.

2.4.1.2. Calculating the shear resistance of the girder

The shear resistance of the girder is calculated and the value is compared to the applied shear.

$$V_{Rd,c} = \left[C_{Rd,c} * k * (100 * \rho_1 * f_{ck})^{\left(\frac{1}{3}\right)} + k_1 * \sigma_{cp} \right] * b_w * d_p \quad \textbf{(2.18)}$$

$$V_{Rd,min} = \left(V_{min} + k_1 * \sigma_{cp} \right) * b_w * d_p \quad \textbf{(2.19)}$$

2.4.1.3. Calculating the torsional resistance of the girder

The torsional resistance of the girder is calculated by computing the design value of shear resistance and the design value of torsional resistance. Then

$$\frac{T_{Ed}}{T_{Rd,c}} + \frac{V_{Ed}}{V_{Rd,c}} = 0.122 \leq 1 \qquad \textbf{(2.20)}$$

2.4.2. Serviceability verification of the girder

The design is based on maintaining the concrete stresses within the specified limits at all stages of the life of the member. Hence the primary design is based on the serviceability limit state.

2.4.2.1. Codes

- Codes used in the analysis and design of the structural elements are principally;

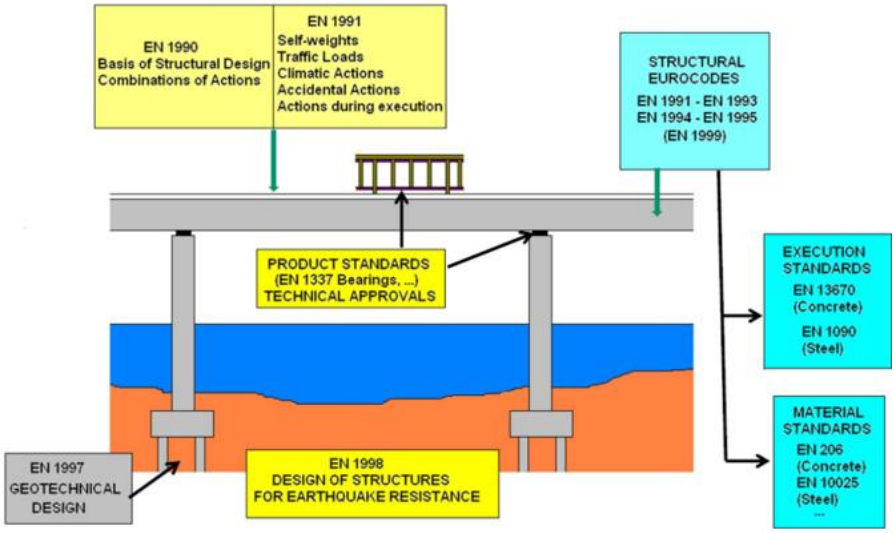

Figure 2.6. Codes used for bridge elements analysis(Aziz et al., 2011).

But for the scope of this study, only the analysis of the superstructure would be done

- In order to evaluate the loss of the prestressing force in prestressing tendons, both the American Association of State Highway Officials (AASHTO) 2017 specification and the EN 1992-1-1:2004 would be used.

2.4.2.2. Determination of minimum section properties

In order that the prestress force and eccentricity exist and permit the stress limits not to be crossed, the minimum values of the section moduli must be satisfied by the chosen section. The chosen section must also have a margin above the values calculated below to also ensure that the practical considerations are met. The following equations are necessary for the determination of the required elastic moduli.

Bottom fibre section modulus

$$Z_b \geq \frac{M_v}{(KF'_{max} - f_{min})} \quad \textbf{(2.21)}$$

Top fibre section modulus

$$Z_b \geq \frac{M_v}{(f_{min} - KF'_{min})} \quad \textbf{(2.22)}$$

Where:

K is the loss factor, K=1-$\%loss$

$$M_v = M_{max} - KM_{min} \quad \textbf{(2.23)}$$

M_{max} is the moment given by the permanent and variable loads.

M_{min} is the moment given by the permanent loads only (including the self-weight of the beam).

2.4.2.3. Selection of prestress force and eccentricity

This is done graphically by drawing the Magnel diagram for critical sections. The equations used to draw the Magnel diagram are:

$$\frac{1}{P_0} \geq \frac{K\left(\frac{1}{A} - \frac{e}{Z_t}\right)}{\left(f_{max} - \frac{M_{max}}{Z_t}\right)} \quad \textbf{(2.24)}$$

$$\frac{1}{P_0} \geq \frac{\left(\frac{1}{A} - \frac{e}{Z_t}\right)}{\left(f'_{min} - \frac{M_{min}}{Z_t}\right)} \quad \textbf{(2.25)}$$

$$\frac{1}{P_0} \leq \frac{K\left(\frac{1}{A} + \frac{e}{Z_b}\right)}{\left(f_{min} + \frac{M_{max}}{Z_t}\right)} \quad \textbf{(2.26)}$$

$$\frac{1}{P_0} \geq \frac{\left(\frac{1}{A} + \frac{e}{Z_b}\right)}{\left(f'_{max} + \frac{M_{min}}{Z_b}\right)} \quad \textbf{(2.27)}$$

Where;

M_{max} is the moment given by the beam's self-weight, permanent loads plus variable loads.

M_{min} is the moment given by the beam's self-weight plus the permanent loads.

This form of construction is known as the Magnel diagram. The additional line 5 shown on the diagram corresponds to a possible physical limitation of the maximum eccentricity allowing for the overall depth of the section, cover to the prestressing tendons, provision of shear links and so on. Figure 2.8 shows the Magnel diagram construction.

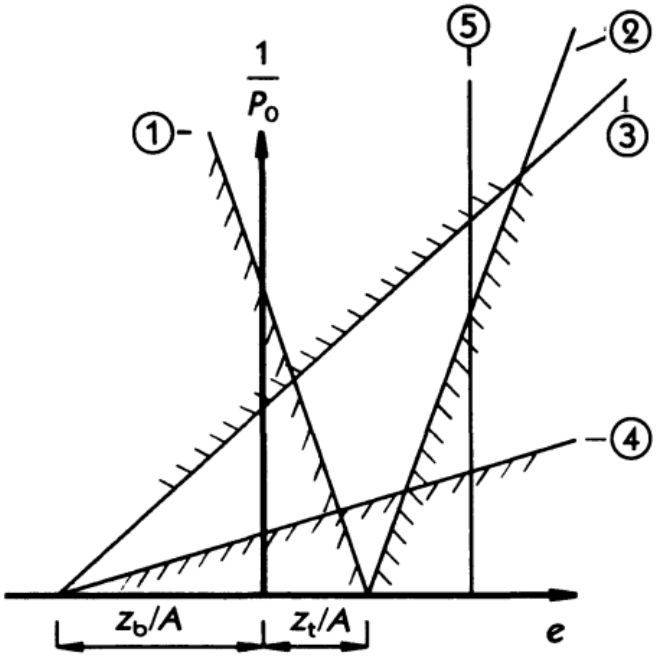

Figure 2.7:Magnel diagram construction (Gilbert et al., 2013).

2.4.2.4. Design of tendon profiles

Having obtained a value of the prestressed force which will permit all stress conditions to be satisfied at the critical section, it is necessary to determine the eccentricity at which this force must be provided, not only at the critical section but also throughout the length of the member.

The design expression can be written as:

At transfer

$$e_{max} \leq \left(\frac{P_0}{A} + \frac{M}{z_t} - f'_{min}\right) * \frac{z_t}{P_o} \quad \textbf{(2.28)}$$

$$e_{max} \leq \left(f'_{max} - \frac{P_0}{A} + \frac{M}{z_b}\right) * \frac{z_b}{P_o} \quad \textbf{(2.29)}$$

At service

$$e_{min} \geq \left(\frac{P_0}{A} + \frac{M}{z_t} - f'_{min}\right) * \frac{z_t}{P_o} \quad \textbf{(2.30)}$$

$$e_{min} \geq \left(f_{min} - \frac{P_0}{A} + \frac{M}{z_b}\right) * \frac{z_b}{P_o} \quad \textbf{(2.31)}$$

Where:

M_{max} is the moment given by the beam's self-weight, permanent loads plus variable loads.

M_{min} is the moment given by the beam's self-weight plus the permanent loads.

These equations are used to evaluate the range of values of eccentricities within which the resultant force lies. For the scope of this work, the member cross section is constant. This implies that the zone within which the centroid of the tendons must lie is governed by the shape of the bending moment envelopes as shown in Figure 2.9

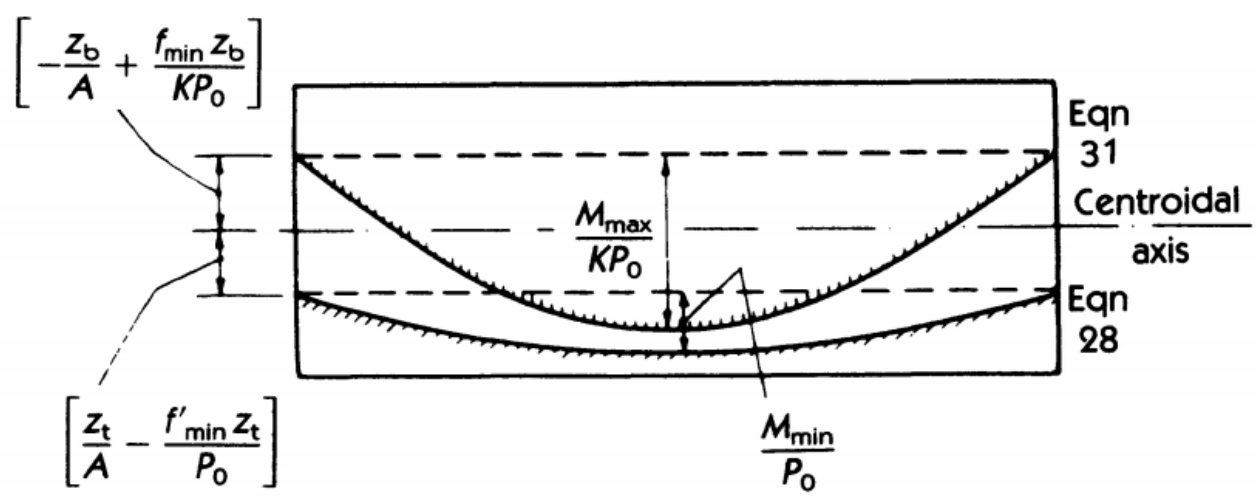

Figure 2.8. Cable zone limits (Gilbert et al., 2013).

2.4.2.5. Stress Limits Check

The governing equations for a single span beam are:

a) At transfer (top fibre in tension and bottom fibre in compression)

- Top fibre

$$f'_t = \frac{P_o}{A} + \frac{M_{min}}{z_t} - \frac{P_o e_{max}}{z_t} \geq f'_{min} \quad \textbf{(2.32)}$$

- Bottom fibre

$$f'_b = \frac{P_o}{A} - \frac{M_{min}}{z_b} - \frac{P_o e_{max}}{z_b} \leq f'_{max} \quad \textbf{(2.33)}$$

b) service (top fibre in compression and bottom fibre in tension)

a) Top fibre

$$f_t = \frac{P}{A} + \frac{M_{max}}{z_t} - \frac{Pe_{max}}{z_t} \leq f_{max} \quad \textbf{(2.34)}$$

b) Bottom fibber

$$f_b = \frac{P}{A} - \frac{M_{max}}{z_b} - \frac{Pe_{max}}{z_b} \geq f_{min} \quad \textbf{(2.35)}$$

Where:

$$P = P_o(1 - \%loss) \quad \textbf{(2.36)}$$

$$M_{min} = q_{min} * {}^{l^2}/_{8} \quad \textbf{(2.37)}$$

$$M_{max} = (q_{live} * {}^{l^2}/_{8}) + M_{min} \quad \textbf{(2.38)}$$

f_{max} and f'_{max} are the compressive strength of concrete at the different life stages of the structure.

It may be required to specify the concrete compressive strength $f_{ck}(t)$, at time t for a number of stages where;

$$f_{ck}(t) = f_{cm}(t) - 8(MPa) \text{ for } 3 < t < 28\ days \quad \textbf{(2.39)}$$

$$f_{ck}(t) = f_{ck} \quad \text{for} \quad t \geq 28 \text{ days} \quad \textbf{(2.40)}$$

The compressive strength of concrete at an age t depends on the type of cement, temperature and curing conditions. For a mean temperature of $20°C$ and curing in accordance with EN 12390, the compressive strength of concrete at various ages $f_{cm}(t)$ may be estimated from equation 2.37.

$$f_{cm}(t) = \beta_{cc}(t)\, f_{cm} \quad \textbf{(2.41)}$$

With

$$\beta_{cc}(t) = \exp\left\{s\left[1 - \frac{28}{t}\right]^{1/2}\right\} \quad \textbf{(2.42)}$$

Where;

$f_{cm}(t)$ is the mean compressive strength at 28 days

$\beta_{cc}(t)$ is the coefficient which depends on the age of the concrete t

t is the age of the concrete in days

2.5. Prestress losses computation

2.5.1. Prestress losses calculation according to EN 1992-1-1:2004

Figure 2.10 illustrates how the initial prestressing force at jacking continuously reduces first due to immediate losses followed by time dependent losses and after all these losses, The final or effective prestressing force necessary for design and good estimation of camber and deflection is obtained.

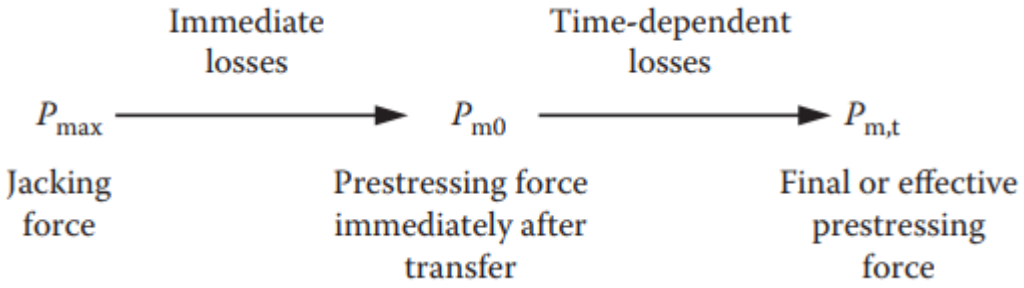

Figure 2.9. Losses of prestress in tendons (Jayaseelan, 2019).

2.5.1.1. Immediate losses

a) Elastic deformation losses

The average stress loss due to elastic shortening is given by the formula

$$\Delta\sigma = \frac{n-1}{2n}\frac{E_p}{E_{cm,0}}\frac{P}{A} \qquad (2.43)$$

n : Number of tendons

$\frac{P}{A}$: Average concrete compressive stress

$\frac{E_p}{E_{cm,0}}$: Modular ratio

b) Friction losses

The average stress loss due to friction is given by the formula

$$\Delta P_\mu(x) = P_{max}(1 + e^{-\mu(\theta+kx)}) \qquad (2.44)$$

P_{max}: Stress in the prestressing steel at jacking

μ : Friction factor

k: Wobble friction coefficient

θ: Sum of the absolute values of angular change of prestressing steel path from jacking ends.

c) seating losses

Figure 2.11 illustrates schematically the way by which the anchorage losses are calculated

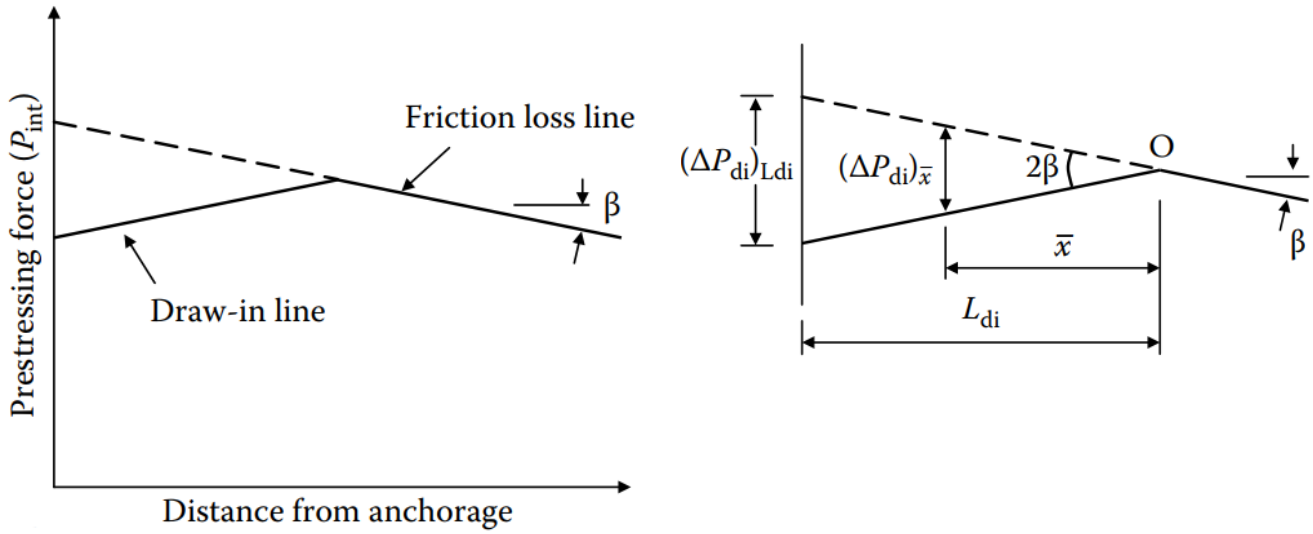

Figure 2.10. Anchorage seating loss calculation (N. Hewson, 2007).

The immediate loss in prestress at anchorage caused by Δ_{slip} is given by

$$(\Delta P_{di})_{L_{di}} = 2 * \beta * L_{di} \quad \textbf{(2.45)}$$

$$L_{di} = \sqrt{\frac{E_p * A_p * \Delta_{slip}}{\beta}} \quad \textbf{(2.46)}$$

β : Slope of the friction loss

L_{di}: Length of the draw in line

A_p : Total cross-sectional area of prestressing strands

Δ_{slip}: Slip distance

E_p : Young's modulus of prestressing strands

2.5.1.2. Time dependent losses

According to the Eurocode, the time dependent loss due to creep, shrinkage and relaxation can be summarised in one formula as shown by equation …

$$\Delta P_{c+s+r} = A_p \Delta\sigma_{p,c+s+r} = A_p \left[\frac{\varepsilon_{cs} E_p + 0.8\Delta\sigma_{p,r} + \frac{E_p}{E_{cm}} \varphi(t,t_o)\sigma_{c,QP}}{1 + \frac{E_p A_p}{E_{cm} A_c}\left(1 + \frac{A_c}{I_c} z_{cp}^2\right)[1 + 0.8 * \varphi(t,t_o)]} \right] \quad \textbf{(2.47)}$$

$\Delta\sigma_{p,c+s+r}$: is the absolute value of the stress in the tendon due to creep, shrinkage and relaxation.

ε_{cs} : Is the absolute value of the estimated shrinkage strain

$\sigma_{p,r}$: It's the absolute value of the variation of stress in tendon at time t due to relaxation.

(t, t_o) : It's the creep coefficient at time t for loads applied at time t_o

$\sigma_{c,QP}$: It's the stress in the concrete adjacent to the tendon due to self-weight, initial prestress and quasi permanent loads.

A_p : It's the total area of all the tendons at a location x.

A_c : It's the area of the concrete cross section.

I_c : It's the second moment of the concrete cross section about its centroidal axis.

z_{cp} : It's the distance between the centre of gravity of the concrete section and the tendons.

2.5.2. Prestress losses calculation according to AASHTO LRFD specifications 2017

According to AASHTO LRFD Time step specifications (2017), the total prestress loss in a prestressed concrete bridge girder is given by

$$\Delta f_{pT} = \Delta f_{pST} + \Delta f_{pLT} \quad \textbf{(2.48)}$$

$$\Delta f_{pLT} = (\Delta f_{pSR} + \Delta f_{pCR} + \Delta f_{pR1})_{id} + (\Delta f_{pSD} + \Delta f_{pCD} + \Delta f_{pR2} - \Delta f_{pSS})_{df} \quad \textbf{(2.49)}$$

Where;

Δf_{pT}:Total prestress losses

Δf_{pLT}: Long term losses

Δf_{pSL}: Short term losses

$(\Delta f_{pSR} + \Delta f_{pCR} + \Delta f_{pR1})_{id}$: Sum of time-dependent losses between transfer and deck placement

Δf_{pSR} : Prestress loss due to shrinkage of girder concrete between transfer and desk placement.

Δf_{pCR} : Prestress loss due to creep of girder concrete between the transfer and deck placement

Δf_{pR1} : Prestress loss due to relaxation of prestressing strands between the time of transfer and deck placement.

$\Delta f_{pSD} + \Delta f_{pCD} + \Delta f_{pR2} - \Delta f_{pSS})_{df}$: Sum of time-dependent losses after the deck placement.

Δf_{pR2} : Prestress loss due to relaxation of prestressing strands after the deck placement.

Δf_{pSD} : Prestress loss due to shrinkage of girder concrete after the deck placement

Δf_{pCD} : Prestress loss due to creep of girder concrete after the deck placement

Δf_{pSS} : Prestress gain due to shrinkage of deck due to composite section.

2.5.2.1. Calculation of instantaneous losses

a) Loss due to elastic shortening

The loss due to elastic shortening in post tensioned members, other than slab systems, may be determined by following equation 2.49

$$\Delta f_{ES} = \frac{N-1}{2N} \frac{A_{ps} f_{pbt}\left(I_g + e_m^2 A_g\right) - e_m M_g A_g}{A_{ps}\left(I_g + e_m^2 A_g\right) + \frac{A_g I_g E_{ci}}{E_p}} \qquad \textbf{(2.50)}$$

Where:

A_{ps}: Area of the prestressing steel

A_g: Gross area of section

E_{ci}: Modulus of elasticity of concrete at transfer

E_p: Modulus of elasticity of prestressing steel

e_m: Average prestressing steel eccentricity at midspan

f_{pbt}: Stress in prestressing steel immediately prior to transfer as

I_g : Moment of inertia of the gross concrete section about the centroidal axis, neglecting the reinforcement.

M_g: Midspan moment due to member self-weight.

N : Number of identical prestressing tendons.

b) Loss due to friction

The path of the cables is parabolic and can be described by the equation $y = ax^2$. This is shown in Figure 2.12.

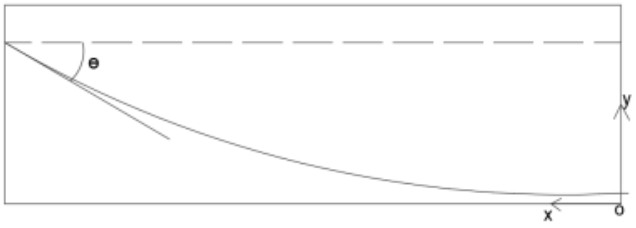

Figure 2.11. Angle of cables.

Losses due to friction between the internal prestressing tendons and the duct wall may be taken as

$$\Delta f_{pF} = f_{pj}(1 - e^{-(Kx+\mu\alpha)}) \qquad \textbf{(2.51)}$$

Where:

f_{pj}: Stress in the prestressing steel at jacking.

μ : Friction factor.

K: Wobble friction coefficient.

α: Sum of the absolute values of angular change of prestressing steel path from jacking ends.

Table 2.7 illustrates how the friction coefficients for post tensioning tendons are obtained depending on the steel type.

Table 2.7. Friction coefficients for posttensioning tendons(Raymond I. G., Neil C. M., 2017).

Type of Steel	Type of Duct	K	μ
Wire or strand	Rigid and semirigid galvanized metal sheathing	0.0002	0.15–0.25
	Polyethylene	0.0002	0.23
	Rigid steel pipe deviators for external tendons	0.0002	0.25
High-strength bars	Galvanized metal sheathing	0.0002	0.30

c) Loss due to anchorage set

$$l_{set} = \sqrt{\frac{E_p A_p \Delta l}{p}}, \tag{2.52}$$

$$\Delta l = 2 p l_{set} \tag{2.53}$$

$$\Delta l = \frac{(Area\ of\ triangle)}{E_p A_p} = \frac{\Delta p l_{set}}{2 E_p A_P} \tag{2.53}$$

$$\Delta f_{pA} = \frac{\Delta l * E_p}{L} \tag{2.54}$$

Figure 2.13 illustrates schematically the way by which the anchorage seating losses are calculated

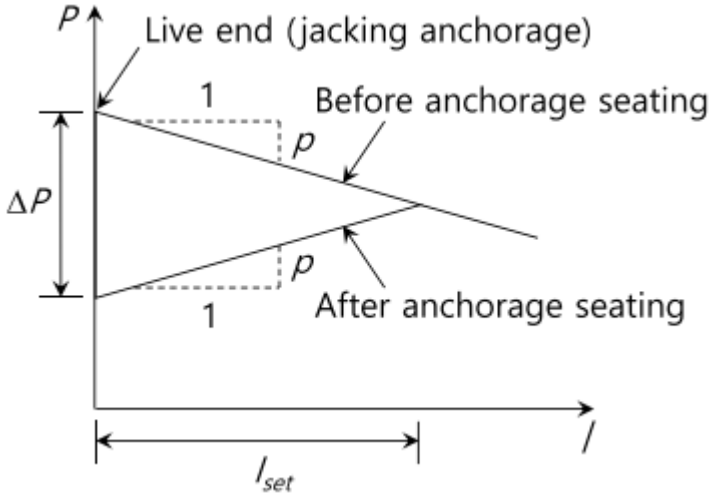

Figure 2.12. Prestressing force distribution affected by anchorage seating loss(N. Hewson, 2007).

Where:

l_{set}: Distance affected by the anchorage seating

E_p: Modulus of elastic strands

A_p: Cross sectional area of the strands

Δl : Draw in slip displacement

p: Friction loss of the prestress force per unit length

Δp: Anchorage seating loss of the prestress force at the live end.

2.5.2.2. Estimation of time-dependent losses between the time of transfer and time of deck placement

a) Shrinkage of concrete girder

The prestress loss due to shrinkage of girder concrete between time of transfer and deck placement, Δf_{pSR}, shall be determined as:

$$\Delta f_{pSR} = \varepsilon_{bid} E_p K_{id} \quad \textbf{(2.55)}$$

In which:

$$K_{id} = \frac{1}{1 + \frac{E_p}{E_{ci}} \frac{A_{ps}}{A_g} \left(1 + \frac{A_g e_{pg}^2}{I_g}\right) [1 + 0.7\psi_b(t_f, t_i)]} \quad \textbf{(2.56)}$$

The strain due to shrinkage is given by

$$\varepsilon_{bid} = k_s k_{hs} k_f k_{td} 0.48x10^{-3} \quad \textbf{(2.57)}$$

In which

$$k_{hs} = (2.00 - 0.014H) \quad \textbf{(2.58)}$$

$$k_s = \left[\frac{\frac{t}{26e^{0.36(V/S)}+t}}{\frac{t}{45+t}}\right]\left[\frac{1064-97(V/S)}{923}\right] \quad \textbf{(2.59)}$$

$$k_f = \frac{5}{1 + f'_{ci}} \quad \textbf{(2.60)}$$

$$k_{td} = \frac{t}{12\left(\frac{100 - 4f'_{ci}}{f'_{ci} + 20}\right) + t} \quad \textbf{(2.61)}$$

The shrinkage coefficient is given by

$$\psi_b(t_f, t_i) = 1.9 k_s k_{hs} k_f k_{td} t_i^{-0.118} \quad \textbf{(2.62)}$$

ε_{bid} : Concrete shrinkage strain of girder between the time of transfer and deck placement

K_{id}: Transformed section coefficient that accounts for the time dependent interaction between concrete and bonded steel in the section being considered for time period between transfer and deck placement.

H: Average annual ambient relative humidity

e_{pg} :Eccentricity of prestressing force with respect to centroid of girder.

$\psi_b(t_f, t_i)$: Girder shrinkage coefficient at final time due to loading introduced at transfer

t_f: Final age

t_i: Age of concrete at time of transfer

k_s: Factor for the effect of volume to surface ratio of the component

k_f: Factor for the effect of concrete strength

k_{td}: Time dependent factor

V/S: Volume to surface ratio

k_{hs}: Humidity factor for shrinkage

f'_{ci} : Design concrete compressive strength at time of prestressing for pretensioned members.

A_c: Area of girder section

I_c: Moment of inertia of girder section

b) Creep of concrete girder

The prestress loss due to creep of girder concrete between time of transfer and deck placement Δf_{pCR}, shall be determined as

$$\Delta f_{pCR} = \frac{E_p}{E_{ci}} f_{cgp} \psi_b(t_d, t_i) K_{id} \quad \textbf{(2.63)}$$

In which

$$\Delta f_{pCR} = \frac{E_p}{E_{ci}} f_{cgp} \psi_b(t_d, t_i) K_{id} \quad \textbf{(2.64)}$$

$$\psi_b(t_f, t_i) = 1.9 k_c k_{hc} k_f k_{td} t_d^{-0.118} \quad \textbf{(2.65)}$$

$$K_{hc} = 1.56 - 0.008H \quad \textbf{(2.66)}$$

$$k_c = \left[\frac{\frac{t}{26e^{0.36(V/S)}+t}}{\frac{t}{45+t}}\right]\left[\frac{1.80+1.77e^{-0.54(V/S)}+t}{2.587}\right] \quad \textbf{(2.67)}$$

Where:

$\psi_b(t_d, t_i)$: Girder shrinkage coefficient at final time due to loading introduced at transfer

t_d: Age at deck placement

f_{cgp}: Sum of concrete stresses at the center of gravity of prestressing tendons due to prestressing force after jacking and self-weight of the member at the member at the sections of maximum moment.

c) Relaxation of prestressing strands

The prestress loss due to relaxation of prestressing strands between time of transfer and deck placement

$$\Delta f_{pR1} = \left[\frac{f_{pt}}{K_L'}\frac{\log(t)}{\log(t_i)}\left(\frac{f_{pt}}{f_{py}} - 0.55\right)\right]\left[1 - \frac{3\left(\Delta f_{pSR} + \Delta f_{pCR}\right)}{f_{pt}}\right]K_{id} \quad \textbf{(2.68)}$$

K_L': Factor accounting for the type of steel, equal to 45 for low relaxation strands and 7 for other prestressing steel.

t: Time between strand tensioning and deck placement

f_{pt}: Stress in the prestressing strands immediately before the transfer

f_{py}: Yield strength of the prestressing strands.

2.5.2.3. Estimation of time-dependent losses after the deck placement

a) Shrinkage of concrete girder

The prestress loss due to shrinkage of girder concrete between the time of deck placement and the final time, Δf_{pSD}, shall be determined as:

$$\Delta f_{pSD} = \varepsilon_{bdf} E_p K_{df} \quad \textbf{(2.69)}$$

In which

$$K_{df} = \frac{1}{1 + \frac{E_p}{E_{ci}}\frac{A_{ps}}{A_c}\left(1 + \frac{A_c e_{pc}^2}{I_c}\right)[1 + 0.7\psi_b(t_f, t_i)\,]} \quad \textbf{(2.70)}$$

ε_{bdf} : Concrete shrinkage strain of girder between the time of deck placement and final time

K_{df}: Transformed section coefficient that accounts for the time dependent interaction between concrete and bonded steel in the section being considered for time period between deck placement and final time

e_{pc} :Eccentricity of prestressing force with respect to centroid of composite section

A_c: Area of section calculated using the gross composite concrete section properties of the girder and the deck-to-girder modular ratio

I_c: Moment of inertia of section calculated using the gross composite concrete section properties of the girder and the deck and the deck-to-girder modular ratio et service

b) Creep of concrete girder

The change in prestress (loss is positive, gain is negative) due to creep of girder concrete between time of deck placement and final time, Δf_{pCD} shall be determined as:

$$\Delta f_{pCD} = \frac{E_p}{E_{ci}} f_{cgp}[\psi_b(t_f, t_i) - \psi_b(t_d, t_i)]K_{df} + \frac{E_p}{E_c}\Delta f_{cd}\psi_b(t_f, t_d)K_{df} \quad \textbf{(2.71)}$$

Where:

Δf_{cd}: Change in stress at centroid of prestressing strands due to long-term losses between the transfer and deck placement, combined with deck weight and superimposed loads.

$\psi_b(t_f, t_d)$: Girder creep coefficient at final time due to loading at deck placement.

c) Relaxation of prestressing strands

The prestress loss due to relaxation of prestressing strands in composite section between time of deck placement and final time, Δf_{pR2}, shall be determined as:

$$\Delta f_{pR2} = \Delta f_{pR1} \quad \textbf{(2.72)}$$

d) Shrinkage of Concrete Deck

The prestress gains due to shrinkage of deck in composite section, $\Delta f_{pSS,}$ shall be determined as:

$$\Delta f_{pSS} = \frac{E_p}{E_c}\Delta f_{cdf} K_{df}[1 + 0.7\psi_b(t_f, t_d)] \quad \textbf{(2.73)}$$

In which:

$$\Delta f_{cdf} = \frac{\varepsilon_{ddf} A_d E_{c\ deck}}{[1 + 0.7\psi_d(t_f, t_d)]}\left(\frac{1}{A_c} - \frac{e_{pc} e_d}{I_c}\right) \quad \textbf{(2.73)}$$

Δf_{cdf}: Change in concrete stress at centroid of prestressing strands due to shrinkage of deck concrete

ε_{ddf}: Shrinkage strain of deck concrete between placement and final time from equation X

A_d: Area of deck concrete

$E_{c\ deck}$: Modulus of elasticity of deck concrete

e_d: Eccentricity of deck with respect to the gross composite section, positive in typical construction where deck is above the girder.

$\psi_d(t_f, t_d)$: Creep coefficient of deck concrete at final time due to loading introduced shortly after deck placement

$\psi_b(t_f, t_d)$: Girder creep coefficient at final time due to loading at deck placement

2.6. Modelling procedure in Midas civil and construction stage analysis

The modelling of the bridge was performed in Midas Civil taking into account the various construction stages, together with their elements, boundary conditions, and loads applied. Using this method of analysis, Prestress losses can be evaluated not only at every single stage during the construction process but also during the service life of the structure. For the analysis, only 3 spans of the bridge were considered since all the spans are identical.

Table 2.8. Detail of the various construction stages of the bridge.

Stages	Days		Details
CS1	10	Structure	Pier and pier cap are activated at the age of 28 days
		Boundary	Substructure supports are activated
		Load	Self-weight of the structure is applied
CS2	21	Structure	Girders of span 1 are activated at 28 days
		Boundary	Girders of span 1 are supported on temporary support
		Load	Girders of span 1 are stressed in sequence
CS3	21	Structure	Diaphragm of span 1 are activated at the age of 14 days Girders of Span 2 are launched at the age of 28 days
		Boundary	Temporary support of span 1 are deactivated Girders of Span 1 are shifted to permanent bearing Girders of Span 2 are supported on temporary support
		Load	Casting of the slab for span 1 begins at the 14th day of CS3, hence wet concrete load of the slab would be acting Girders of Span 2 are stressed in sequence
CS4	21	Structure	Deck slab of span 1 is activated at the age of 14 days Diaphragm of span 2 are activated at the age of 14 days Girders of span 3 are activated at the age of 28 days
		Boundary	Temporary support of span 2 are deactivated Girders of Span 2 are shifted to permanent bearing Girders of Span 3 are supported on temporary support
		Load	Casting of the slab for span 2 begins at the 14th day of CS3, hence wet concrete load of the slab would be acting Wet concrete load of span 1 is deactivated Girders of Span 3 are stressed in sequence

CS5	21	Structure	Deck slab of span 2 is activated at the age of 14 days Diaphragm of span 3 are activated at the age of 14 days
		Boundary	Temporary support of span 3 are deactivated Girders of Span 3 are shifted to permanent bearing
		Load	Casting of the slab for span 3 begins at the 14th day of CS3, hence wet concrete load of the slab would be acting Wet concrete load of span 2 is deactivated
CS6	21	Structure	Deck slab of span 3 is activated at the age 14 days
		Load	Wet concrete load of span 3 would be deactivated
CS7	10000		To check the long-term stresses during the service life of the structure

This modelling procedure and analysis is better illustrated in **Annex 1.**

2.7. Method of comparison of results

The comparison of the results would be based on the design parameters incorporated by both codes, the material properties, the modular ratio, the partial safety and strength reduction factors, the creep, shrinkage and friction coefficients. Curves would be drawn together with bar charts and pie charts for every single tendon in order to better compare the results. From these design parameters, the more accurate and more detailed method would be chosen as well as the necessary conditions required for the application of this method.

2.8. Proposition for prestress losses reduction

The propositions given to ensure the reduction of prestress losses would be based on the results of the calculation and also on both technical reports on post-tensioned durability and the case study investigated.

Conclusion

The aim of this chapter was to present in a chronological manner, the steps necessary to calculate prestress losses using both the Eurocode and the AASHTO Specifications. This was done firstly, by site recognition through documentary research. Furthermore, the site visit and the data collection. In order to perform righteous analysis, a clear methodology to obtain the solicitations via corresponding load condition is presented and the verifications at limit states followed. After this followed the computation of the various prestress losses following the two methods. These losses help us to obtain the comparison criteria, to carry out analysis and propose solutions for their reduction.

CHAPTER 3: RESULTS AND DISCUSSION

Introduction

The correct evaluation of the performance of a structure starts with its correct analysis. Firstly, the case study to be modelled and its corresponding material properties with respect to the methodology discussed in chapter 2 are presented in section 3.2. Secondly the various analysis performed would be presented followed by the verification of the structural model both at ultimate and at serviceability limit states. Furthermore, Prestress losses results would be presented from the analytical model followed by a comparative analysis between losses obtained from AASHTO LRFD specifications and those obtained by the EN 1992-1-1:2004. Finally, solutions regarding the reduction of prestressed losses would be proposed.

3.1. General presentation of site

It consists in presenting the geographical location of the site on a map, the climate, the geology of the region, its economic activity and geology. Figure 3.1 shows the longitudinal view of the bridges.

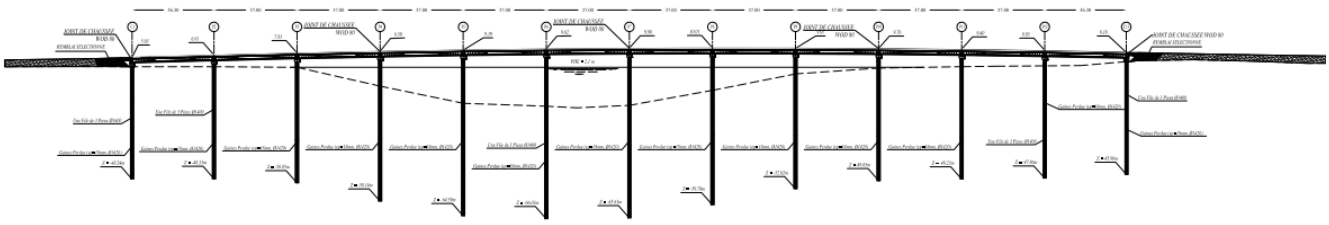

Figure 3.1. Longitudinal view of the bridge.

3.1.1. Geographic location

The Edea - Douala axis of the national road (RN3) is one of the busiest roads in Cameroon. It links the city of Douala to the rest of the country and to the neighbouring countries (Chad, Central African Republic, Gabon, Equatorial Guinea). The bridge over the Dibamba River located on this axis, is about 20 km south-east of Douala city centre and 45 km North-East of the town of Edea. The project site is located at the junction between the territory of the urban community of Douala, district of Douala II in the department of Wouri and the township of the Dibamba, district of Dibamba in the department of Sanaga maritime, both part of the Littoral region. Geographically, the project is at $3^{\circ}57'03''$N and $11^{\circ}32'26''$E. The satellite view of the project site is shown in Figure 3.2 while Figure 3.3 gives us a plan view of the bridge to be constructed. A better view of the project's site is given in **Annex 2.**

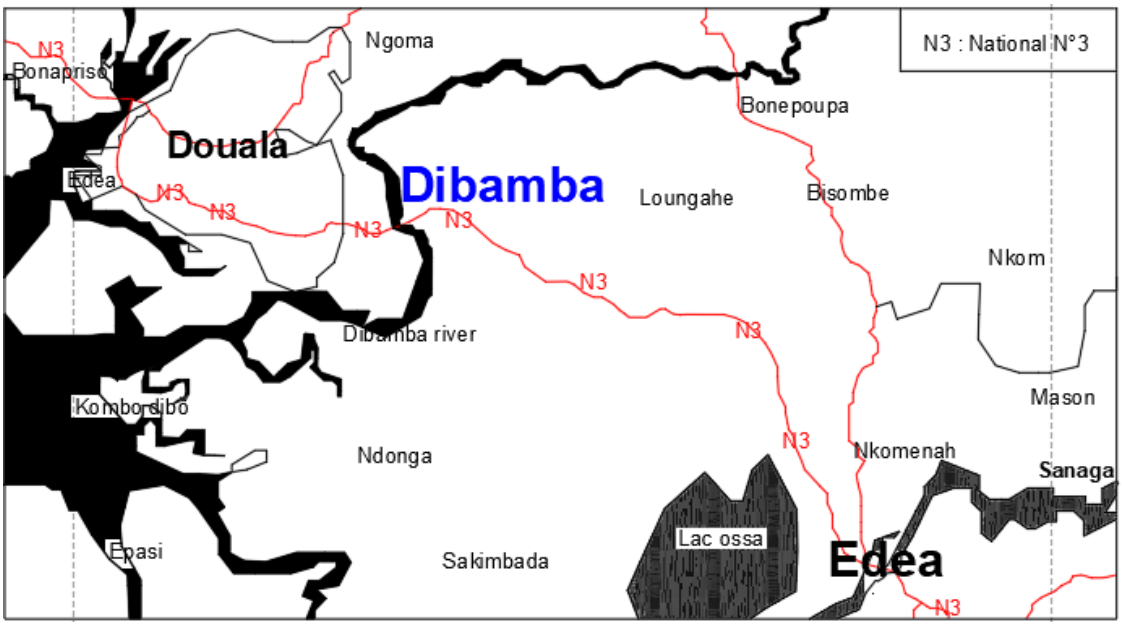

Figure 3.2. Satellite view of the project site.

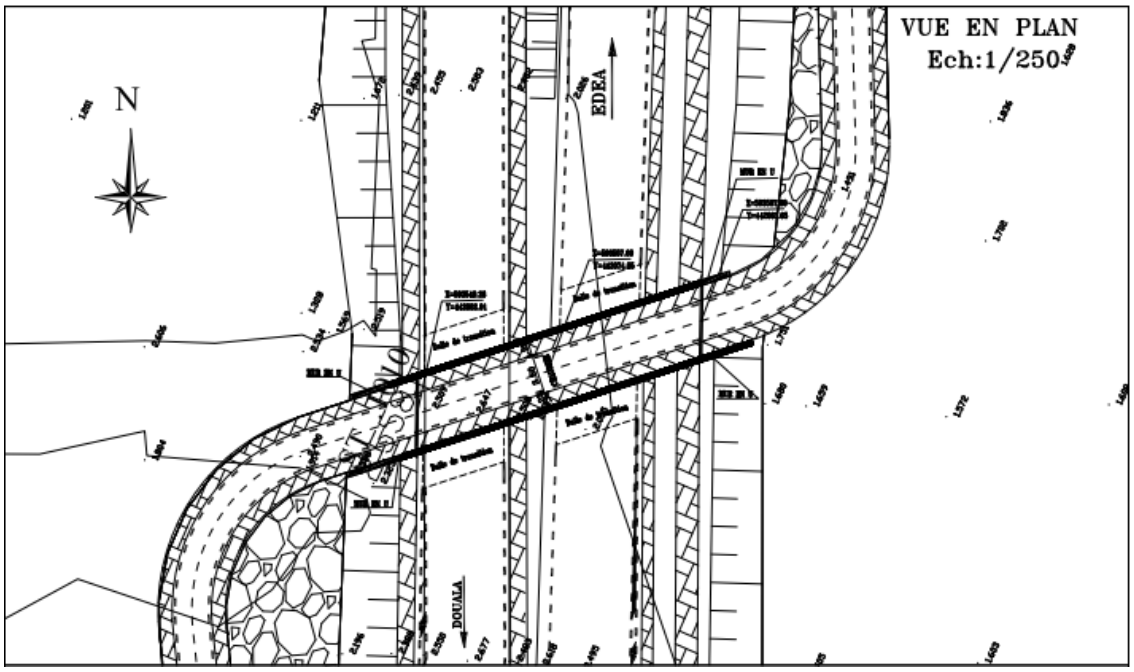

Figure 3.3. Plan view of the bridge on the Dibamba river.

3.1.2. Relief and soils

The site has a fairly flat to undulating relief made up of hills and plateaus, with fairly gentle slopes (hillsides). The soils are mostly clayey-sandy in the thalwegs and sandy-clay in the valleys. They are generally ferralitic soils with a yellowish colour. These soils are quite rich in laterite concretions at shallow depths, which justifies the numerous laterite quarries that are exploited by public works companies in the vicinity. The banks of the river are muddy to sandy-clay on the surface, active where they are exposed and are sensitive to water phenomena. The

bed of the Dibamba is generally covered with sediments exploited for construction purposes. This factor must be taken into consideration as a physical constraint.

3.1.3. Climate

The climate in this area is tropical and humid, with two distinct seasons: a dry season that lasts between 4 and 5 months, and an important rainy season that generally lasts from March to October. Average monthly temperatures vary between 24 and 28°C. The average annual precipitation is 2606 mm. The information related to climate is illustrated in Figure 3.4

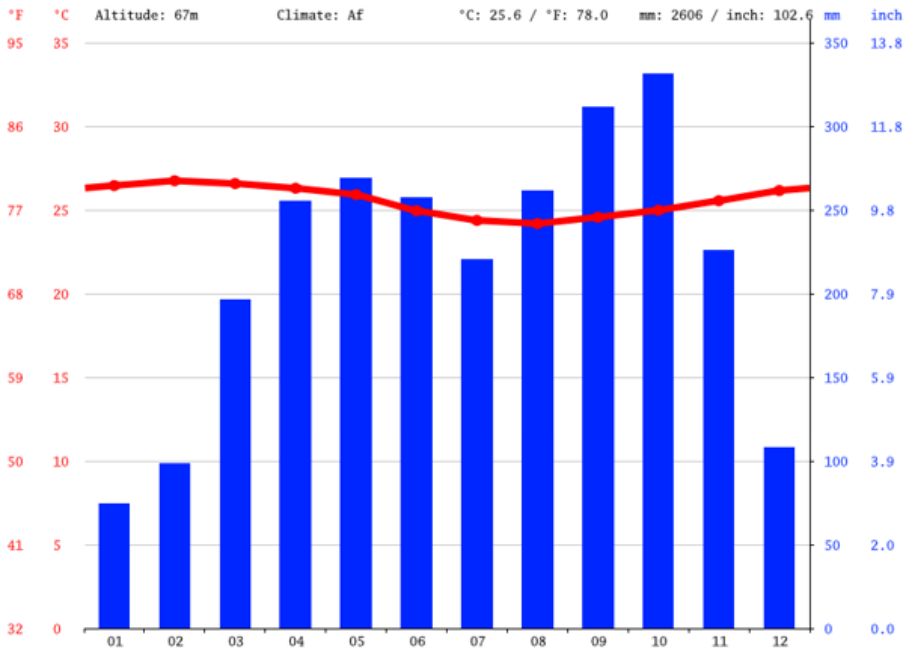

Figure 3.4: Ombro-thermal chart of Dibamba

3.1.4. Hydrography

The study area is watered by the Dibamba, Mone and Missolé rivers. Overall, there exist several rivers and streams that water the villages of the township (Ngombé, Welmakoulou, Ybong (Ngombé, Welmakoulou, Ybong, Manyo-Manyo, Bibalé, Manaté, Mayané, Ossa, Mitotom) abundant in diversified fish resources. The Dibamba is 150 km long, has a basin of 2,400 km² and an estimated average flow of 480 m3/s at its mouth. The waters of this river join the Wouri River estuary through the mangrove forests that extend mangrove forests south of Douala at Souelaba point1. The river is crossed by a 370-metre-long bridge made of precast concrete girders and prestressed concrete dating from 1983-1984, located at the level of a very shallow meander of the river. The Public River Domain is sparsely occupied by buildings.

3.1.5. Demographics and economy

The whole of the Dibamba with a total area of 1600 km² has an estimated population of about 14 000 inhabitants with about 8.75 inhabitants per km². For the moment, economic activities are limited to the incessant ballet of trucks entering and exiting the bridge loaded with sand, trucks refueling at the petrol stations, fishermen on their pirogues all day long, and the trade in agricultural produce, fresh and smoked fish displayed on makeshift stalls on the roadside.

3.2. Presentation of the project

The proposed structure is a prestressed concrete girder bridge with twelve (12) independent spans of 37m each. The total length of the structure (between extreme roadway joints) is 445 m. The deck, whose total width is 16.00 m, supports two traffic lanes which are 3.50 m wide each, a cycle track 3.0 m wide, a pavement 2.00 m wide on the cycle track side, 1.25 m wide on the side of the road and 1.25m wide on the central side between the two structures. The transverse section of the studied bridge is given by Figure 2.1.

3.2.1. Transverse deck arrangement

The deck is supported on five precast prestressed I beam that are linked together by a reinforced concrete slab. The thickness of the slab is 250 mm and is constant throughout the length of the bridge. The transverse section of the bridge superstructure is shown in Figure 3.5.

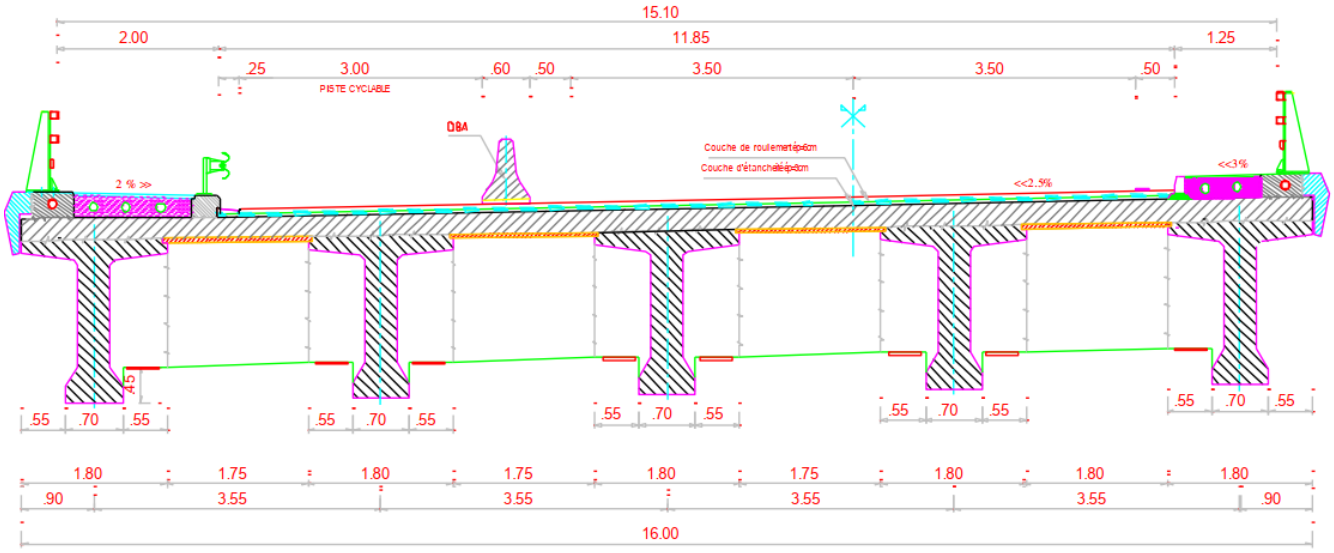

Figure 3.5. Transverse section of the deck.

The section of the precast prestressed girder is shown in Figure 3.6.

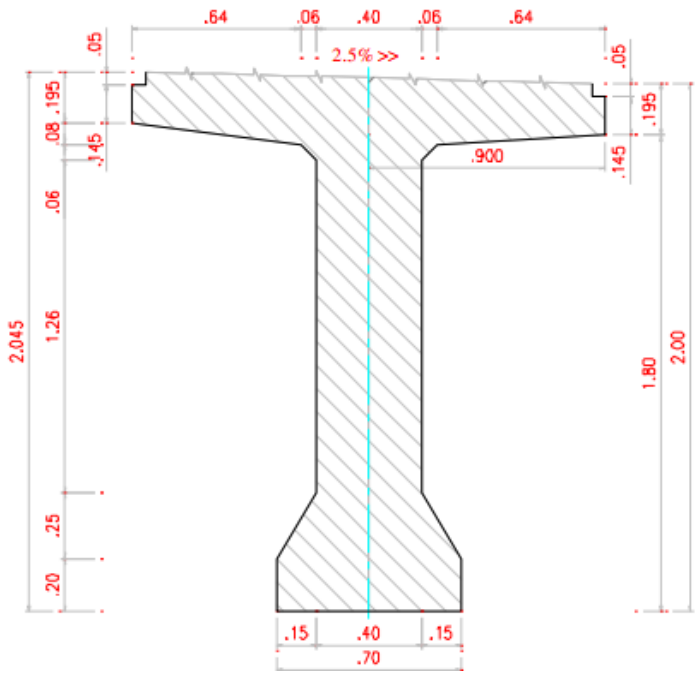

Figure 3.6. Prestressed beam girder section.

The prestressed precast girder is more detailly presented with the prestressing tendons and their eccentricities in Figure 3.7

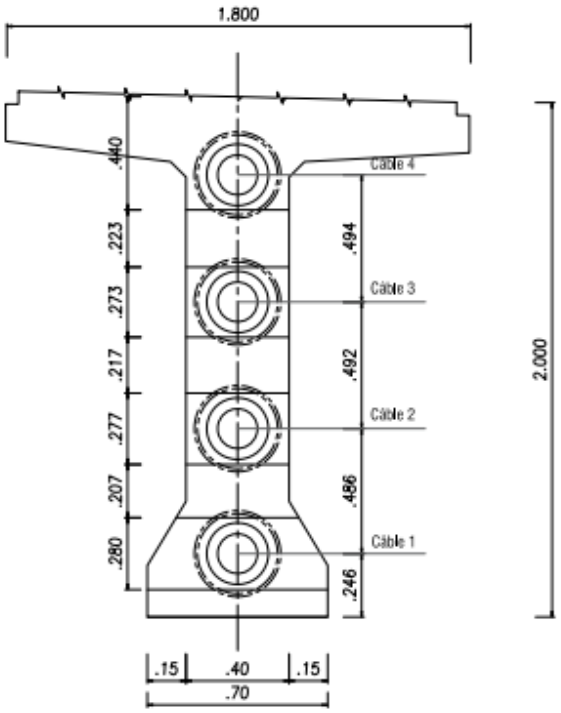

Figure 3.7. Section with tendons.

3.2.2. Articulation of the structure

The types of bearings proposed for the structure is the elastomeric bearings which will each accommodate rotational and translational displacements. Each of the five beams is supported by an elastomeric bearing. Figure 3.8 shows the arrangement of the bearings on the bridge while Figure 3.9 illustrates a typical type of bearing which is the elastomeric bearing used in the project.

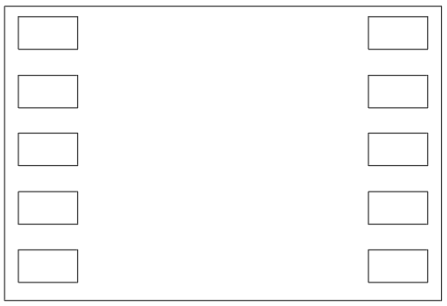

Figure 3.8. Bearing layout.

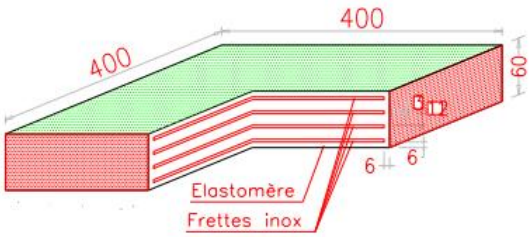

Figure 3.9. Elastomeric bearings(Insight, 2021).

3.2.3. Geometric properties of deck components

The main properties of the interest are; the Area (A), centre of gravity (Y_G), moment of inertia about the bending axis (I_{XX}), torsional moment of inertia (J_t) and the section moduli (Z_b and Z_b)

3.2.3.1. Prestressed girder and cross beams

The geometric properties of the cross beams as well as that of the precast girder before and after the application of the composite action are summarised in Table 3.2 and Table 3.1 respective

Table 3.1. Geometric properties of the prestressed girder section and composite section.

	Value(Before)	Value(After)	Unit
Area	1.572700e+006	2.427883e+006	mm^2
Asy	7.853419e+005	1.497979e+006	mm^2
Asz	6.635406e+005	7.646338e+005	mm^2
Ixx	7.492404e+010	8.383220e+010	mm^4
Iyy	7.194558e+011	1.105250e+012	mm^4
Izz	4.852190e+011	1.383339e+012	mm^4
Cyp	1.440000e+003	1.440000e+003	mm
Cym	1.440000e+003	1.440000e+003	mm
Czp	7.046937e+002	4.124474e+002	mm
Czm	1.340306e+003	1.632553e+003	mm
Qyb	0.000000e+000	0.000000e+000	mm^2
Qzb	0.000000e+000	0.000000e+000	mm^2
Peri:O	9.968852e+003	1.756885e+004	mm
Peri:I	0.000000e+000	0.000000e+000	mm
Center:y	1.440000e+003	1.775000e+003	mm
Center:z	1.340306e+003	1.632553e+003	mm
y1	-1.440000e+003	-1.440000e+003	mm
z1	7.046937e+002	4.124474e+002	mm
y2	1.440000e+003	1.440000e+003	mm
z2	7.046937e+002	4.124474e+002	mm
y3	3.500000e+002	3.500000e+002	mm
z3	-1.340306e+003	-1.632553e+003	mm
y4	-3.500000e+002	-3.500000e+002	mm
z4	-1.340306e+003	-1.632553e+003	mm

Table 3.2. Geometric properties of the cross beams.

	Value	Unit
Area	2.500000e+005	mm^2
Asy	2.083333e+005	mm^2
Asz	2.083333e+005	mm^2
Ixx	4.388288e+009	mm^4
Iyy	1.302083e+009	mm^4
Izz	2.083333e+010	mm^4
Cyp	5.000000e+002	mm
Cym	5.000000e+002	mm
Czp	1.250000e+002	mm
Czm	1.250000e+002	mm
Qyb	7.812500e+003	mm^2
Qzb	1.250000e+005	mm^2
Peri:O	2.500000e+003	mm
Peri:I	0.000000e+000	mm
Center:y	5.000000e+002	mm
Center:z	1.250000e+002	mm
y1	-5.000000e+002	mm
z1	1.250000e+002	mm
y2	5.000000e+002	mm
z2	1.250000e+002	mm
y3	5.000000e+002	mm
z3	-1.250000e+002	mm
y4	-5.000000e+002	mm
z4	-1.250000e+002	mm

3.2.4. Material properties

The materials are concrete, prestressing steel and reinforcing steel

3.2.4.1. Concrete

The strength of the concrete for both the prestressed and the reinforced concrete is the same so as to ensure some degree of monolithic behaviour of the beams and slab. The different material properties are summarized in Table 3.3.

Table 3.3. Material properties of concrete sections.

Concrete for the Slab and Girders			
Concrete class	C 35/45		
Characteristic cubic strength	R_{ck}	45	MPa
Compressive strength at 28 days	f_{ck}	35	MPa
Compressive strength at 7 days	$f_{ck}(t)$	23.179	MPa
Mean cylindrical resistance	$f_{cm} = f_{ck} + 8$	43	MPa
Mean tensile resistance	f_{ctm}	2.7	MPa
Mean tensile resistance at 7 days	$f_{ctm}(t)$	1.991	MPa
Elastic modulus	E_{cm}	35981.73	MPa
ULS Safety factor	γ_c	1.5	MPa
Design value of concrete compressive strength	$f_{cd} = \frac{\alpha_{cc} f_{ck}}{\gamma_c}$	19.83	MPa
Concrete tensile strength 5% fractile	$f_{ctk,0.05} = 0.7 * f_{ctm}$	1.4	MPa
Design tensile strength	$f_{cdt} = \frac{\alpha_{cc} f_{ctk,0.05}}{\gamma_c}$	0.79	MPa
Poisson's ratio	v	0.2	
Shear modulus	$G = \frac{E_{cm}}{2(1+v)}$	14992.39	MPa
Coefficient of thermal expansion	A	$1x10^{-5}$	
Specific weight of concrete	γ	25	KN/m^2

3.2.4.2. Steel

The steel selected for the prestressing are of high strength and have a diameter of 15.2 mm each. The properties of steel used in both prestressed and reinforced concrete is summarized in Table 3.4

Table 3.4. Material properties for prestressing and reinforcing steel.

Prestressing steel			
Class	Class 2		
Strand type	T1860S7		
Nominal Diameter	$\emptyset$	15.2	mm
Characteristic tensile stress	f_{pk}	1863.26	MPa
Characteristic stress at 0.1% strain	$f_{p0.1k}$	1569	MPa
Cross sectional area	A	150	mm²
Total cross-sectional area	A_p	1650	mm²
Jacking force per cable	P_o	2455.20	kN
Maximum initial stress	σ_{in}	1488	MPa
Maximum relaxation at 1000 hours		2.5%	
Elastic modulus	E_s	200000	MPa
Reinforcing steel			
Steel class	B500C		
Characteristic yield strength	f_{yk}	500	MPa
Design yield strength	f_{yd}	434.78	MPa
Partial safety factor of steel	γ_s	1.15	
Specific weight of steel	γ	78.5	kN/m^3
Poisson ratio	v	0.3	
Modulus of Elasticity	E	210000	MPa

3.2.5. Concrete cover

The calculation for the concrete cover for the various bridge parts is summarized on Table 3.5.

Table 3.5. Concrete cover for different structural elements.

Structural element	Exposure class	$C_{min}(mm)$	$\Delta\, cdev(mm)$	C_{min}(mm)
Main beams	XC4	35	5	40
Slab	XC4	20	5	25
Foundations	XC2	30	5	35
Cross beams	XC4	20	5	25
Abutments	XC4	20	5	25

3.3. Values of bridge loads

The various load types acting on the structure were defined in section 2.3

3.3.1. Values of permanent or dead loads

The dead loads refer to the self-weight to the structural elements and to the non-structural superimposed loads. Table 3.6 illustrates values of the self-weight and the self-imposed dead loads.

The self-weight of the bridge is automatically taken into account by the software.

Table 3.6. Values of dead loads.

Static load types	Value	Unit
Self-imposed dead loads	2.5	kN/m
Safety barriers	1.6	kN/m
Wet Concrete Span 1	9.5	kN/m
Wet Concrete Span 2	9.5	kN/m

3.3.2. Value of wind load

The horizontal forces acting on the bridge is calculated, and the resultant couple of forces on the edge beams for Phase 0 and Phase 1. With this, the vertical forces acting on the bridge is calculated. The calculation of the wind load at phase 0 and phase 1 are summarized on Table 3.7.

Table 3.7. Wind load calculations.

Region	Littoral			
Reference base velocity	v_{bo}	22	m/s	
Basic wind velocity	v_b	22	m/s	
Average air density	ρ	1.25	kg/m^3	
Reference kinetic pressure	q_b	0.3025	kg/m^2	
Terrain category		III		
Reference height	z	13.445	m	
Exposure factor	$ce(z)$	1.9		
Width of bridge	b	15.1	m	
Height considered	d_t	2.045	m	Phase 0
		5.045	m	Phase 1
Distance between edge beams	d	14.2	m	
Width to height ratio	b/d_t	7.384		Phase 0
		2.993		Phase 1
Force coefficient	$cf_{x,0}$	1.3		Phase 0
		1.65		Phase 1
Peak velocity pressure	F_w	0.75	kN/m^2	Phase 0
		0.95	kN/m^2	Phase 1
Distributed load on edge beams	F	1.72	kN/m	Phase 0
		2.18	kN/m	Phase 1

3.3.3. Value of traffic load

The traffic loads according to the load model 1 consists of the tandem loads and uniformly distributed loads acting on each notional lane of the bridge deck. Table 3.8 shows the width and number of notional lanes.

Table 3.8. Width and number of notional lanes.

Driveway surface width	W	10
Number of conventional lanes	n_l	3m
Length of conventional lanes	L_c	3m
Width of remaining area	L_r	1m

The methods of application of loads according to LM1 on the bridge is shown in Figure 3.9 and the sum of these uniformly distributed loads and tandem loads are shown in Table 3.9.

Table 3.9. Traffic load intensity for load model 1.

Uniformly distributed loads				
Position	q(kN/m²)		Width (m)	qtot (kN/m)
Lane 1	q_1	9	3	27
Lane 2	q_2	2.5	3	7.5
Lane 3	q_3	2.5	3	7.5
Left sidewalk	q_4	2.5	2.25	5.625
Right sidewalk	q_5	2.5	1.75	4.375
Remaining Area	q_5	2.5	2.1	5.25
Total				57.25
Tandem loads				
Position	Q(kN)		# of axels	$Q_{tot}(kN)$
Lane 1	Q_1	300	2	600
Lane 2	Q_2	200	2	400
Lane 3	Q_2	200	2	400
Remaining Area	-	0	0	0
Total				1400

3.3.4. Value of temperature effects

The force due to temperature variation would be applied from the data due to climate and a value of 32 °C will be applied as the maximum positive temperature. With a minimum temperature of 22 °C, positive and negative gradients Δt of +/-10 °C will be applied to the bridge.

3.3.5. Value of creep and shrinkage coefficients

Creep and shrinkage are taken into account in this analysis by considering creep and shrinkage properties when defining the concrete material. The relative humidity of the environment is assumed to be 85%. Creep starts three days after casting. Figures 3.10 and 3.11 show the variation curves of the creep and shrinkage coefficients in concrete obtained with the AASHTO LRFD Specification 2017.

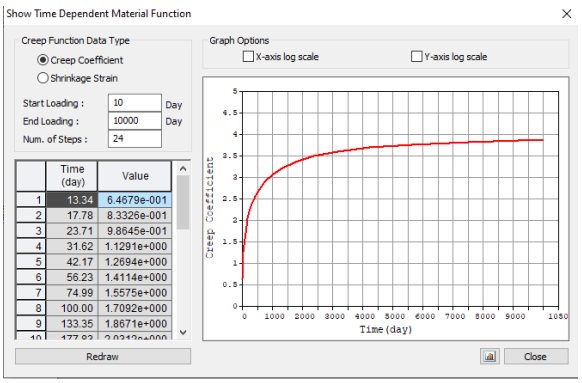

Figure 3.10. Creep function.

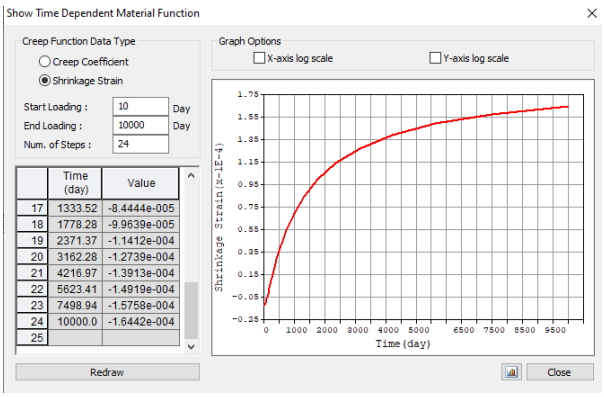

Figure 3.11. Shrinkage function.

From Figure 3.11 it can be concluded that the shrinkage coefficient at $t = \infty$ is given by $\varepsilon_{cs} = -1.6442x10^{-4}$ and $\rho = 3.87896$

3.3.6. Prestress loads

Our bridge is a post tensioned girder bridge. So, a Prestress Load of 1288 MPa is applied to every single tendon of the bridge. It should also be noted that this force is applied after the girder concrete is casted.

3.4. Diagrams of solicitations

After application of the various loads, analysis was performed and the girder having the maximum Shear, Axial and Moment diagram was chosen. A detail analysis of this girder was performed together with the calculation of the loss of prestress force.

Figure 3.12 shows a transverse arrangement of the bridge and the circled girder is the critical girder with which detail analysis would be performed.

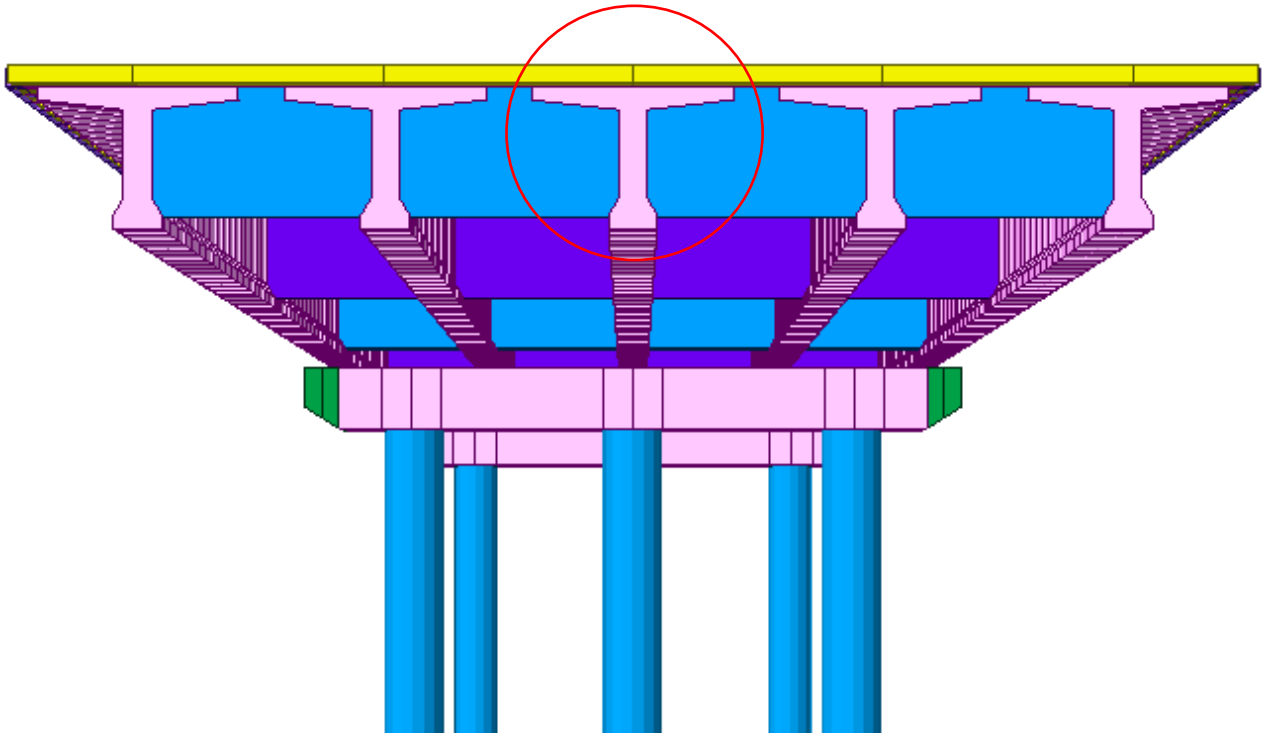

Figure 3.12. Bridge structure with critical girder.

The various load cases, their description together with the results are presented by Table 3.10.

Table 3.10. Solicitation description after construction stage analysis (Charbel et al., 2012).

Load Case	Results	Description
1. CS: Dead Load		Results due to all loadings excluding Erection Load and the effects of Creep, Shrinkage and Tendon Prestress
2. CS: Erection Load		Results due to dead loads, which are separated from CS: Dead Load, defined in Construction Stage Analysis Control Data dialog
3. CS : Tendon Primary	Reaction	
	Deformation	Deformation resulting from tendon prestress
	Force	Member forces resulting from tendon prestress
4. CS: Tendon Secondary	Reaction	Reactions caused by Tendon Prestress in an indeterminate structure.
	Force	Member forces caused by Tendon Prestress in an indeterminate structure.
5. CS: Creep Primary	Reaction	
	Deformation	Deformation due to imaginary forces required to cause creep stain
	Force	Imaginary forces required to cause creep stain
6. CS: Creep Secondary	Reaction	Reactions caused by creep in an indeterminate structure
	Force	Member forces caused by creep in an indeterminate structure
7. CS: Shrinkage Primary	Reaction	
	Deformation	Deformation due to imaginary forces required to cause shrinkage stain
	Force	Imaginary forces required to cause shrinkage stain
8. CS: Shrinkage Secondary	Reaction	Reactions caused by shrinkage in an indeterminate structure
	Force	Member forces caused by shrinkage in an indeterminate structure
CS: Summation	Reaction	1+2+4+6+8
	Deformation	1+2+3+5+7
	Force	1+2+3+4+6+8

3.4.1. Bending moment and shear diagrams due to self-weight

Figure 3.13 shows the moment and shear diagram of the girder due to the self-weight of the bridge.

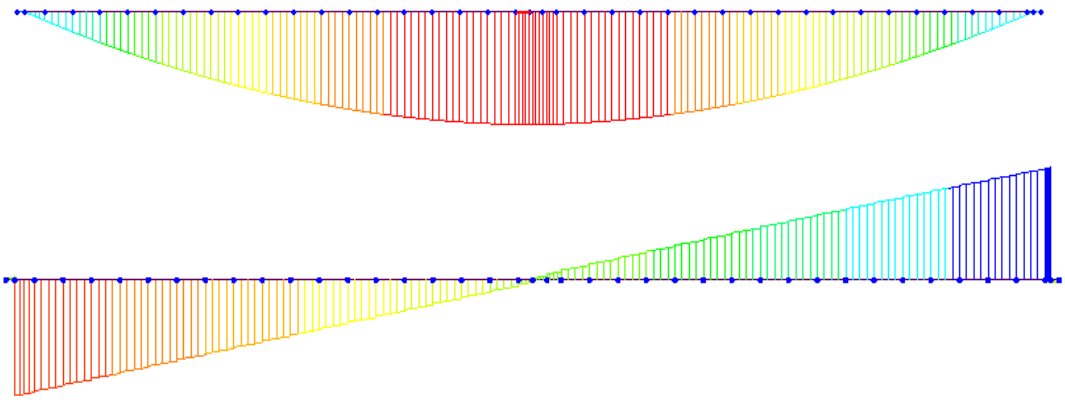

Figure 3.13. Bending moment and shear due to self-weight.

Maximum moment $M_{max} = 140.5\ kNm$

Maximum shear force $V_{max} = 26.1\ kN$

3.4.2. Bending moment and shear diagrams due to erection loads

Figure 3.14 shows the moment and shear diagram of the girder due to the erection loads.

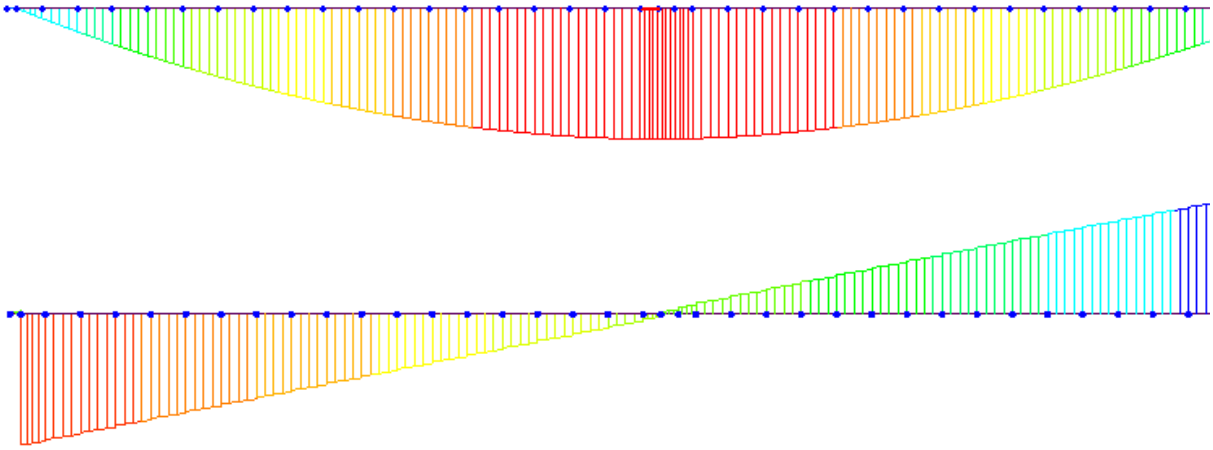

Figure 3.14. Bending moment and shear due to erection loads.

Maximum moment $M_{max} = 2984\ kNm$

Maximum shear force $V_{max} = 362.8\ kN$

3.4.3. Bending moment and shear diagrams due to the effect of creep.

Figure 3.15 and 3.16 shows the moment and axial diagrams of the girder due to the effect of concrete creep both primary and secondary respectively.

a) Creep primary

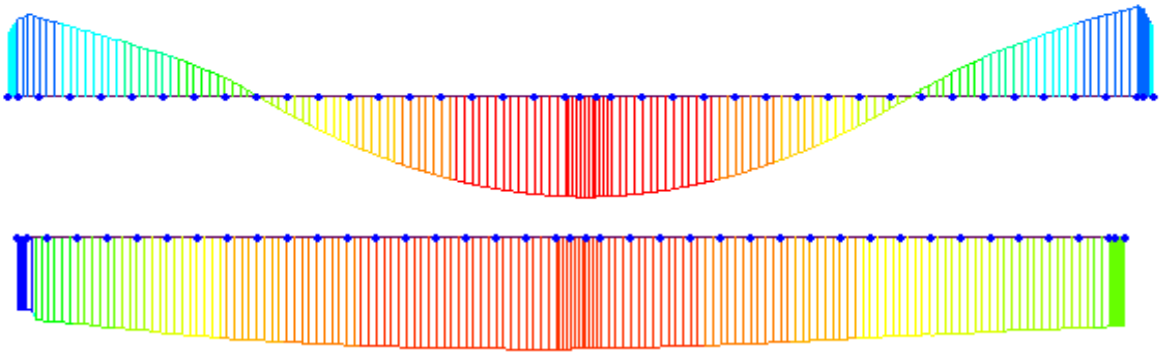

Figure 3.15. Bending moment and axial force due to creep primary.

Maximum moment $M_{max} = 7487\ kNm$

Maximum axial force $N_{max} = 8427\ kN$

b) Creep secondary

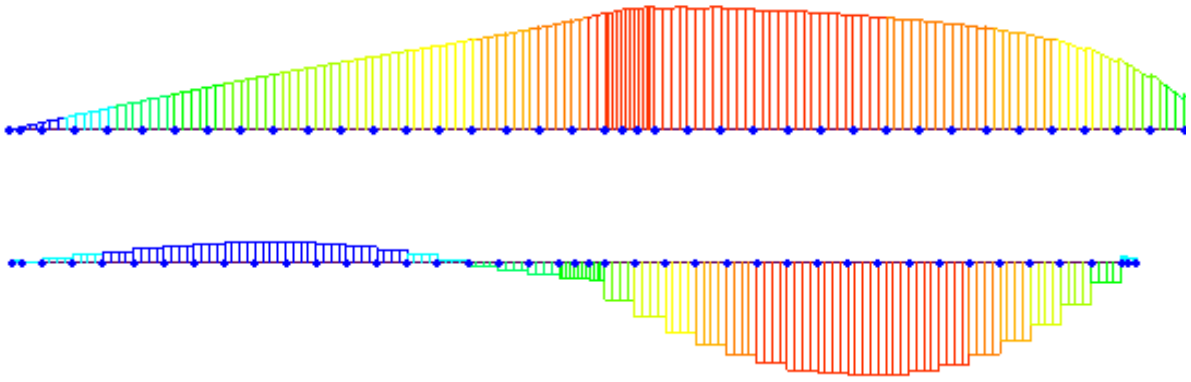

Figure 3.16. Bending moment and axial force due to creep secondary.

Maximum moment $M_{max} = 26.53$ kNm

Maximum axial force $N_{max} = 21.05\ kN$

3.4.4. Bending moment and shear diagrams due to shrinkage

Figure 3.17 and 3.18 shows the moment and axial diagrams of the girder due to the effect of concrete shrinkage both primary and secondary respectively.

c) Shrinkage primary

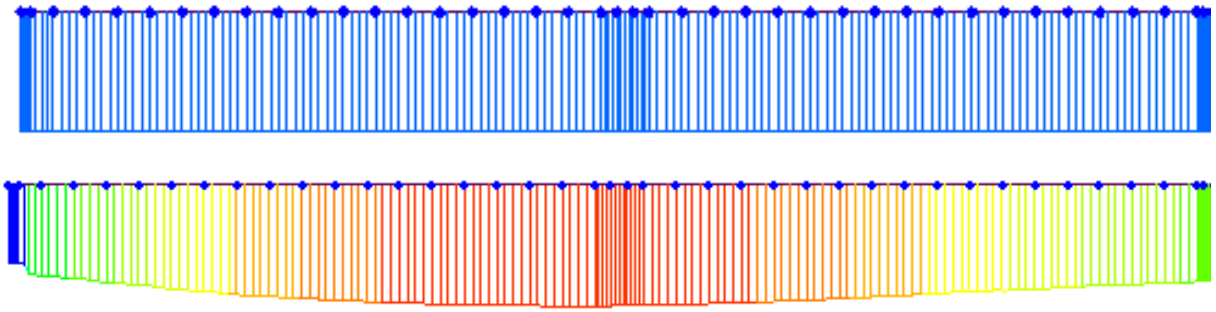

Figure 3.17. Bending moment and axial force due to shrinkage primary.

Maximum moment $M_{max} = 7487$ kNm

Maximum axial force $V_{max} = 8427\ kN$

d) Shrinkage secondary

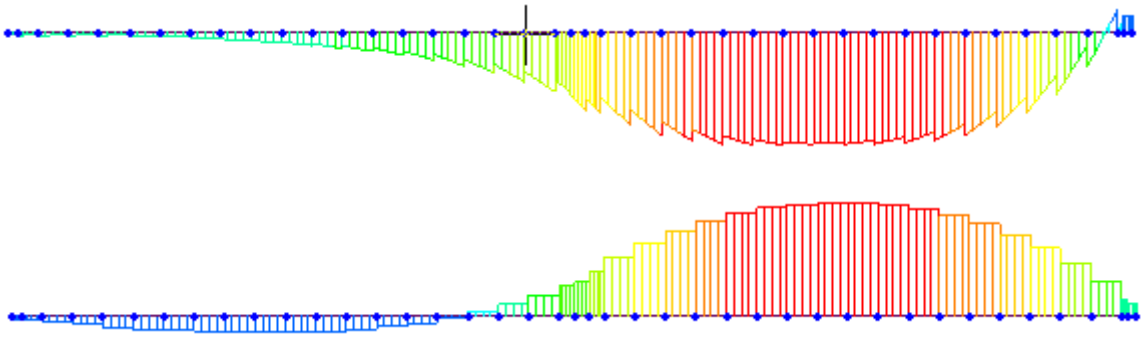

Figure 3.18. Bending moment and axial force due to shrinkage secondary.

Maximum moment $M_{max} = 159.5\ kNm$

Maximum axial Force $V_{max} = 337.8\ kN$

3.4.5. Bending moment and axial diagrams due to prestressing force in tendons

Figure 3.17 and 3.18 shows the moment and axial diagrams of the girder due to the prestressing force both primary and secondary respectively.

e) Tendon primary

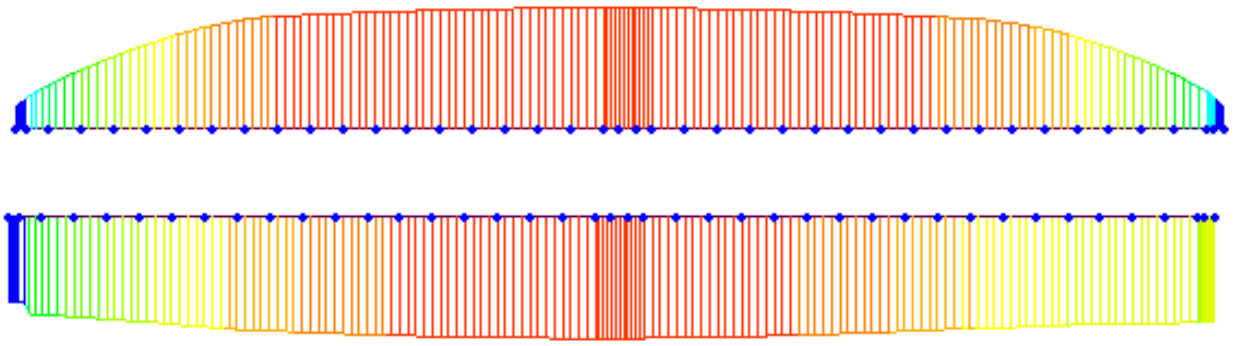

Figure 3.19. Bending moment and axial force due to tendon primary.

Maximum moment $M_{max} = 1718\ kNm$

Maximum axial force $V_{max} = 5202\ kN$

f) Tendon secondary

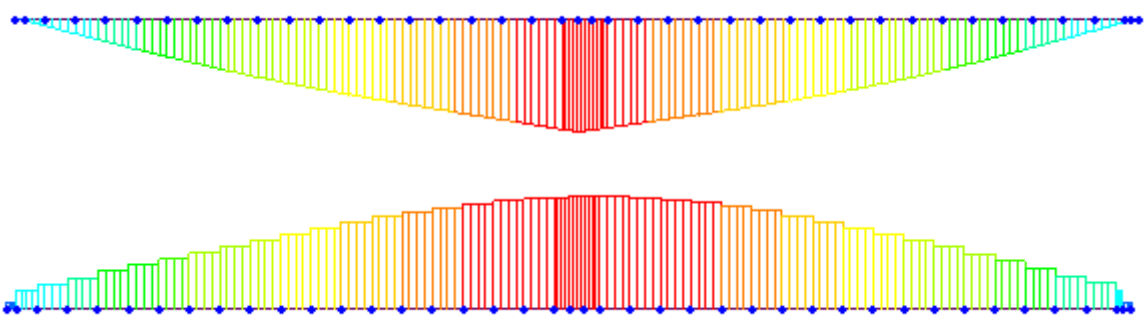

Figure 3.20. Bending moment and axial force due to tendon secondary.

Maximum moment $M_{max} = 25.3\ kNm$

Maximum axial force $V_{max} = 0.735\ kN$

3.4.6. Summation

Figure 3.21 shows the diagram of the moment, shear and axial diagrams due to the sum of effects of all the loads and at ultimate limit state.

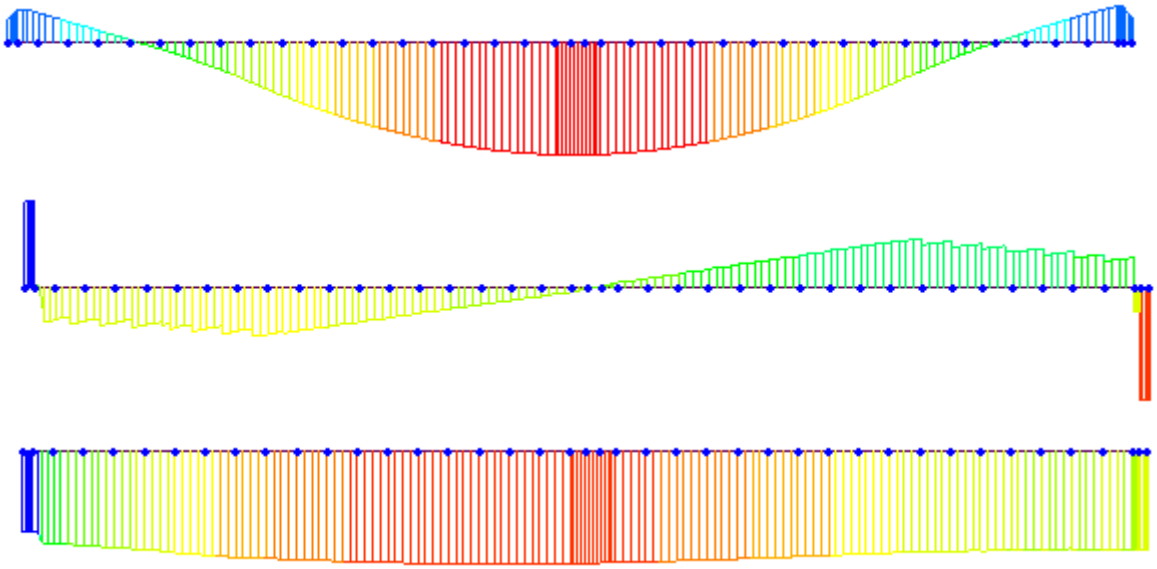

Figure 3.21. Summation of solicitation diagrams.

Maximum moment $M_{max} = 16809.221 kNm$

Maximum shear force $V_{max} = 96.5\ kN$

Maximum axial force $N_{max} = 5205\ kN$

3.5. Ultimate limit state verification of the beam

The ultimate limit state verification of a prestressed beam has to do with ultimate moment verification, Shear verification and Torsional resistance verification. The load combination used for this verification was ULS 1 from equation 2.8.

3.5.1. Check for flexural resistance

From ULS1 combination and from Figure 3.21, The applied bending moment $M_{ED} =$ 16809.221 KNm. The calculation of the ultimate resisting moment is summarized in Table 3.11.

Table 3.11. Check for flexural resistance.

Concrete compressive strength	f_{ck}	35	MPa
Concrete design strength	f_{cd}	19.83	MPa
Design strength of reinforcing steel	f_{yd}	434.78	MPa
Compression force for girder	$F_{c(g)}$	3488.35	KN
Compression force for slab	$F_{c(s)}$	4978.58	KN
Compression reinforcement force	$F_{s'}$	7179.75	KN
Tension force in reinforcement	F_s	3155.67	KN
Tension force in tendon	F_p	9005.40	KN
Depth of neutral axis	x	88.38	mm²
Area of Concrete stress brock for girder	$A_{ca(g)}$	22350	mm
Area of concrete stress block for slab	$A_{ca(s)}$	251021	mm²
Compression reinforcement areas	$A_{s'}$	31935.42	mm²
Tension reinforcement Areas	A_s	7258.05	mm²
Resistant Moment	M_{RD}	26166.95	MPa
Maximum applied moment	M_{ED}	16809.22	MPa
Check	$\boldsymbol{M_{RD} \geq M_{ED}}$	**VERIFIED**	

3.5.2. Check for shear resistance

The diagram for maximum shear force is shown in Figure 3.21 with a maximum applied shear of $V_{ED} = 96.5\ kN$. Figure 3.22 shows how the shear stresses vary along the girder and that all these stresses are found in the stress envelop.

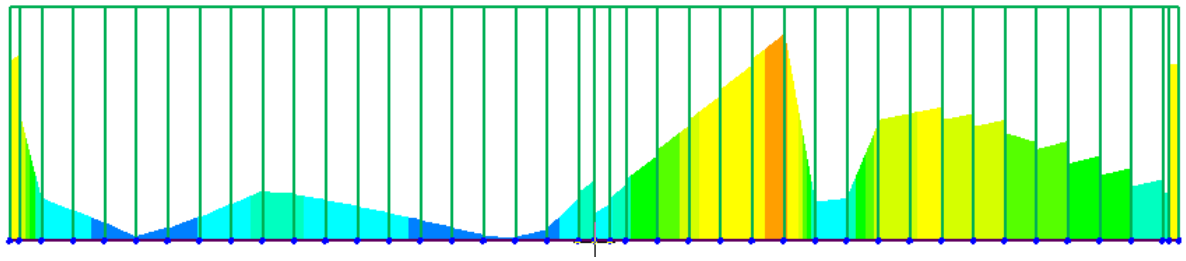

Figure 3.22. Shear envelope.

The shear resistance of concrete is summarised in Table 3.13. Table 3.12 presents the necessary parameters necessary for the shear resistance calculation.

Table 3.12. Parameters used for shear resistance check.

$C_{Rd,c}$	V_{min}	k_1	k	ρ_1	A_{sl}	b_w	d_p	σ_{cp}	N_{ED}	A_c
0.120	0.30	0.1	1.29	0.08	7258.05	400	2235	2.80	7424.8	2650988.57
					mm²	mm	mm	MPa	KN	mm²

Table 3.13. Check for shear resistance.

Design strength of concrete	f_{cd}	19.83	MPa
Design strength of reinforcing steel	f_{yd}	434.78	MPa
Flexural tensile stress	f_b	5.97	MPa
Design tensile stress of concrete	f_{ctd}	1.50	MPa
Design value for shear resistance	$V_{Rd,c}$	800.88	KN
Minimum shear resistance	$V_{Rd,min}$	649.70	KN
Maximum applied shear	V_{ED}	96.50	KN
Check	$\boldsymbol{V_{Rd,c} \geq V_{ED}}$	**VERIFIED**	

3.5.3. Check for torsional resistance

The torsional resistance of both the flange and the web section is summarised in Table 3.14.

Table 3.14. Check for torsional resistance of the girder flange and web.

Check for torsional resistance of flange			
Design strength of concrete	f_{cd}	19.83	MPa
Design strength of reinforcing steel	f_{yd}	434.78	MPa
Design tensile strength of concrete	f_{ctd}	1.50	MPa
Concrete tensile strength 5% fractile	$f_{ctk,0.05}$	1.40	MPa
Mean tensile resistance	f_{ctm}	2.70	MPa
Maximum applied torsion	T_{Ed}	5.79	KNm
Design value for torsional cracking moment	$T_{Rd,c}$	1032.13	KNm
Applied shear force	V_{Ed}	96.50	KN
Design value of shear resistance	$V_{Rd,c}$	800.88	KN
Check	$\frac{T_{Ed}}{T_{Rd,c}} + \frac{V_{Ed}}{V_{Rd,c}} = 0.06 \leq 1$	**VERIFIED**	
Check for torsional resistance of web			
Design strength of concrete	f_{cd}	19.83	MPa
Design strength of reinforcing steel	f_{yd}	434.78	MPa
Design tensile strength of concrete	f_{ctd}	1.50	MPa
Concrete tensile strength 5% fractile	$f_{ctk,0.05}$	1.40	MPa
Mean tensile resistance	f_{ctm}	2.70	MPa
Maximum applied torsion	T_{Ed}	5.79	KNm
Applied shear force	V_{Ed}	93.50	KN
Design value of shear resistance	$V_{Rd,c}$	800.88	KN
Design value for torsional cracking moment	$T_{Rd,c}$	1032.13	KNm
Check	$\frac{T_{Ed}}{T_{Rd,c}} + \frac{V_{Ed}}{V_{Rd,c}} = 0.122 \leq 1$	**VERIFIED**	

3.6. Serviceability limit state verification of the beam

The serviceability limit state verification aims at verifying the stresses at cross section, the tensile stress of prestressing tendons, checking for deflection and finally checking for cracking.

3.6.1. Stress at cross section

The stresses are checked both during the construction stage and during the service life of the bridge. Figure 3.23 Shows the stresses in the girder not only during the construction stages but also during the service life of the bridge. All the stresses are found in the stress envelop which has a green colour as shown in Figure 3.23.

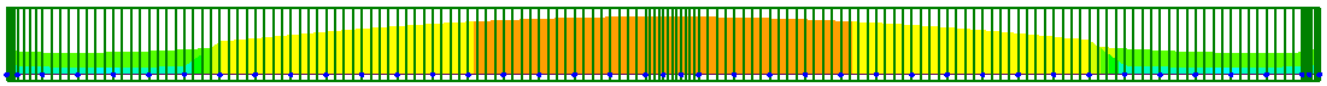

Figure 3.23. Stress envelope.

3.6.1.1. During the construction stages

The stresses are verified from the time of transfer of the prestressing force to the last construction stage (Construction stage 7). The stress verification check during the construction stages is summarised in Table 3.15.

Table 3.15. Stress verification during construction stages.

Combined stress due to bending moment about the major axis M_y and axial force at top fibre	FT	8.53	MPa
Combined stress due to bending moment about the major axis M_y and axial force at bottom fibre	FB	7.70	MPa
Combined stress due to bending moment about the major axis M_y, minor axis M_z and axial force at top left fibre	FTL	8.53	MPa
Combined stress due to bending moment about the major axis M_y, minor axis M_z and axial force at bottom left fibre	FBL	7.70	MPa
Combined stress due to bending moment about the major axis M_y, minor axis M_z and axial force at top right fibre	FTR	8.53	MPa
Combined stress due to bending moment about the major axis M_y, minor axis M_z and axial force at bottom right fibre	FBR	7.70	MPa
Maximum combined stress	FMAX	8.53	MPa
Allowable stress of cross section at construction stage	ALW	21.00	MPa
Check FMAX ≤ ALW	**Verified**		

For post tensioned members, the limiting stress ALW is given by

$$\text{ALW} = k_1 * f'_{ci} \qquad \textbf{(Eq. 3.1)}$$

Where;

$f'_{ci} = 35\ (MPa)$ with $k_1 = 0.6$

3.6.1.2. During the service life

The frequent combination has been used to check the stresses during the service life of the bridge. Table 3.16 presents the stress verification check of the bridge during its service life.

Table 3.16. Stress verification during the service life.

Combined stress due to bending moment about the major axis M_y and axial force at top fibre	FT	18.38	MPa
Combined stress due to bending moment about the major axis M_y and axial force at bottom fibre	FB	16.38	MPa
Combined stress due to bending moment about the major axis M_y, minor axis M_z and axial force at top left fibre	FTL	18.31	MPa
Combined stress due to bending moment about the major axis M_y, minor axis M_z and axial force at bottom left fibre	FBL	16.40	MPa
Combined stress due to bending moment about the major axis M_y, minor axis M_z and axial force at top right fibre	FTR	18.46	MPa
Combined stress due to bending moment about the major axis M_y, minor axis M_z and axial force at bottom right fibre	FBR	16.37	MPa
Maximum combined stress	FMAX	18.46	MPa
Allowable stress of cross section at construction stage	ALW	21.00	MPa
Check	**Verified**		

For post tensioned members, the limiting stress ALW is given by ALW = $k_1 * f'_{ci}$ where

$f'_{ci} = 35\ (MPa)$ with $k_1 = 0.6$

3.6.2. Tensile stress in prestressing tendons

The tension in the prestressing tendons is checked and results are displayed in Table 3.17.

Table 3.17. Tensile stress verification.

		Tendon 1	Tendon 2	Tendon 3	Tendon 4	
Stress in Tendons at anchorage	FDL1	1287.71	1287.70	1287.68	1287.64	MPa
Maximum stress in tendon after anchor set	FDL2	1287.42	1287.20	1287.35	1287.04	MPa
Maximum stress after all losses at last stage	FLL1	1201.62	1152.80	1194.87	1191.87	MPa
Allowable stress after anchor set at anchorage	AFDL1	1412.15	1412.15	1412.15	1412.15	MPa
Allowable stress after anchor set elsewhere	AFDL2	1333.70	1333.70	1333.70	1333.70	MPa
Allowable stress at service state after losses	AFLL1	1397.45	1397.45	1397.45	1397.45	MPa
Check $AFDL2 \leq AFLL1$		**Verified**	**Verified**	**Verified**	**Verified**	

3.6.3. Cracking verification

The combination used for cracking verification is the frequent combination 1.

$$F_d = G_k + P_k + \psi_{11} Q_{1k} + \sum_{i=2}^{i=n} \psi_{2i} Q_{ik} \qquad \textbf{(Eq. 3.2)}$$

The various cracking parameters as well as the results obtained after having verified the girder section for cracking is displayed in Table 3.18 and 3.19 respectively.

Table 3.18. Cracking verification parameters.

σ_s	$f_{ct,eff}$	α_e	$\rho_{\rho,eff}$	$A_p^{'}$	$A_{c,eff}$	x	k_t	ε_1	ε	$\emptyset_s$	$\emptyset_p$
469.63	3.210	5.86	0.086	6600	105000	265.1	0.6	0.518	0.500	43.002	80.211
MPa	MPa			mm²	mm²	mm					

k_1	k_2	k_3	k_4
0.8	0.5	3.4	0.425

Table 3.19. Cracking verification.

Bar equivalent diameter	$\emptyset$	43	mm
Applied axial force	N_{Ed}	19733.10	KN
Applied bending moment	M_{Ed}	16682.14	KNm
Concrete cover of longitudinal reinforcement	c	60	mm
Mean strain in concrete and reinforcement	$\varepsilon_{sm} - \varepsilon_{cm}$	2.1796E-03	
Maximum spacing of longitudinal bars	S_{limit}	407.5	mm
Actual spacing of longitudinal bars	S_{bar}	150	mm
Maximum crack spacing	$S_{r,max}$	289	mm
Crack width limit	$W_{k,max}$	0.2	mm
Actual crack width	W_k	0.15	mm
Check	$W_k \leq W_{k,max}$	**VERIFIED**	

3.7. Prestress losses computation

For the prestress losses computation in Midas civil, one girder of the first span of the bridge was chosen since all the girders have identical sections. This girder was chosen first because it's the most loaded girder of this span and this span is the first to be constructed. During the construction process, the construction of the other spans induces stresses and prestress losses in the girders of the first span. It is important to emphasize that accurate assessment of losses is not possible because of many uncertainties involved in the parameters governing loss calculations. Figure 3.24 shows the critical girder with the tendon arrangement inside. The first tendon is that having the smallest eccentricity.

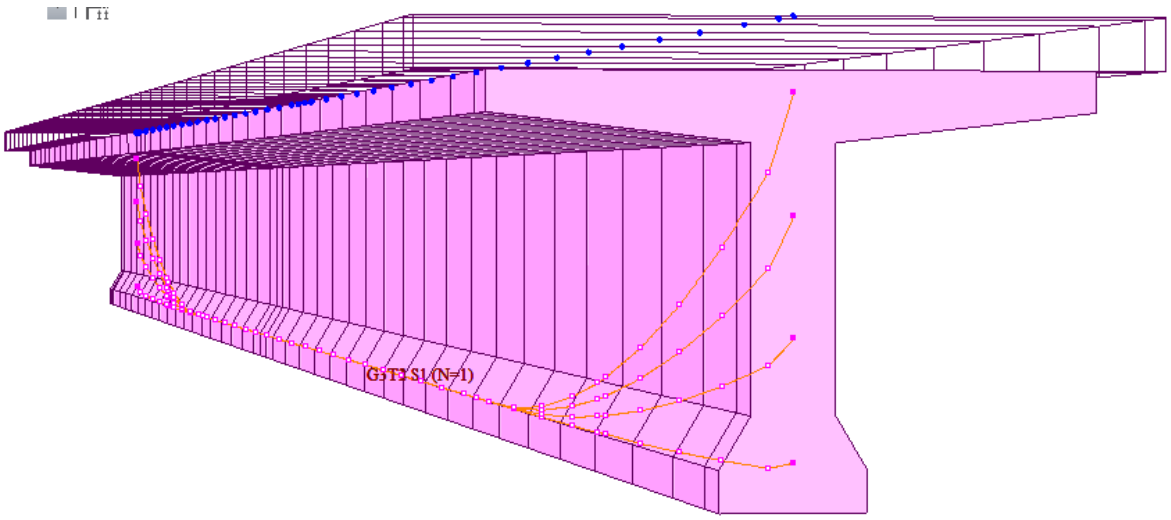

Figure 3.24. Critical girder with tendons.

3.7.1. Computation of prestress losses according to AASHTO LRFD specifications

3.7.1.1. Short term losses

Short term losses were computed after all the construction stages since the construction of other spans induces stresses and losses in the first span.

a) Loss due to friction

The frictional losses for the four cables are represented in Figure 3.24 below

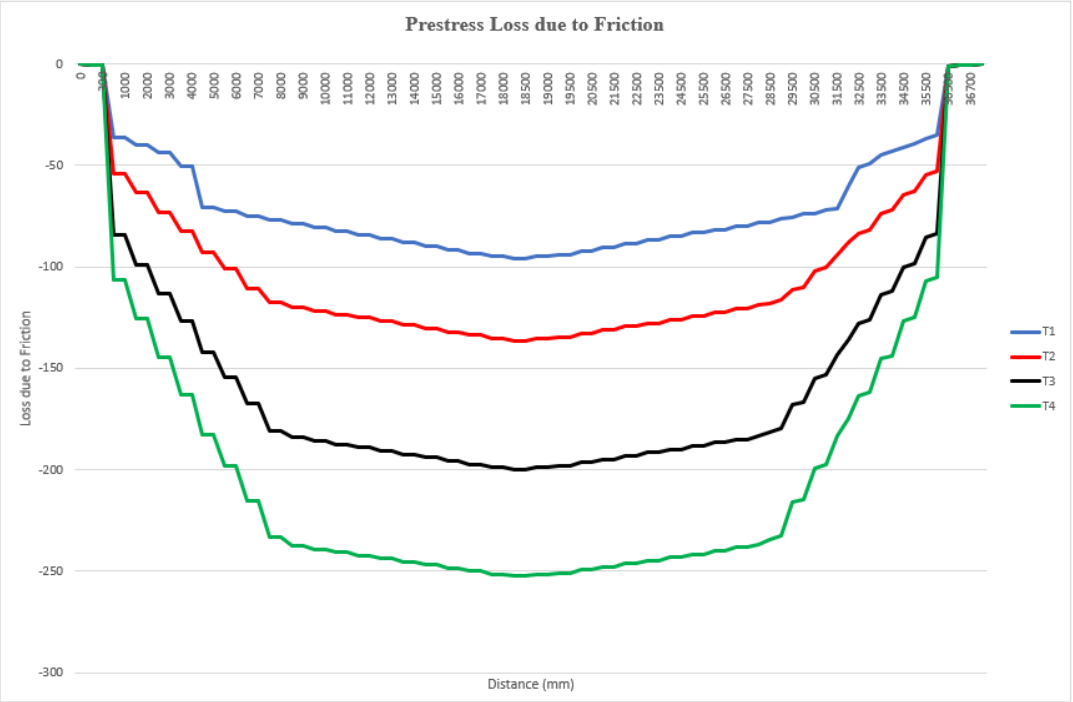

Figure 3.25. Prestress loss due to friction.

It can be concluded for Figure 3.24 that the loss due to friction is greatest in tendon 4. This is because tendon 4 has the greatest eccentricity. A summary of this loss quantity and their percentage can be seen in Table 3.20. From this table, it can be seen clearly that the friction losses increase from tendon one to tendon four.

Table 3.20. Percentage loss due to friction.

	Losses due to friction		
	Stress after loss (MPa)	Loss value	Percentage (%)
Tendon 1	1192.97	95.03	7.38
Tendon 2	1152.45	135.55	10.52
Tendon 3	1089.08	198.92	15.44
Tendon 4	1036.32	251.68	19.54

b) Loss due to anchorage seating

Anchorage setting losses in the four tendons are shown graphically in figure 3.26 It can be observed that the Loss due to anchorage setting is greatest in tendon 4 followed by tendon 3,

tendon 2 and finally tendon 1. This is as a result of a greater loss of friction per unit length in tendon 4 than in all the remaining tendons.

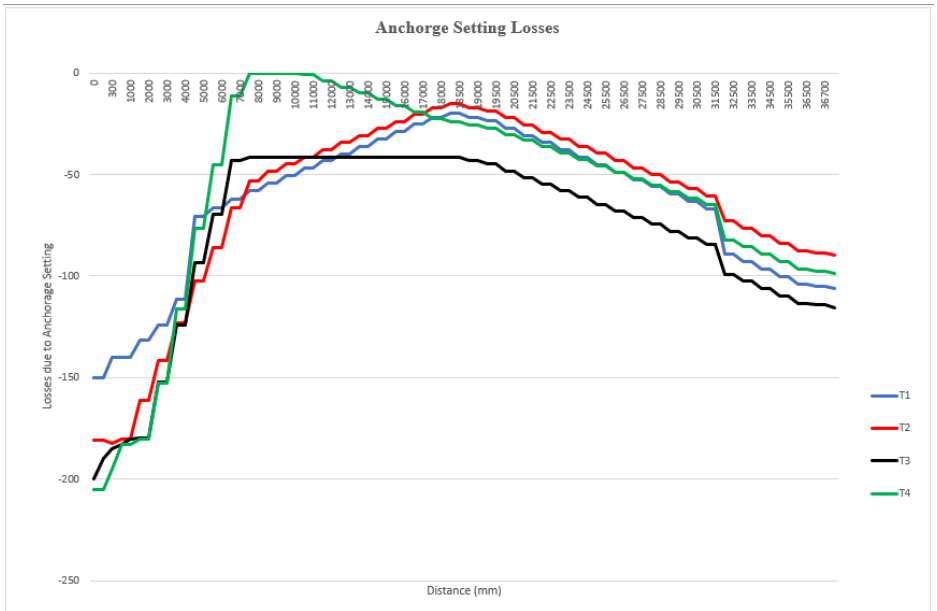

Figure 3.26. Prestress loss due to anchorage seating.

The percentage loss due to anchorage seating that occur in each tendon is illustrated in Table 3.21.

Table 3.21. Percentage loss due to anchorage seating.

	Losses due to Anchorage Slip		
	Stress after loss (MPa)	Loss value	Percentage (%)
Tendon 1	1138	37.5	11.65
Tendon 2	1105.7	45.5	14.15
Tendon 3	1088	50	15.53
Tendon 4	1083	51.25	15.92

c) Loss due to elastic shortening

The loss in prestress due to elastic shortening in the four tendons are shown graphically in Figure 3.27. Losses due to elastic shortening takes place in post tensioned members when the tendons are stressed sequentially. No elastic shortening loss will occur if only one tendon is

stressed. The loss in prestress due to elastic shortening in tendon 1 is as a result of tensioning of Tendon 2. This is the reason why the loss in elastic shortening in tendon 3 is zero since it's the last cable to be stressed. tendon 2 is the first cable to be stressed followed by tendon 1, then tendon 4 and finally tendon 3.

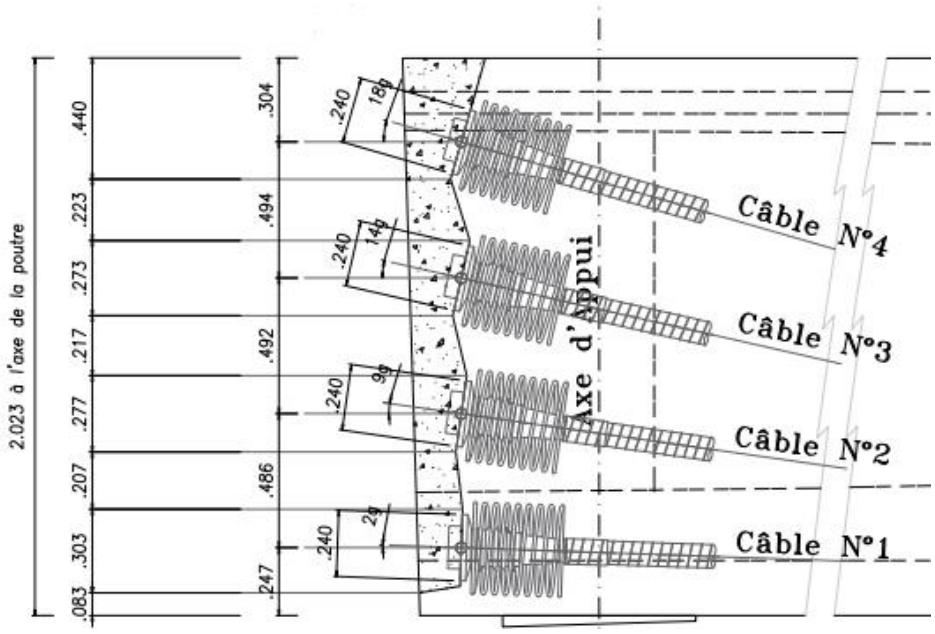

Figure 3.27. Prestressing tendons and eccentricities.

It can be concluded that the loss due to elastic shortening is greatest in tendon 2 due to the sequence of tensioning. Figure 3.28 illustrates the variation of elastic shortening losses with distance for the four tendons.

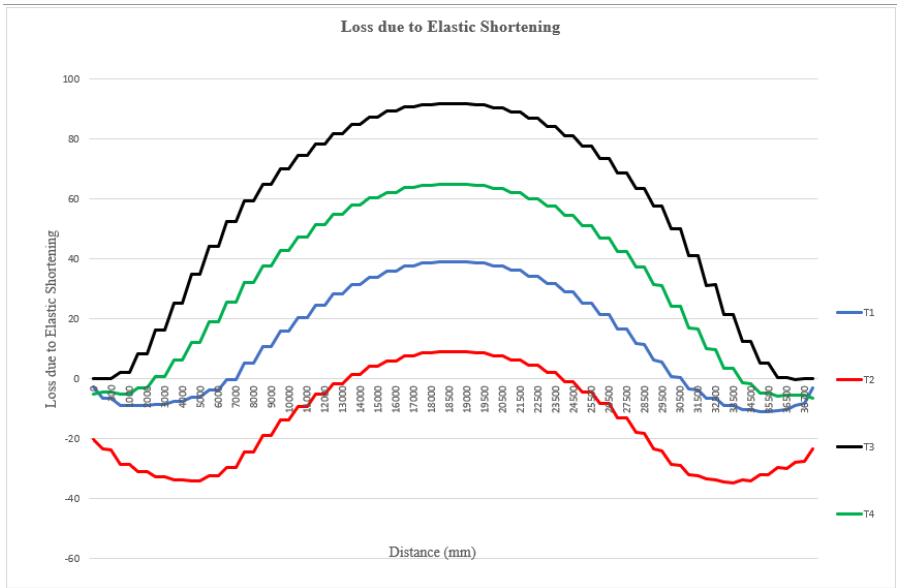

Figure 3.28. Prestress losses due to elastic shortening.

The percentage loss due to elastic shortening that occur in each tendon is illustrated in Table 3.22.

Table 3.22. Percentage loss due to elastic shortening.

	Losses due to Elastic Shortening		
	Stress after loss (MPa)	Loss value	Percentage (%)
Tendon 1	1248.93	39.07	3.03
Tendon 2	1279.01	8.99	0.70
Tendon 3	1196.13	91.87	7.13
Tendon 4	1222.98	65.02	5.05

3.7.1.2. Long term losses

The long-term losses were computed for a life span 100 years.

a) Losses due to tendon relaxation

The loss in prestress due to Tendon relaxation is shown graphically in figure 3.29. The first 2 tendons (tendon 1 and tendon 2) have the greatest losses. This is due to the fact that these two tendons are the first two tendons to be stressed. The tensioning of other tendons of the same beam or same span or even other spans induces stresses into these two tendons and consequently losses.

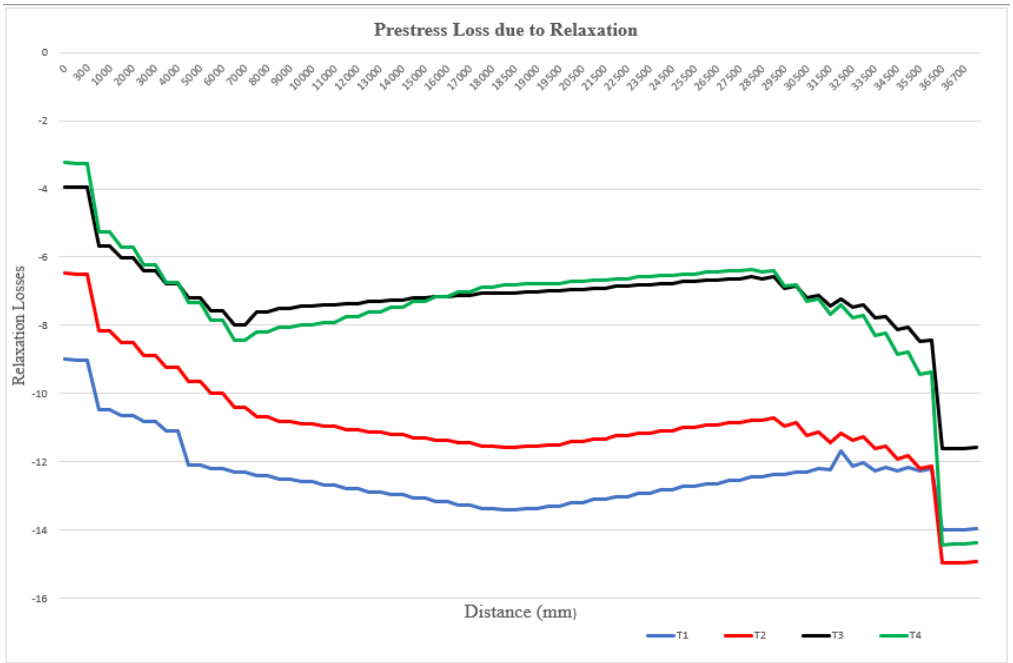

Figure 3.29. Prestress losses due to tendon relaxation.

The percentage loss of prestress due to tendon relaxation in each of the four tendons is represented in Table 3.23.

Table 3.23. Percentage loss due to relaxation of tendons.

	Losses due to Relaxation of tendons		
	Stress after loss (MPa)	Loss value	Percentage (%)
Tendon 1	1273.9977	14.0023	1.09
Tendon 2	1273.0344	14.9656	1.16
Tendon 3	1276.3864	11.6136	0.90
Tendon 4	1273.5759	14.4241	1.12

b) Prestress losses due to creep and shrinkage

The losses in prestress due to creep and shrinkage in every tendon are represented graphically in Figure 3.30. The software Midas Civil display the losses due to creep and shrinkage together. Figure 3.30 shows an initial increase in prestress losses and then a decrease in the losses till the 18.5m which is the midspan of the girder.

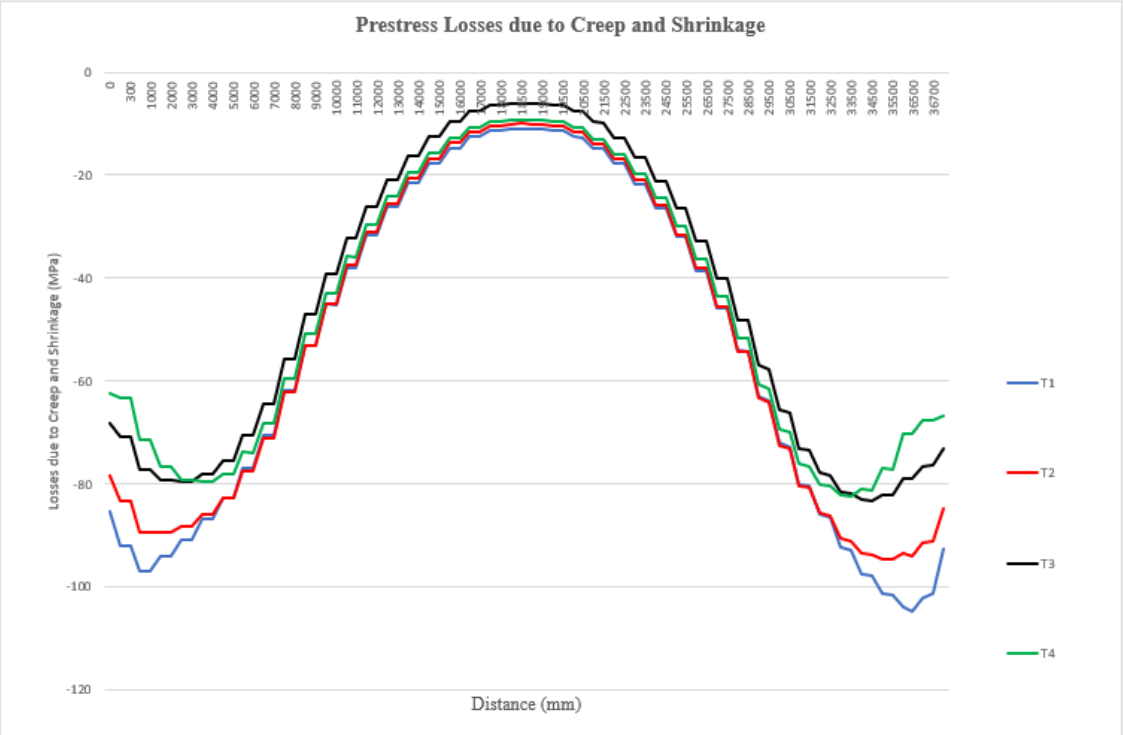

Figure 3.30. Prestress losses due to creep and shrinkage.

The percentage loss of prestress due to creep and shrinkage in each of the four tendons is represented in Figure 3.24.

Table 3.24. Percentage loss due to creep and shrinkage.

	Losses due to Creep and Shrinkage		
	Stress after loss (MPa)	Loss value	Percentage (%)
Tendon 1	1175.36	104.64	8.12
Tendon 2	1185.39	94.61	7.34
Tendon 3	1196.81	83.19	6.46
Tendon 4	1197.69	82.31	6.39

3.7.1.3. Summary table of all losses in every tendon

Table 3.25 provides a summary of all the loss types, their values and percentage for each of the four tendons.

Table 3.25. Summary of all losses.

		Friction	Anchorage Slip	Elastic Shortening	Tendon Relaxation	Creep and Shrinkage	Total
Tendon 1	Value	95.03	37.50	39.07	14.00	104.64	290.25
	Percentage (%)	32.74	12.92	13.46	4.82	36.05	
Tendon 2	Value	135.55	45.58	8.99	14.97	94.61	299.69
	Percentage (%)	45.23	15.21	12.01	4.99	31.57	
Tendon 3	Value	198.92	50.00	91.87	11.61	83.19	435.59
	Percentage (%)	45.67	11.48	21.09	2.67	19.10	
Tendon 4	Value	251.68	51.25	65.02	14.42	82.31	464.68
	Percentage (%)	54.16	11.03	13.99	3.10	17.71	

3.7.1.4. Pie chart for all losses in every tendon

The information of Table 3.25 is represented from Figure 3.31 to 3.34 for each tendon in the form of a pie chart in order for it to be read more easily

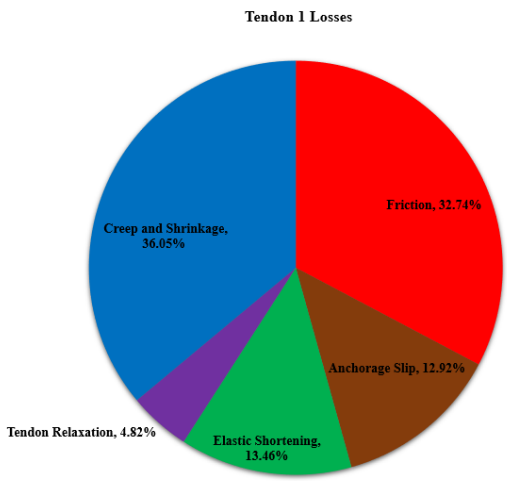

Figure 3.31. Percentage of each loss in tendon 1 with AASHTO.

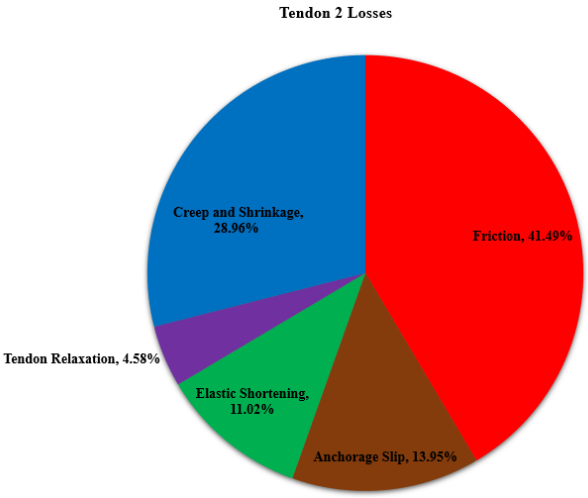

Figure 3.32. Percentage of each loss in tendon 2 with AASHTO.

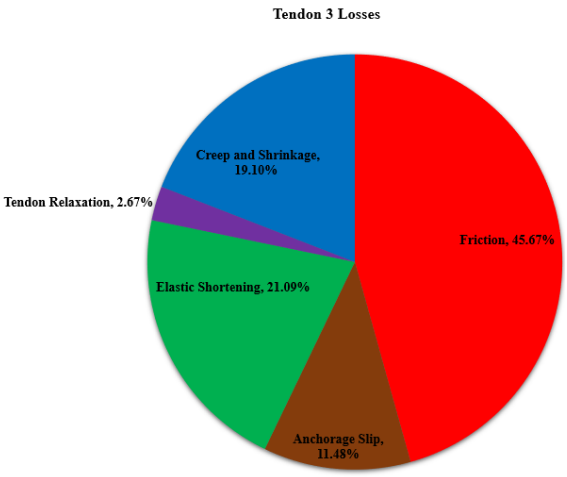

Figure 3.33. Percentage of each loss in tendon 3 with AASHTO.

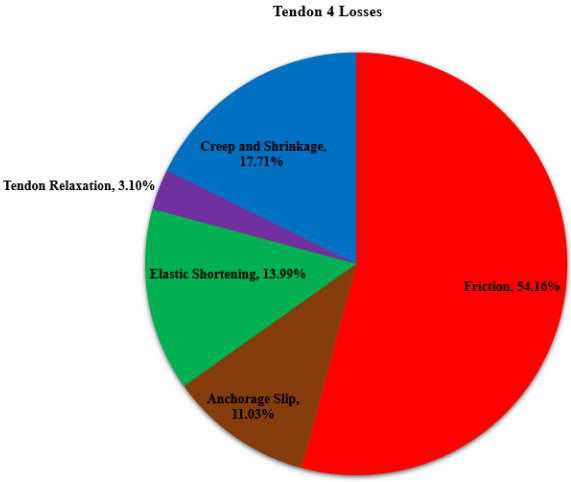

Figure 3.34. Percentage of each loss in tendon 4 with AASHTO.

From the above pie charts, the greatest percentage of prestress losses in post tension members are losses due to friction followed by losses due to creep and shrinkage. The smallest losses are those due to tendon relaxation.

3.7.2. Computation of prestress losses according to EN 1992-1-1:2004

The prestress losses computed by the method of the Eurocode are those that take place from the time of transfer till the end of the service life of the bridge. Eurocode does not divide the losses into that before, during and after the deck placement as it's the case with AASHTO LRFD.

3.7.2.1. Short term losses

a) Loss due to Friction

The losses in prestress due to friction calculated according to the Eurocode 2 are represented in Table 3.26.

Table 3.26. Prestress loss due friction with EN 1992-1-1:2004.

	Losses due to Friction		
	Stress after loss (MPa)	Loss value	Percentage (%)
Tendon 1	1218.71	69.29	5.38
Tendon 2	1190.95	97.05	7.54
Tendon 3	1146.85	141.15	10.96
Tendon 4	1109.47	178.53	13.86

b) Loss due to anchorage seating

The losses in prestress due to anchorage seating calculated according to the Eurocode 2 are represented in Table 3.27.

Table 3.27. Prestress loss due anchorage seating with EN 1992-1-1:2004.

	Losses due to anchorage seating		
	Stress after loss (MPa)	Loss value	Percentage (%)
Tendon 1	1116.21	15.65	13.34
Tendon 2	1087.21	20.53	15.59
Tendon 3	1073.37	25.23	16.66
Tendon 4	1054.50	28.35	18.13

c) Loss due to Elastic Shortening

The losses in prestress due to elastic shortening calculated according to the Eurocode 2 are represented in Table 3.28.

Table 3.28. Prestress loss due elastic shortening with EN 1992-1-1:2004.

	Losses due to elastic shortening		
	Stress after loss (MPa)	Loss value	Percentage (%)
Tendon 1	1252.17	35.83	2.78
Tendon 2	1282.16	5.84	0.45
Tendon 3	1196.13	91.87	7.13
Tendon 4	1224.53	63.47	4.93

3.7.2.2. Long term losses

The long-term losses (creep, shrinkage and tendon relaxation losses) calculated according to the Eurocode 2 are represented in Table 3.29.

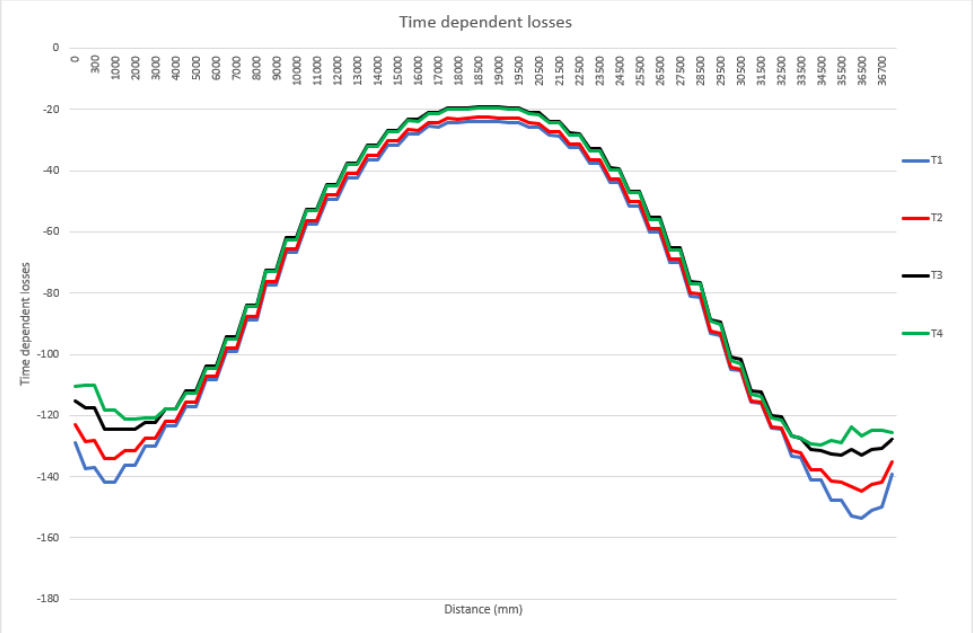

Figure 3.35. Long term losses by Eurocode.

The percentage of the long-term losses in each tendon is illustrated by Table 3.29.

Table 3.29. Long-term losses using EN 1992-1-1:2004 method.

	Losses due creep, shrinkage and tendon relaxation		
	Stress after loss (MPa)	Loss value	Percentage (%)
Tendon 1	1177.50	110.50	8.58
Tendon 2	1188.25	99.75	7.74
Tendon 3	1195.97	92.03	7.14
Tendon 4	1195.25	92.75	7.20

3.7.2.3. Summary table of all losses in every tendon

Table 3.30. Summary of all losses using EN 1992-1-1:2004 method.

		Friction	Anchorage slip	Elastic shortening	Creep shrinkage and relaxation	Total
Tendon 1	Value	62.29	15.65	35.83	110.50	224.27
	Percentage	27.78	6.98	15.97	49.27	
Tendon 2	Value	97.05	20.53	5.84	99.75	223.17
	Percentage	43.49	9.20	2.62	44.69	
Tendon 3	Value	141.15	25.23	91.87	92.03	350.27
	Percentage	40.30	7.20	26.23	26.27	
Tendon 4	Value	178.53	28.35	63.87	92.75	363.49
	Percentage	49.11	7.80	17.57	25.52	

3.7.2.4. Pie chart for all losses in every tendon

The information of Table 3.30 is represented from Figure 3.36 to Figure 3.39 for each tendon in the form of a pie chart in order for it to be read more easily

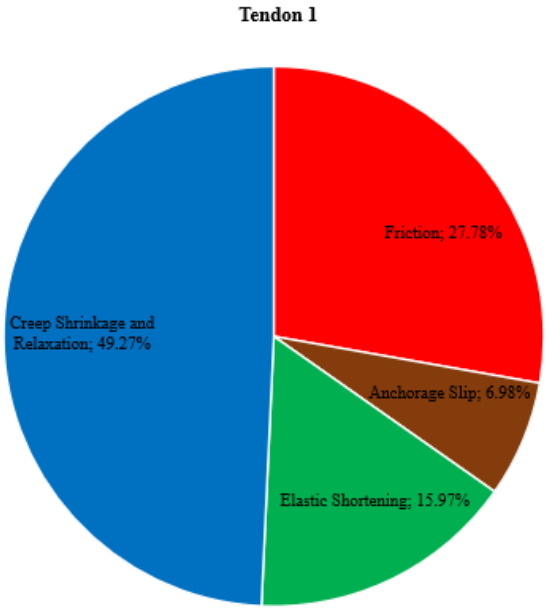

Figure 3.36. Percentage of each loss in tendon 1 with Eurocode.

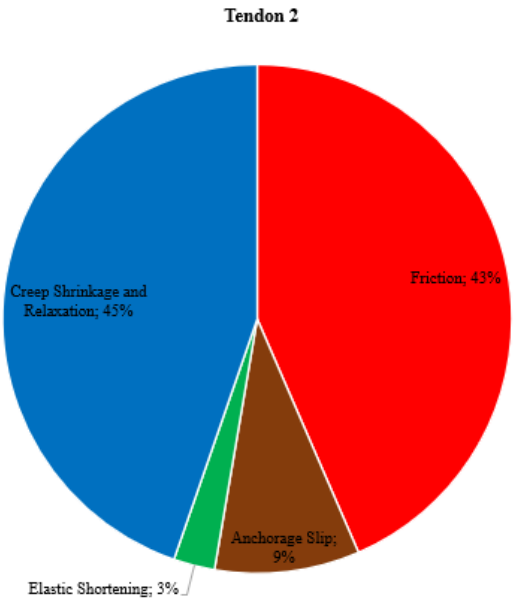

Figure 3.37. Percentage of each loss in tendon 2 with Eurocode.

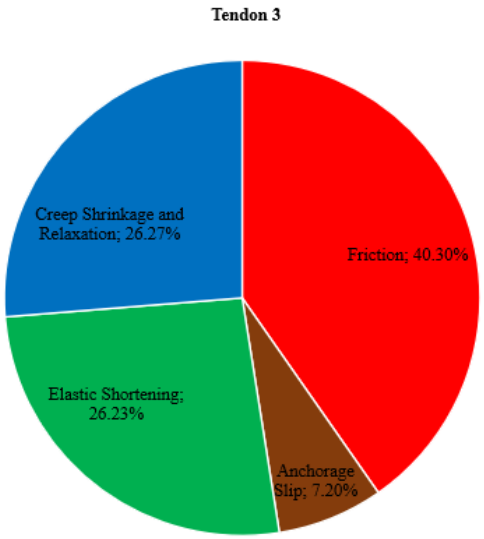

Figure 3.38. Percentage of each loss in tendon 4 with Eurocode.

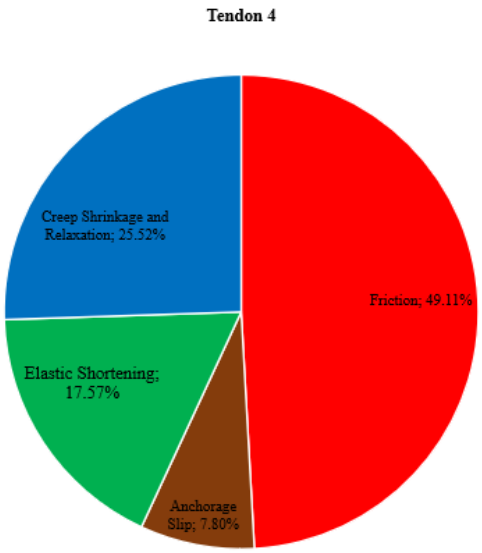

Figure 3.39. Percentage of each loss in tendon 4 with Eurocode.

From figure 3.36 to Figure 3.39, the greatest percentage of prestress losses in post tension members are losses due to friction and time dependent losses. The smallest losses are those due to anchorage seating.

3.8. Comparison between losses computed with AASHTO LRFD Specifications and those computed with EN 1992-1-1:2004

3.8.1. Comparison from a tabular presentation of results

The results obtained after the calculation of prestress losses using both the AASHTO LRFD Specifications and those computed with EN 1992-1-1:2004 are illustrated in Table 3.31 together with the percentage difference between the two methods in each of the four tendons.

Table 3.31. Difference in prestress losses between Eurocode and AASHTO.

		Friction	Anchorage Slip	Elastic Shortening	Long term	Total
Tendon 1	Eurocode	62.29	15.65	35.83	110.50	224.27
	AASHTO	95.03	37.50	39.07	118.65	290.25
	Difference (%)	20.81	41.10	4.33	3.55	8.82
Tendon 2	Eurocode	97.05	20.53	5.84	99.75	223.17
	AASHTO	135.55	45.58	8.99	109.58	299.69
	Difference (%)	16.55	37.88	21.20	4.70	9.63
Tendon 3	Eurocode	141.15	25.23	91.87	92.03	350.27
	AASHTO	198.92	50.00	91.87	94.80	435.59
	Difference (%)	16.99	32.92	50.00	1.49	10.86
Tendon 4	Eurocode	178.53	28.35	63.87	92.75	363.49
	AASHTO	251.68	51.25	65.02	96.73	464.68
	Difference (%)	17.00	28.77	0.89	2.10	12.22

From Table 3.31, the greatest difference in total losses between the two codes occur in tendon 4 which is 12 %. This is globally due to the use of different partial safety and strength reduction

factors interchangeably between the two codes. The different values in material properties are also one cause of this discrepancy.

3.8.2. Comparison from bar charts

The comparison between the two methods is done in this section in the form of a bar chart for each loss type.

3.8.2.1. Losses due to Friction

Figure 3.40 illustrates the difference between the losses due to friction obtained both with the AASHTO LRFD specification and the EN 1992-1-1:2004.

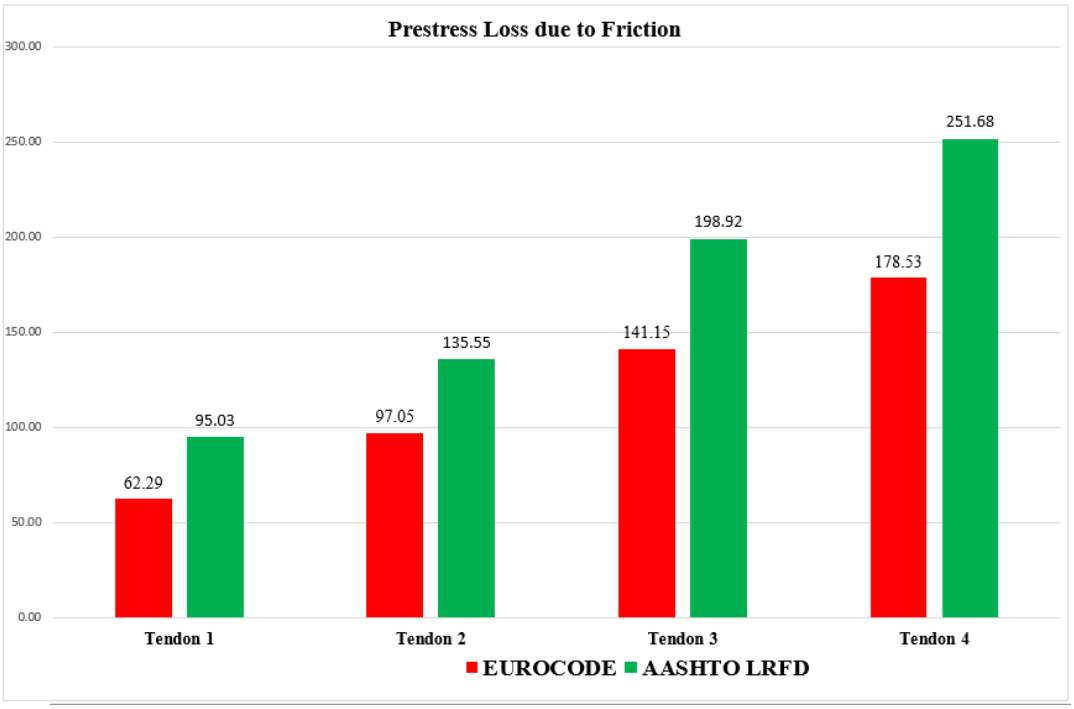

Figure 3.40. Comparison between friction losses obtained with Eurocode and that obtained with AASHTO method.

We notice from Figure 3.40 first that the losses due to friction for both codes increase as from tendon 1 to tendon 4. This increase is as a result of increase in eccentricity. Secondly, the losses provided by AASHTO LRFD Specifications are greater than those provided by EN 1992-1-1:2004 in every tendon. The greatest difference takes place in tendon 4 which is about 17 %. The major causes of these differences are that these two codes suggest friction loss formulas with some kind of differences. Furthermore, there exist significant differences in numerical values between the Wobble friction coefficient of the Eurocode 2 and that of AASHTO. Finally, the

losses provided by AASHTO are also greater and more accurate because it takes into account the friction losses during the construction stages and during the service life of the bridge.

3.8.2.2. Losses due to elastic shortening

Figure 3.41 illustrates the difference between the prestress losses due to elastic shortening obtained for each of the four tendons for the two methods.

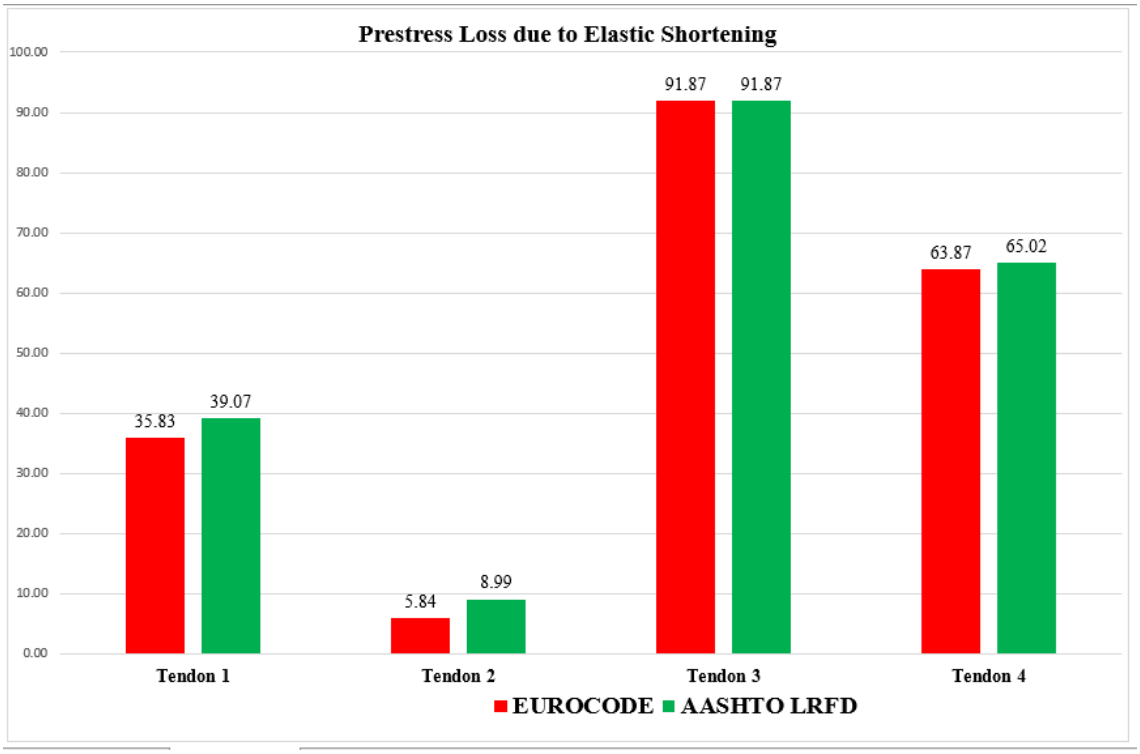

Figure 3.41. Comparison between losses due to elastic shortening obtained with Eurocode and that obtained with AASHTO method.

The slight differences between the values of the losses due to Elastic shortening computed with the two codes are due to the difference in the values of the modular ratios. The two codes have different elastic modulus of concrete at seven days. This is due to the different equations used in calculating the 7 days elastic modulus hence resulting in varying modular ratio. Both methods however give an accurate value for the losses due to elastic shortening. The greatest difference takes place in Tendon 1 which is about 4 % hence very insignificant.

3.8.2.3. Losses due to anchorage slip

Figure 3.42 illustrates the difference between the prestress losses due to anchorage slip for each of the four tendons for the two methods.

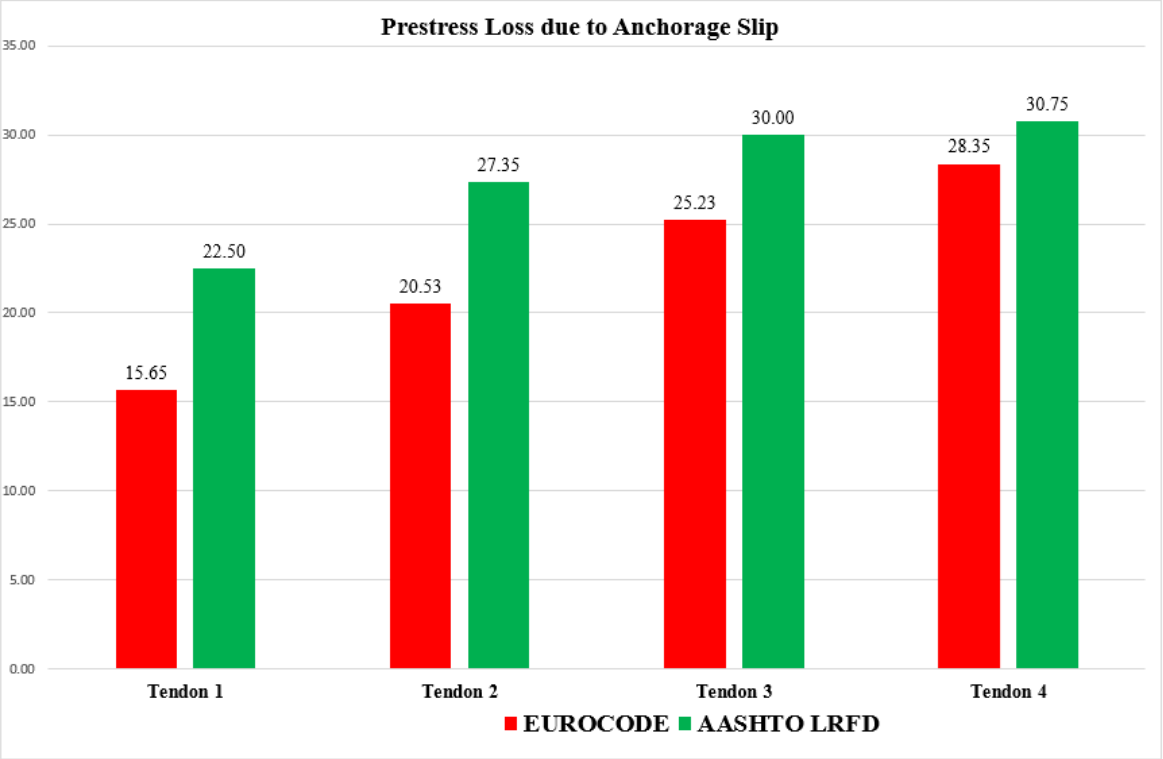

Figure 3.42. Comparison between anchorage slip losses obtained with Eurocode and that obtained with AASHTO method.

The losses due to anchorage slip are from Figure 3.42 Are increasing from the first to the last tendon for both Eurocode 2 and AASHTO. However, there is a great difference between the losses for each tendon. This is because the two codes adopt different material properties calculations which results to difference in anchorage seating losses. Also, the AASHTO takes into account the losses due to anchorage seating in a particular girder induced by the construction of other girders and other spans. The greatest difference is noticed in tendon 2 which is of the other of 14.27 %.

3.8.2.4. Time dependent losses

Figure 3.43 illustrates the difference between the time dependent losses for each of the four tendons for the two methods.

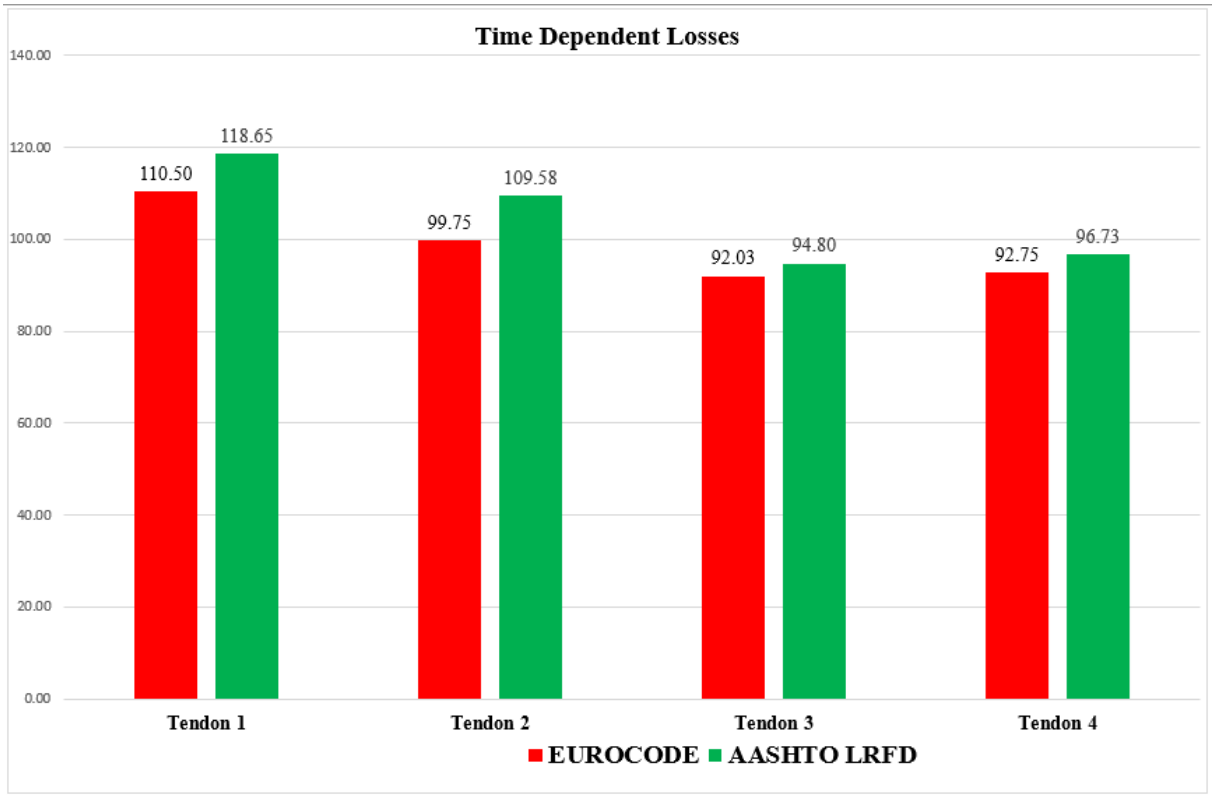

Figure 3.43. Comparison between time dependent losses obtained with Eurocode and that obtained with AASHTO method.

Figure 3.43 shows that both the AAHSTO LRFD and the Eurocode 2 both provide an accurate method for the determination of time dependent losses. The minor difference in losses in each tendon is due to the fact that the two codes use different design parameters. The design charts used to obtain the creep and shrinkage coefficient are different and the Eurocode 2 needs an ambient relative humidity to obtain a relevant creep coefficient. Concerning the difference in relaxation losses, the Eurocode 2 provides numerical data for maximum steel relaxation after 1000 hours but with the AASHTO, the duration coefficient, the stress coefficient and the annual temperature function are obtained beforehand. Also, the AASHTO uses a detailed procedure for computing time dependent losses not only before but also after the deck placement meanwhile the Eurocode 2 method was developed to determine the time dependent losses without having to break the life history of the beam into several time intervals. The greatest difference was to be 4.70 % in tendon 2.

3.9. Propositions to reduce prestress losses

3.9.1. Effects of variation of elastic modulus of concrete

The AASHTO LRFD Specification takes into account the variation of the modulus of elasticity with time. That is, it takes into account the effective modulus of elasticity of concrete which is an indirect function of the concrete creep coefficient. The modulus of elasticity is influenced by many factors such as the porosity and elastic modulus of hydrated cement, the porosity of aggregates, the concrete wetness condition, the mix proportion, the concrete age and the curing regime of the concrete. Figure 3.44 present the time dependent losses obtained after an increase of the elastic modulus while Table 3.32 presents the percentages of losses in each ten

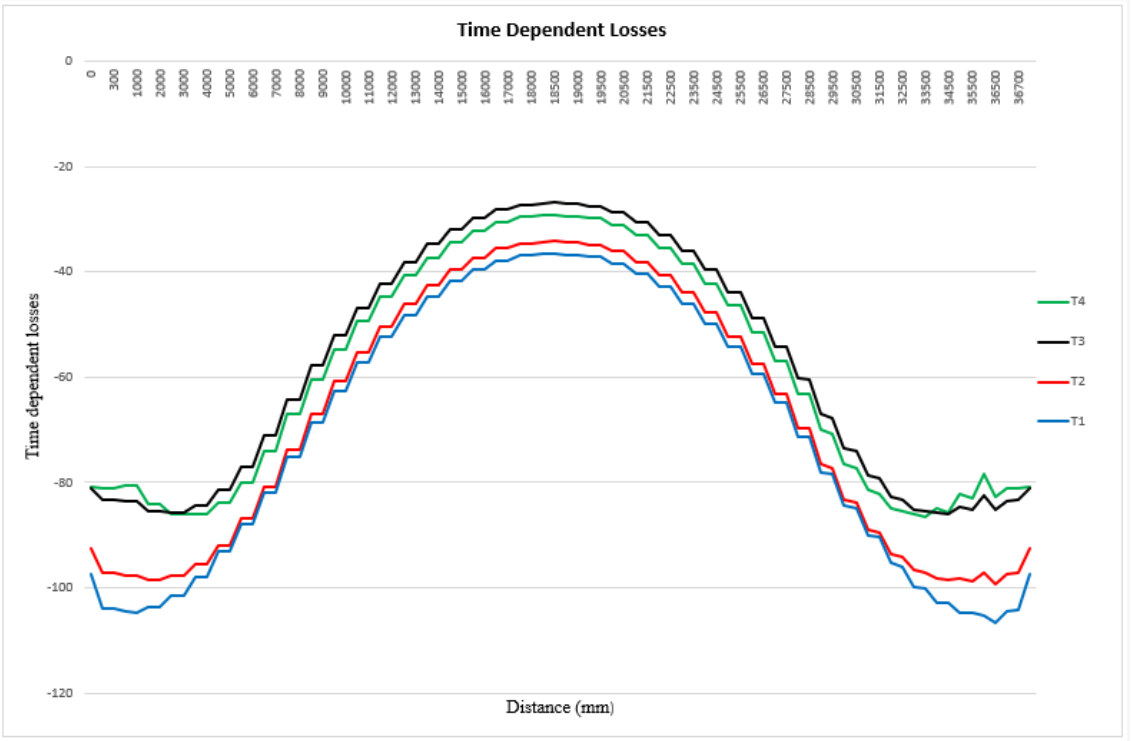

Figure 3.44. Time dependent losses after increasing the elastic modulus.

Table 3.32. Long term losses after increasing the elastic modulus.

	Losses due Creep, Shrinkage and Tendon relaxation		
	Stress after loss (MPa)	Loss value	Percentage (%)
Tendon 1	1213.32	74.68	5.80
Tendon 2	1218.43	69.57	4.50
Tendon 3	1223.46	64.54	3.01
Tendon 4	1236.00	52.00	2.04

The information of Table 3.32 is represented in Figure 3.45. It shows clearly the discrepancy between the prestress losses results obtained before and after the increase of the elastic modulus.

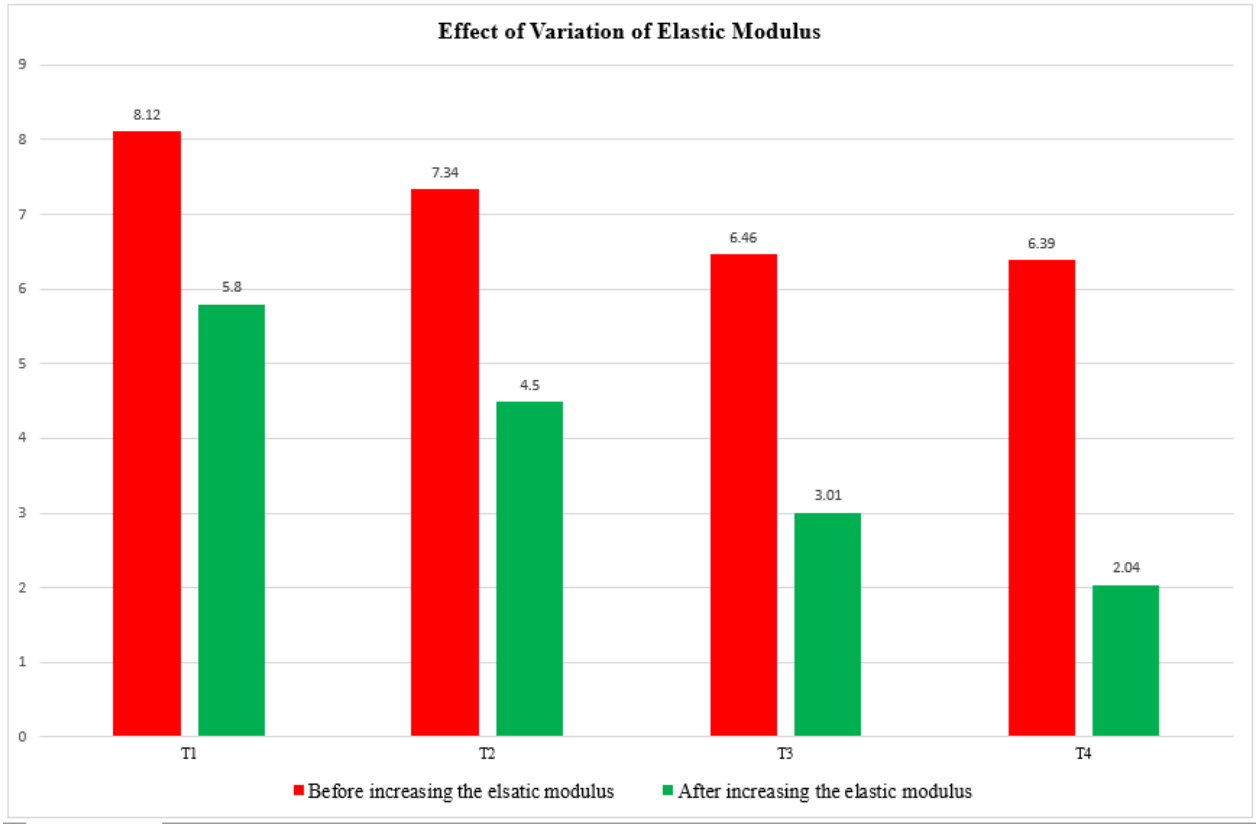

Figure 3.45. Comparison between the losses obtained before and after the increase of the elastic modulus.

Figure 3.45 Shows the effect of the variation of the elastic modulus on prestress losses. It can be concluded that an increase of the elastic modulus by 10 % reduces the prestress losses by 4.35 %

3.9.2. Effect of variation of the creep coefficient

The creep coefficient which is the ratio between the creep strain to the elastic strain is influenced by various factors such as the volume to surface ratio of the concrete member, the type and volume of aggregate, the age of concrete at the time of loading and the geometry of the concrete member. The AASHTO LRFD Specification accounts for the variation of the creep coefficient of the concrete. The reduction in the value of the creep coefficient increases the effective modulus and hence causes a reduction in creep effect and prestress loss. Figure 3.46 illustrates the effect of variation of the creep coefficient on prestress losses.

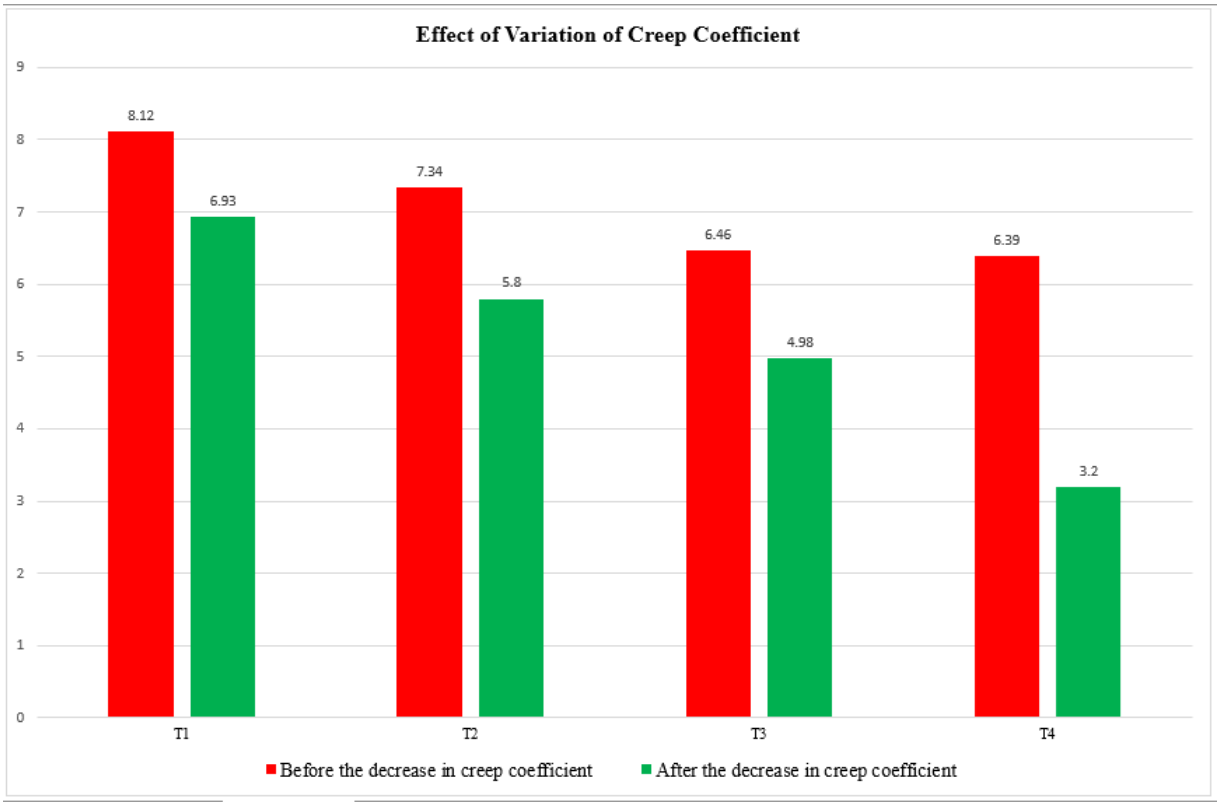

Figure 3.46. Comparison between the losses obtained before and after the decrease of the creep coefficient.

It can be noticed clearly that a 20 % decrease in the creep coefficient of concrete lowers the long-term losses by 3.19 %.

3.9.3. Effect of the addition of mild strands

Mild reinforcing are basic reinforcements of characteristic yield strength of 250MPa. They reduce prestress losses when included in prestressed concrete sections. As the concrete section shortens, whether through elastic shortening, creep, or shrinkage, the shortening causes additional compressive strains and stresses in the composite anchored mild reinforcing steel, thus redistributing the forces within a prestressed concrete cross section that actively resists the prestressing forces. The mild reinforcing steel provides an ever increasing “transformed” cross section that reduces the time-dependent shortening of the concrete section and thereby reduces the total prestress losses. Unfortunately, both the Eurocode 2 and the AASHTO don’t have a way to account for the inclusion of mild reinforcing steel. So, if one of these methods is used, including mild reinforcing steel has no effect on the estimated total prestress losses.

3.9.4. Effect of the addition of top prestressing strands

The effects of the addition of top prestressing in the prestress concrete bridges were analysed by adding two and four top strands to the beam cross section. The addition of the top strands reduces

the eccentricity of the prestressing force and thereby causes reduction in prestress loss when compared to the base case with no top prestressing strands.

3.9.5. Reduction of friction losses

In post tensioned members, the tendons are housed in ducts which may either be made of steel or plastic. On tensioning these strands, losses occur due to friction between the strands and the surrounding. There are principally two major effects that leads to losses due to friction.

- The curvature effect which mainly depends on the tendon form or alignment. This effect can be reduced by reducing the eccentricity of tendons or by changing the form of the tensons from a circular path to a trapezoidal path.
- Loss due to the wobble effect which depends upon the local deviations in the alignment of the cables. This loss effect can be reduced by taking precautions during construction in other to ensure the correct alignments of the duct and of the tendons.

Friction losses can also be reduced by jacking the tendons from both ends of the beam, over tensioning the tendons by an amount equal to the maximum friction loss. Finally, Emulsifiable oils (oils containing emulsifiers like lecithin) can also be used in post tensioned construction to reduce the losses and to provide temporary corrosion protection for tendons.

Conclusion

The main aim of this chapter was to evaluate prestress losses of the critical member of a post tensioned prestressed bridge using both the AASHTO LRFD 2017 Specifications and the EN 1992-1-1:2004, to compare the results provided by both methods and finally to propose solutions for the reduction of these losses. A general presentation of the site based on its geographical location, its geology, its climate, its hydrology and socio-economic activities was conducted. After running the construction stage analysis, the numerical model was validated followed by the analytical results. With the validated model, verifications were carried out both at ultimate and at serviceability limit state. Prestress loss results were next presented detailly and for both methods. Both methods revealed that more than 50 % of prestress losses are friction losses followed by time dependent losses. Reporting the performance of each method and comparing them, a difference in prestress losses calculated using the two methods is noticed. A difference of 17 % for losses due to friction, 4 % for losses due to elastic shortening, 14.42 % for anchorage seating losses and 4.70 % for time dependent losses is noticed. These discrepancies are due to the fact that the design parameters incorporated by these two codes are different. Furthermore, some solutions are proposed for the reduction of prestress losses. For an increase of the elastic modulus by 10 %, a decrease in prestress losses by 4.35 % was noticed and for a reduction of the creep coefficient by 20 %, a reduction of the prestress losses by 3.19 % was noticed.

GENERAL CONCLUSION

Haven come to the end of the study entitled “Loss of preload in prestressed bridge cables”, the main objective is first recalled. It was to reduce prestress losses in prestressed concrete bridges. In order to achieve this objective, prestress losses were evaluated using both the AASHTO LRFD 2017 Specifications and the EN 1992-1-1:2004. The results obtained using both norms were compared and solutions were proposed for prestress losses reduction. This work was structured around three chapters. The concept of prestressed concrete technologies in chapter 1 was reviewed, the methodology to be used in chapter 2 was presented. The structure with the help of the computer program Midas Civil 2022 (v 1.2) was modelled, analyzed and results shown in chapter 3. The following conclusions could be drawn from this study: firstly, the stress limits at all the stages of life and the deformation at the critical phases of the prestressed beam were below the limits, thus satisfactory. Secondly, the numerical results of prestress losses for both methods showed a good similitude. Using the AASHTO LRFD specifications, approximately 50 % of prestress losses were frictional losses, 30 % were time dependent losses (losses due to creep, shrinkage and tendon relaxation), 13 % of the losses were due to elastic shortening and about 7 % were due to anchorage slip. Regarding the Eurocode, approximately 45 % of prestress losses were frictional losses, 35 % were time dependent losses, 12 % were losses due to elastic shortening and 8 % of the losses are due to anchorage slip. The main reasons for these great differences between these two methods were linked to the fact that the design parameters incorporated by both methods are different. The material properties, modular ratio, the creep, shrinkage and friction coefficients as well as the partial safety and strength reduction factors are all different. The AASHTO LRFD 2017 specifications provided more accurate results because it does not only take into account the time dependent material properties and the age modulus of concrete but provides more detail results on the loss of prestress not only during the construction stage of the structure but also during its service life. This norm has an overall better performance and reliability, but comes with more complex equations and demands more time for prestress losses calculations. After detail analysis of the critical element, it was noticed that increasing the elastic modulus by 10 % and decreasing the creep coefficient by 20 % reduced prestress losses by 4.35 % and 3.19 % respectively. The lack of experimental results to verify the accuracy of the numerical model appeared as a limit to the effectiveness of the current thesis.

As perspective, since both norms don’t consider the effect of the addition of mild strands or top prestressing strands on prestress losses, further research has to be conducted in order to determine what magnitude of prestress losses can be reduced by adopting these two methods.

BIBLIOGRAPHY

Anania, L., Badalà, A., & D'Agata, G. (2018). Damage and collapse mode of existing post tensioned precast concrete bridge: The case of Petrulla viaduct. *Engineering Structures*, *162*, 226–244. https://doi.org/10.1016/J.ENGSTRUCT.2018.02.039

Aziz, H. Y., Ma, J., Mohammed, A. A., & Liu, N. (2011). Design of substructure bridge with different codes and analysis manually and by using plaxis program 3D. *ICTE 2011 - Proceedings of the 3rd International Conference on Transportation Engineering*, *41184*(March 2020), 1517–1523. https://doi.org/10.1061/41184(419)251

Bald, R. E., Crom, J. M., Crowley, F. X., Doull, R. M., Feeser, L. J., Heger, F. J., & Willett, J. a. (1997). *ACI 373R-07 - Design and Construction of Circular Prestressed Concrete Structures*. 657–672.

Bhuiyan, I. H., Amin, A., Riyad, R. H., & Sadi, R. (2021). *Structural Analysis of Pre-tensioning and Post-tensioning Concrete with Normal Concrete Beam*. *September*.

Boukendakdji, M., Touahmia, M., & Achour, M. (2017). Comparative Study of Prestress Losses. *Engineering, Technology & Applied Science Research*, *7*(3), 1633–1637. https://doi.org/10.48084/etasr.1172

Brenkus, T. G., & Natassia. (2021). Durability of Anchorage Pour-backs and Improvements Prepared by : *ODOT Research Reports*, *FHWA/OH-2021-02*.

Bymaster, J. C., Dang, C. N., Floyd, R. W., & Hale, W. M. (2015). Prestress losses in pretensioned concrete beams cast with lightweight self-consolidating concrete. *Structures*, *2*(January), 50–57. https://doi.org/10.1016/j.istruc.2015.01.003

Charbel, F. T., Debrun, G., & Webinar, A. (2012). *midas Civil Contents :*

Cho, K., Cho, J. R., Kim, S. T., Park, S. Y., Kim, Y. J., & Park, Y. H. (2016). Estimation of prestress force distribution in multi-strand system of prestressed concrete structures using field data measured by electromagnetic sensor. *Sensors (Switzerland)*, *16*(8). https://doi.org/10.3390/s16081317

Choudhary, K., & Akhtar, S. (2019). Application of partial prestressing for crack control in reinforced concrete structures. *AIP Conference Proceedings*, *2158*(September).

https://doi.org/10.1063/1.5127151

Craig, J. (2018). Atlantic Bridge. *Atlantic*, 235–251.

EN-1992-1-1_2. (2009). *Partie 1-1 : Règles générales et règles pour les bâtiments*. *33*(0).

EOTA. (2016). *Post-Tensioning Kits for Prestressing*. *September*.

fib. (2004). *Precast concrete bridges, fib Bull.29*. Federation Internationale du Beton.

Gilbert, R. I., Mickleborough, N., & Ranzi, G. (2013). *Design of Prestressed concrete according to Eurocode 2* (Vol. 53, Issue 9).

Giovanni, F. (2017). *Effetti del degrado sul comportamento strutturale di elementi in c . a . p .* 1–6.

Gosaye, J., & Kaba, F. (2015). *Behaviour and design of prestressed steel structures*. *February*.

Hassoun, M. N. A.-M. (2012). *Structural Concrete Theory and Design (Vol. 91, Issue 5,P.1067*.

Hewson, N. (2007). Balanced cantilever bridges. *Concrete (London)*, *41*(10), 59–60.

Hewson, P. C. (2011). *Prestressed concrete in bridgeworks*. https://doi.org/10.1680/pcb.41134.001

HÖKELEKLİ, G. (2016). (May), 31–48. http://etd.lib.metu.edu.tr/upload/12620012/index.pdf

Insight, B. (2021). *midas Bridge Elastomeric Bearings for Bridges : Stiffness and Tips for Modeling Table of Contents Elastomeric Bearings for Bridges : Stiffness and Tips for Modeling*. 1–16.

Jayaseelan, H. (2019). *Prestress losses in concrete and the estimation of long-term deflections and camber for prestressed concrete bridges [electronic resource] /. June*.

Kim, S. H., Park, S. Y., Kim, S. T., & Jeon, S. J. (2022). Analysis of Short-Term Prestress Losses in Post-tensioned Structures Using Smart Strands. *International Journal of Concrete Structures and Materials*, *16*(1), 1–15. https://doi.org/10.1186/s40069-021-00488-3

Kim, S. T., Park, S. Y., Kim, Y. J., & Park, Y. H. (2017). *Construction Stage Analysis*. 1–20.

Magnel, G. (1950). Prestressed steel structures. *The Structural Engineer*, *28*, 285–295.

Members, P. S., & Connor, J. J. (2001). *Structural Applications and Feasibility of Certified by*.

Menn. (1990). In *Gastronomía ecuatoriana y turismo local.* (Vol. 1, Issue 69).

Mohandoss, P., Kompella, S. K., & Pillai, R. G. (2019). Bond performance of pretensioned concrete systems. *Lecture Notes in Civil Engineering*, *11*(December), 277–286. https://doi.org/10.1007/978-981-13-0362-3_22

Naaman, A. E., & Ph, D. (1983). Prestressed concrete analysis and design: Fundamentals. *International Journal of Cement Composites and Lightweight Concrete*, *5*(2), 139. https://doi.org/10.1016/0262-5075(83)90035-0

Naito, Guppy, K. H., Ph, D., Charbel, F. T., Debrun, G., & Al, E. T. (2018). *H Emodynamic E Valuation of B Asilar*. *51*(2), 327–334.

Raymond I. G., Neil C. M., G. R. (2017). *Design of prestressed Concrete to Eurocode 2 Second Edition*. CRC press.

Schacht, G., & Marx, S. (2014). *Concrete Hinges – Historical development and contemporary Use CONCRETE HINGES – HISTORICAL DEVELOPMENT AND*. *May 2010*, 1–22.

Zia., Barr, P. J., Kukay, B. M., & Halling, M. W. (2017). *Zia_Preston_Scott_Workman.pdf*.

ANNEXES

Annex 1: Detail procedure for the construction stage analysis with deformation diagrams due to prestressing effect.

a) Construction stage 1 (CS1)

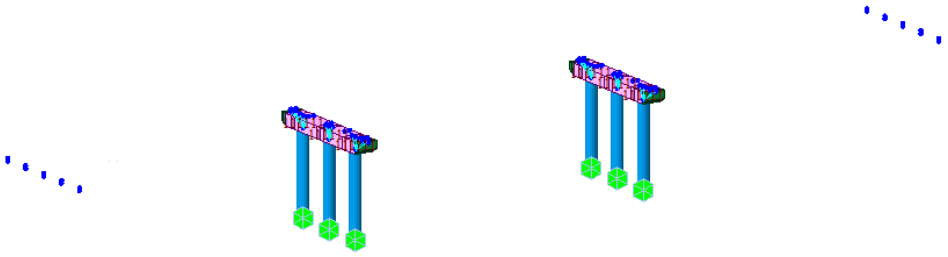

b) Construction stage 2 (CS2)

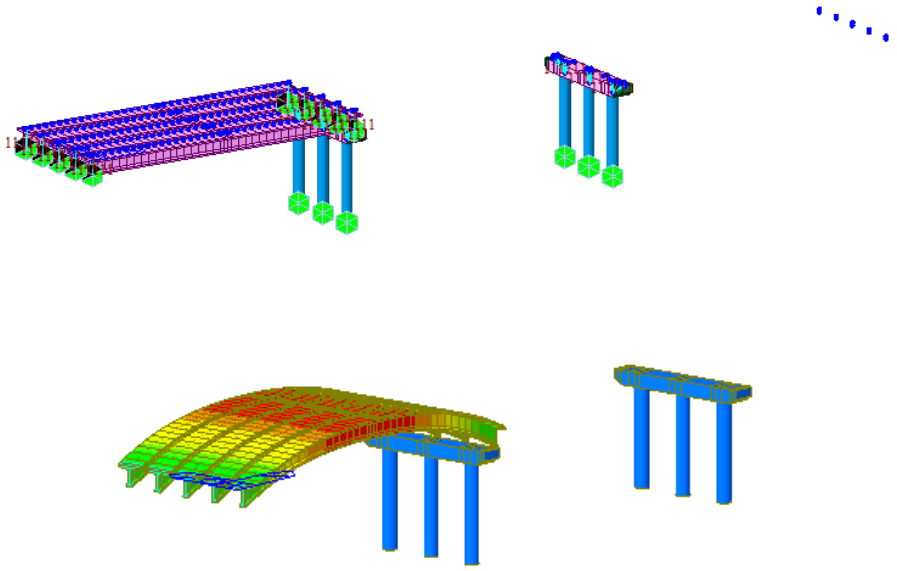

c) Construction stage 3 (CS3)

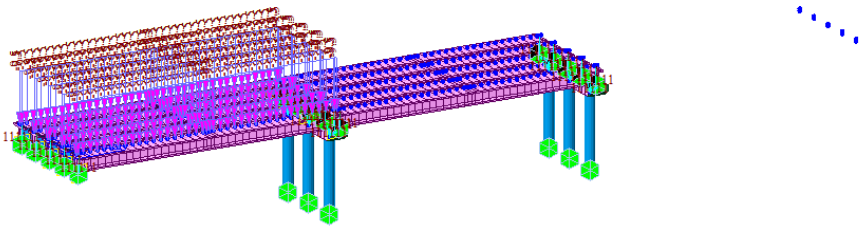

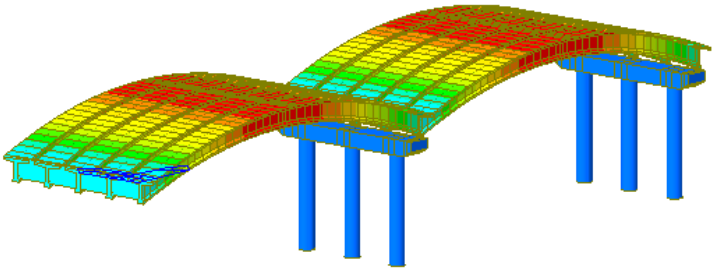

d) Construction stage 4 (CS4)

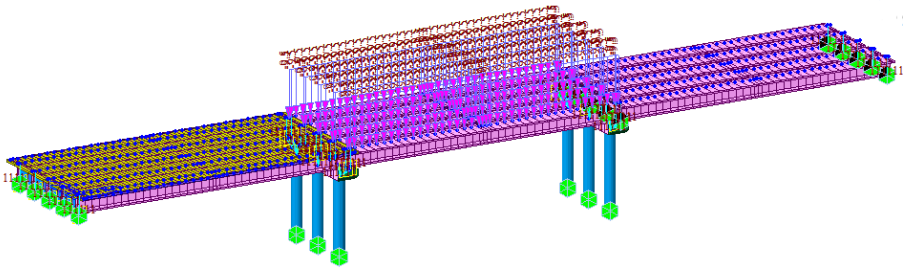

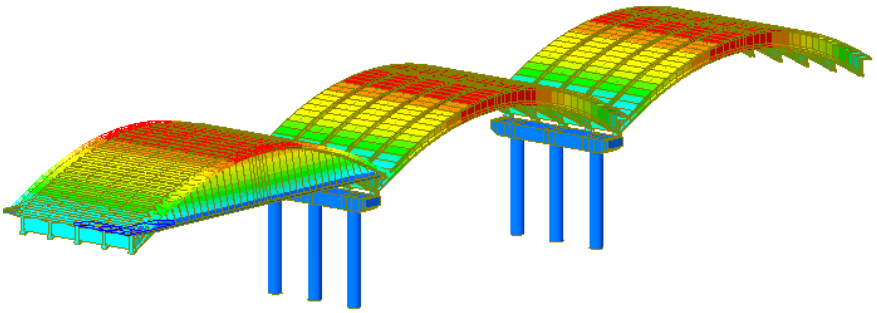

e) Construction stage 5 (CS5)

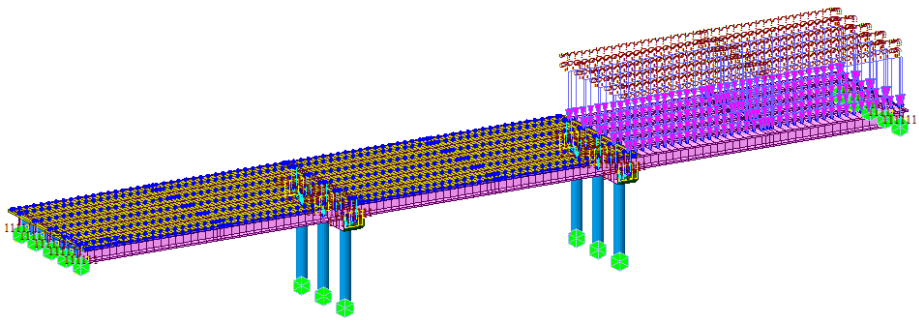

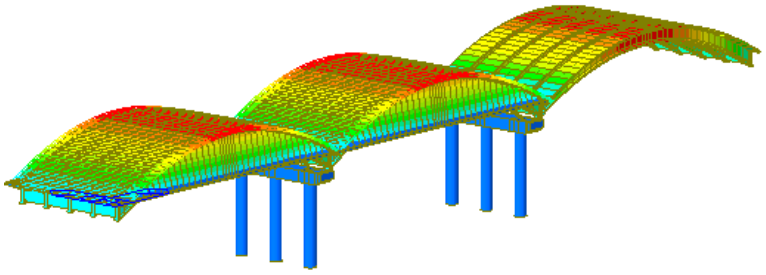

f) Construction stage 6 (CS6)

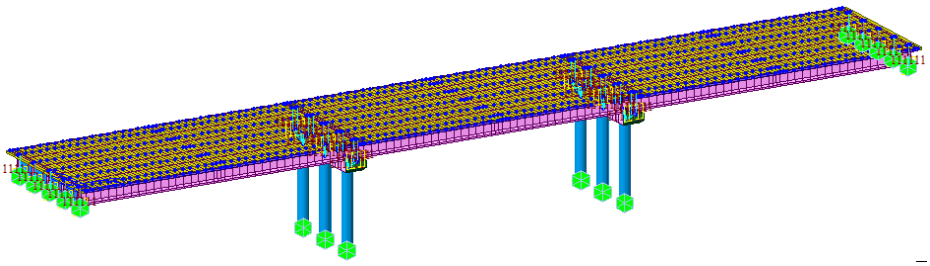

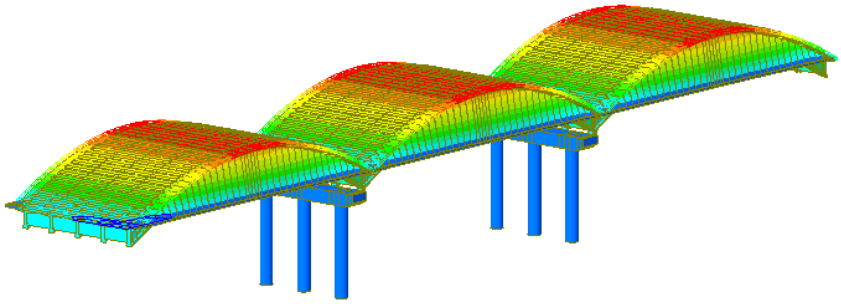

g) Construction stage 7 (CS7) (service life)

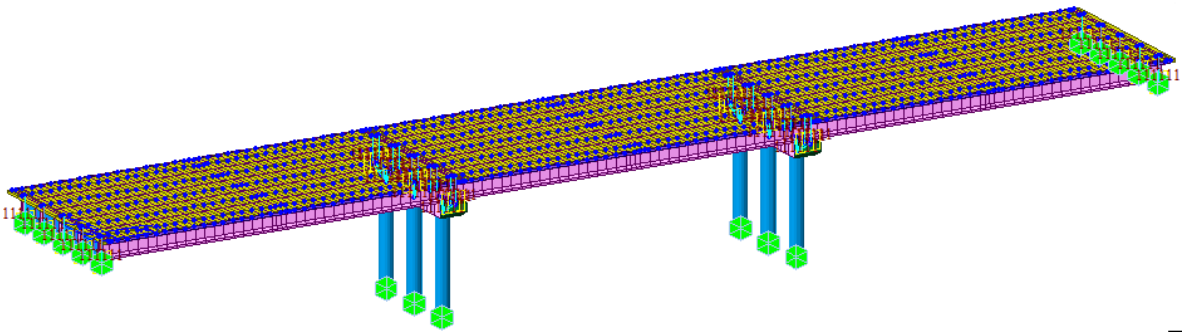

Annex 2: Deformation and displacement contour diagram of the bridge under maximum loading

a) Bridge deformation

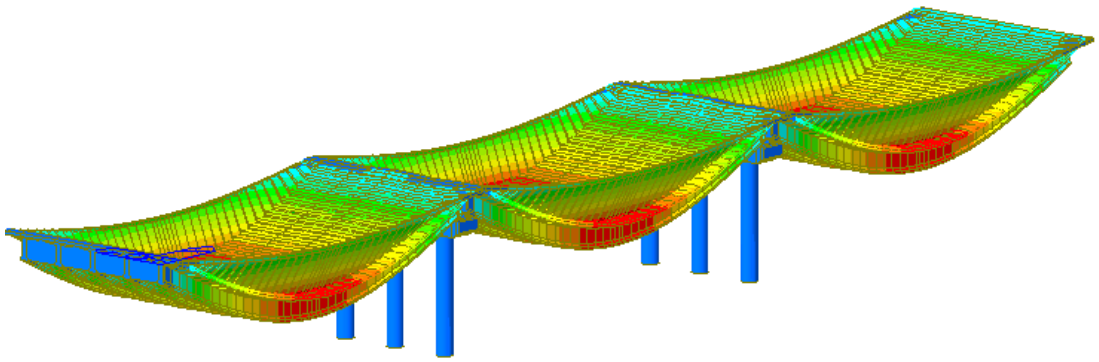

b) Displacement contour under maximum loading

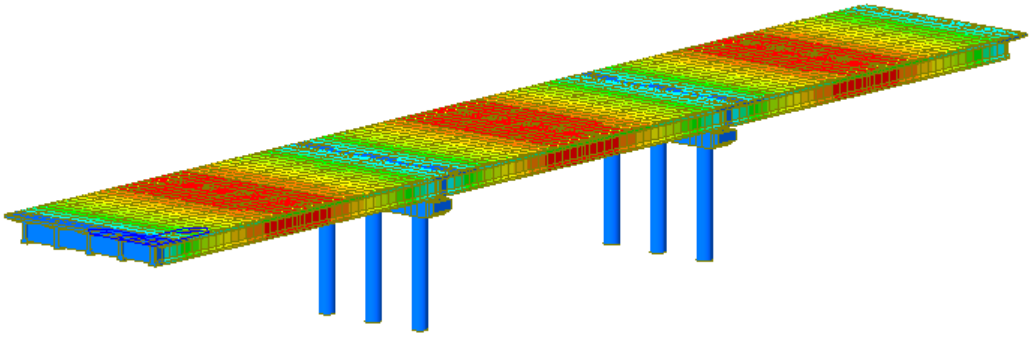

c) Solicitation diagram of the bridge under maximum loading for critical member selection

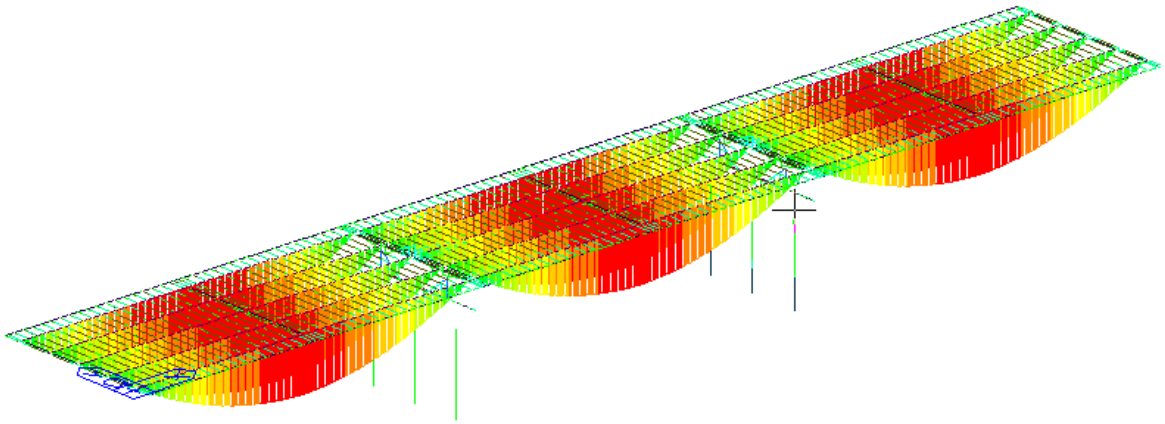

Annex 3: Pictures taken on the project site.